



HAL
open science

The *Phytophthora parasitica* effector Avh195: an antagonist of host autophagy and promoter of the infection cycle

Serena Testi

► **To cite this version:**

Serena Testi. The *Phytophthora parasitica* effector Avh195: an antagonist of host autophagy and promoter of the infection cycle. Molecular biology. Université Côte d'Azur, 2018. English. NNT : 2018AZUR4087 . tel-02275821

HAL Id: tel-02275821

<https://theses.hal.science/tel-02275821>

Submitted on 2 Sep 2019

HAL is a multi-disciplinary open access archive for the deposit and dissemination of scientific research documents, whether they are published or not. The documents may come from teaching and research institutions in France or abroad, or from public or private research centers.

L'archive ouverte pluridisciplinaire **HAL**, est destinée au dépôt et à la diffusion de documents scientifiques de niveau recherche, publiés ou non, émanant des établissements d'enseignement et de recherche français ou étrangers, des laboratoires publics ou privés.

THÈSE DE DOCTORAT

L'effecteur Avh195
de *Phytophthora parasitica* :
antagoniste de l'autophagie chez l'hôte
et promoteur du processus infectieux.

Serena TESTI

UMR ISA, INRA CNRS UCA – Équipe Interactions Plantes-Oomycètes

**Présentée en vue de l'obtention
du grade de docteur** en Science de la Vie
et de la Santé
d'Université Côte d'Azur

Dirigée par :
Franck Panabières / Harald Keller

Soutenue le : 26 Octobre 2018

Devant le jury, composé de :

Elodie Gaulin, Maître de conférences HDR,
Université Toulouse III
Franck Panabières, Directeur de Recherche,
UMR Institut Sophia Agrobiotech
Gilles Peltier, Chercheur CEA HDR,
CEA Cadarache
Pierre Frenod Professeur,
Université Côte d'Azur

**L'effecteur Avh195 de *Phytophthora parasitica* :
antagoniste de l'autophagie chez l'hôte et
promoteur du processus infectieux.**

Président du Jury

Pierre Frenco, Professeur, Université Côte d'Azur

Rapporteurs

Céline Masclaux-Daubresse, Directeur de Recherche, INRA Versailles-Grignon

Elodie Gaulin, Maître de conférences HDR, Université Toulouse III

Examineurs

Gilles Peltier, Chercheur CEA HDR, CEA Cadarache

Directeurs de thèse

Franck Panabières, Directeur de Recherche, UMR Institut Sophia Agrobiotech

Harald Keller, Directeur de Recherche, UMR Institut Sophia Agrobiotech

L'effecteur Avh195 de *Phytophthora parasitica* : antagoniste de l'autophagie chez l'hôte et promoteur du processus infectieux.

L'agent pathogène *Phytophthora parasitica* est un oomycète qui a des effets dévastateurs sur l'agriculture et les écosystèmes naturels. En tant qu'organisme hémi-biotrophe, il infecte les racines des plantes en établissant d'abord un contact intime avec les cellules hôtes (biotrophie) avant de les tuer (nécrotrophie) et de terminer son cycle d'infection. Pour contrôler ces processus, les oomycètes sécrètent des protéines effectrices, qui sont internalisées dans les cellules végétales par un motif de translocation (appelé RxLR-EER) pour manipuler la physiologie et les réponses immunitaires de l'hôte. Les études des échanges moléculaires entre *Phytophthora parasitica* et la plante qui ont été menées par le laboratoire d'accueil ont permis d'identifier un effecteur RxLR, dénommé Avh195. La séquence en acides aminés de l'effecteur est caractérisée par la présence de cinq motifs AIM (« ATG8 Interacting Motive ») qui indiquent une interaction potentielle avec la protéine centrale de l'autophagie, ATG8. Avh195 co-localise avec la fraction membranaire de l'ATG8, et un système double-hybride en levure permettant la détermination d'interactions entre protéines membranaires, a confirmé une interaction non sélective entre Avh195 et plusieurs isoformes d'ATG8. La caractérisation de la perturbation de l'autophagie dépendante de Avh195 a été réalisée dans l'algue unicellulaire *Chlamydomonas reinhardtii* après génération de lignées transgéniques surexprimant l'effecteur. Les analyses par cytométrie de flux ont révélé que Avh195 ne modifie pas la physiologie et la « fitness » de l'algue dans des conditions de croissance normales et pendant l'autophagie induite par la rapamycine. La microscopie électronique à transmission a révélé que l'effecteur provoque dans les cellules de l'algue un retard dans le flux autophagique, se traduisant par une réduction de la coalescence et de la clairance des vacuoles et une forte accumulation d'amidon dans les chloroplastes. Cependant, ce phénotype est transitoire et seulement légèrement lié aux modifications de la régulation transcriptionnelle de la machinerie autophagique. L'analyse de la fonction effectrice chez les plantes a montré que Avh195 retarde le développement de la mort cellulaire hypersensible, déclenchée par un éliciteur d'oomycète. Cette activité dépend de trois AIM sur cinq, ce qui renforce encore l'importance de l'interaction Avh195-ATG8 pour la fonction de l'effecteur. La surexpression stable d'Avh195 chez *A. thaliana* a permis de déterminer que l'effecteur n'altère pas les réponses immunitaires des plantes, mais favorise globalement le développement de l'agent pathogène, accélérant le passage de la biotrophie à la nécrotrophie au cours de l'infection. À notre connaissance, le travail présenté dans cette thèse représente la première preuve qu'un effecteur d'oomycète possède une activité transitoire, ciblant de manière non sélective la protéine ATG8 dans différents organismes photosynthétiques pour ralentir le flux autophagique, favorisant ainsi le mode de vie hémi-biotrophe d'un agent pathogène.

Mots clé : Plante, *Phytophthora parasitica*, Effecteur; Autophagie, *Chlamydomonas reinhardtii*

**The *Phytophthora parasitica* effector Avh195 :
An antagonist of host autophagy and promoter of the infection cycle.**

The plant pathogen *Phytophthora parasitica* is an oomycete with devastating impacts on both agriculture and natural ecosystems. As a hemi-biotrophic organism it infects the roots of plants first establishing an intimate contact with host cells (biotrophy) before killing them (necrotrophy) and completing its infection cycle. To control these processes, oomycetes secrete effector proteins, which are internalized in plant cells by a translocation motif (called RxLR-EER) to manipulate the physiology and the immune responses of the host. Studies of the molecular exchanges between *Phytophthora parasitica* and the plant that were conducted by the hosting laboratory led to the identification of an RxLR effector, designed to as Avh195. The amino acid sequence of the effector is characterized by the presence of five AIMs (ATG8 interacting motifs), that indicate a potential interaction with the autophagic core protein, ATG8. Avh195 colocalizes with the membrane-bound fraction of ATG8, and a yeast two-hybrid system, which allows to determine interactions between membrane proteins, confirmed a non-selective interaction between Avh195 and several ATG8 isoforms. The characterization of Avh195-dependent autophagy perturbation was carried out in the unicellular alga *Chlamydomonas reinhardtii* after generation of transgenic lines overexpressing the effector. Analyses by flow cytometry revealed that Avh195 does not modify the physiology and fitness of the alga, both under normal growth conditions and during rapamycin-induced autophagy. Transmission electron microscopy of cells revealed that the effector provokes a delay in the autophagic flux, manifested as a reduced coalescence and clearance of autophagic vacuoles and a strong accumulation of starch in chloroplasts. However, this phenotype was transient and only slightly related to modifications in the transcriptional regulation of the autophagic machinery. The analysis of effector function *in planta* showed that Avh195 delays the development of hypersensitive cell death, which is triggered by an oomycete elicitor. This cell death-delaying activity is dependent on three out of five AIMs, further consolidating the importance of the Avh195-ATG8 interaction for the function of the effector. The stable overexpression of Avh195 in *A. thaliana* allowed to determine that the effector does not impair plant defense responses, but overall promotes the development of the pathogen, accelerating the switch from biotrophy to necrotrophy during infection. To our knowledge, the work presented in this thesis represents the first evidence for an oomycete effector to possess a transitory activity, which targets in a non-selective manner the protein ATG8 in different organisms from the green lineage to slow down autophagic flux, thus promoting the hemibiotrophic life style of a pathogen.

Keywords: Plant, *Phytophthora parasitica*, Effector; Autophagy, *Chlamydomonas reinhardtii*

Remerciements

Je tiens d'abord à remercier les membres du jury pour l'intérêt que vous avez manifesté pour ce travail. Merci à Céline Masclaux-Daubresse, et Elodie Gaulin pour avoir accepté d'évaluer mon travail en tant que rapportrices. Merci à Gilles Peltier pour avoir accepté d'être examinateur et merci à Pierre Frendo pour avoir accepté d'être président du jury.

Merci au financement Labex Signallife (ANR-11-LABX-0028-0). Je remercie aussi toutes les personnes qui ont contribué à la réalisation de ce travail de thèse. Merci à Claire Veneault-Fourrey et Christophe Roux pour la discussion fructueuse lors du Comité de thèse. Merci à Gilles Peltier, Fantao Kong et Pascaline Auroy pour la génération des Chlamydomonas transformées. Merci à Nathalie Zucchini-Pascal pour tous ses efforts sur les cellules HeLa. Merci à Georges de Sousa et Éric Boncompagni pour tous les produits qu'ils m'ont fourni et à Olivier Pierre pour ses précieux conseils sur la microscopie. Merci à Valérie Allasia pour avoir complété une partie importante de ce travail. Merci à Sophie Pagnotta et Julie Cazareth pour leur temps et leur engagement dans la réalisation des expériences de TEM et de cyrtométrie en flux.

Merci Franck et Harald de m'avoir accueilli dans votre laboratoire et équipe. Avoir deux directeurs de thèse c'est parfois redouté mais dans mon cas cela a représenté une valeur ajoutée : j'ai vraiment apprécié pouvoir échanger avec deux scientifiques exceptionnels aux compétences si variés. Merci pour l'énorme aide que vous m'avez donné pour la réussite de cette thèse et merci pour tout ce que vous m'avez appris au cours de ces quatre années. Merci aussi pour tous les bons moments que nous avons passé ensemble lors des congrès. Merci pour la confiance que vous m'avez accordée et merci de m'avoir poussé plusieurs fois à sortir de ma zone de confort.

Merci à toute l'équipe IPO qui m'a accueilli comme une grande famille. Merci à Valérie, Agnès, Jo-Yanne et Naïma (mais aussi Sandrine et Elodie) pour tous les sujets de conversations incroyables abordées au café (et aussi pour les bons chocolats !) : je ne suis pas une grande bavarde mais j'ai vraiment adoré passer du temps avec vous. Merci à Cathy et Éric : ça a été un vrai plaisir d'avoir partagé le laboratoire avec vous pendant ces quatre années. Éric, merci pour les discussions scientifiques (et non) que nous avons eu, pour tous tes conseils et encouragements.

Benoît et Laurent : merci pour toutes vos bêtises, vous m'avez redonné le sourire même dans les journées les plus noires. Merci Benoît, tout simplement parce que c'est toi (et aussi parce que t'as supporté avec patience mon dépaysement lors de mes premiers pas dans le labo). Et merci Laurent pour avoir toujours la réponse à tout, maintenant il te manque juste d'imparare un po' di italiano !

Merci à tous les doctorants que j'ai croisée au cours de ces quatre ans. Un remerciement spécial va à Laïla Danila et Martina. Vous êtes des collègues exceptionnelles. Merci pour tous les bons moments que nous avons a passée ensemble au labo, sur la plage ou d'arrière une pinte de bière. J'ai adoré partager cette expérience avec vous et je ne vous oublierai jamais : je vous souhaite tout le meilleur pour votre futur.

Marie Line, je ne t'ai pas oublié : tu es ici parmi mes remerciements les plus personnels car tu as été non seulement une encadrante mais aussi une amie et parfois une maman. Tu m'as accompagné depuis le début de cette aventure et nous avons partagés ensemble les joies et les douleurs de ce doctorat (et plein de nuits passées avec les doigts croisées). Je pense qu'il n'y a pas de mots pour exprimer ma gratitude pour tout ce que t'as fait pour moi et tu le sais que je ne t'oublierai jamais. Merci et encore merci pour tout ton aide, ton soutien et ta gentillesse envers moi.

Merci à ma petite boule de poil, Freya, pour toute la joie et l'amour qu'elle a apporté à ma vie comme seulement un chat sait faire. Merci d'avoir dormi avec patience à mon côté lors de longues heures de rédaction.

Thanks to Nathaly and Caterina (in order of arrival in my life, not of importance!). It's been four years we met: we begun this huge journey together and finally we are going to see the light at the end of the tunnel together. Maybe we haven't had the time to meet as much as we planned but I want you to know how much I loved every single moment (and kilometres) we spent together. I will keep our friendship precious in my heart and I really wish all the best to both of you, while waiting to go for a walk in Nice when we will be three old grumpy ladies.

Grazie ai miei genitori. Vi voglio bene e ovunque andrò i chilometri non ci terranno mai lontani perché siete sempre nel mio cuore. Grazie per tutti gli sforzi che avete fatto per farmi arrivare dove sono e per avermi sempre supportato in ogni mio sogno.

Grazie Andrea, perché questa tesi è anche merito tuo. Quattro anni fa mi hai incoraggiato ad iniziare un dottorato pur sapendo che questo avrebbe significato vivere lontani. Quattro anni sono interminabili ma tu mi sei sempre stato accanto: sei la mia forza e la ragione che mi spinge ogni giorno a dare sempre il meglio. Grazie per tutto il tuo amore e sostegno. Grazie di esserci. Grazie di credere sempre in me, molto più di quanto sarò mai capace di fare.

Table of Contents

Abbreviations	1
Figures and Tables.....	3
Chapter 1: Oomycetes.....	5
General Introduction	5
1.1 The species <i>Phytophthora parasitica</i>	9
1.2 Molecular dialogue between plants and Oomycetes.....	14
Chapter 2: Autophagy	21
General Introduction	21
2.1 A focus on macroautophagy.....	22
2.2 Autophagy in plants.....	28
Objectives of the PhD project	35
Chapter 3: Results.....	37
3.1 Molecular characterization of Avh195	38
3.2 Avh195 interacts with ATG8.....	47
3.3 Characterization of Avh195 in <i>Chlamydomonas reinhardtii</i>	55
3.4 Role of Avh195 during the host-pathogen interaction	83
3.5 Trans-kingdom activity of Avh195.....	89
Chapter 4: Discussion.....	97
Conclusions and Perspectives	105
Materials and Methods	111
I - Bioinformatic analysis	111
II - Vector construction.....	111
III - RNA extractions and gene expression analysis	114
IV - SDS-page and Western blot analysis.....	115
V - Recombinant protein production and purification	116
VI - Yeast two-hybrid assay	117
VII - <i>Arabidopsis thaliana</i> assays.....	118
VIII - <i>Solanum lycopersicum</i> assays	120
IX - <i>Nicotiana</i> species assays.....	121
X - <i>Chlamydomonas reinhardtii</i> assays.....	123
XI - HeLa cells assays.....	126
XII - Statistical analysis.....	126
XIII - Sequences.....	127
XIV - Growth media.....	128
XV - Primers	131
XVI - Vector constructions	133

Bibliography 135
Supplementary Figures..... 151

Abbreviations

3-MA	3-methyladenine
aa	Amino acid
A/Ade	Adenine
AIM	ATG8 interacting motif
At	<i>Arabidopsis thaliana</i>
ATG	Autophagy related (gene/protein)
ATP	Adenosine triphosphate
AVR	Avirulence protein
BRET	Bioluminescence Resonance Energy Transfer
C/Cys	Cysteine
cAMP	Cyclic Adenosine mono-phosphate
cDNA	Complementary DNA
CFSE	Carboxyfluorescein succinimidyl ester
CMV	Cytomegalovirus (promoter)
CQ	Chloroquine
Cr	<i>Chlamydomonas reinhardtii</i>
CRN	Crinkling and necrosis
ct	Cycle threshold in qPCR
CVT	cytosol-to-vacuole targeting
CVT	Cytosol-to-vacuole targeting
D/Asp	Aspartic acid
DAPI	4'-6-diamino-2 phenylindole dihydrochloride
DMEM	Dulbecco's Modified Eagle Medium
DNA	Deoxyribonucleic acid
E/Glu	Glutamic acid
ECL	Enhanced Chemiluminescence
EHM	Extrahaustorial membrane
EHMx	Extrahaustorial matrix
ER	Endoplasmic reticulum
EST	Expressed sequence tags
ET	Ethylene
ETI	Effector triggered immunity

FSC	Forward light scattering
FW	Conidiospores per mg fresh weight
G/Gly	Glycine
GFP	Green fluorescent protein
GTP	Guanosine triphosphate
H/His	Histidine
Hpa	<i>Hyaloperonospora arabidopsidis</i>
hpi	Hours post inoculation
HR /HR-PCD	Hypersensitive Response (- programmed cell death)
HRP	Horse Radish Peroxidase
HSP	Heat shock protein
HT	Host-targeting signal
I/Ile	Isoleucine
JA	Jasmonic acid
kDa	Kilo Dalton
L/Leu	Leucine
LB	Luria-Bertani medium
LC3	Mammalian ortholog of ATG8 proteins
LIR	LC3 interacting region
LIRCPs	LIR motif-containing proteins
M/Met	Methionine
MAPK	Mitogen activated protein kinase
Mbp	Mega base pairs
mbSUS	Mating-based split-ubiquitin system
miRNA	Micro RNA
ML	Maximum Likelihood
MS	Murashige and Skoog medium
Mya	Million years ago
NCBI	National Center for Biotechnology Information
OA	Oxalic acid
OD₆₀₀	Optical density measured at 600 nm

OE	Overexpressor
ORF	Open reading frame
p35S	Cauliflower Mosaic Virus (CaMV) 35s promoter
PAMPs	Pathogen associated molecular patterns
PAS	Phagophore assembly site
pb	Base pairs
PCD	Programmed cell death
PCR	Polymerase chain reaction
PE	Phosphatidyl ethanolamine
Pi	<i>Phytophthora infestans</i>
pI	Isoelectric point
PKA	cAMP-dependent protein kinase
poli(A)	Poli adenylation signal
Pp	<i>Phytophthora parasitica</i>
PPRs	Pattern recognition receptors
PR	Pathogenesis related
Ps	<i>Phytophthora sojae</i>
PSSM	Position-specific scoring matrix
PtdIns	Phosphatidyl inositol
PtdIns3K	Phosphatidyl-inositol 3 kinase
PtdIns3P	Phosphatidyl inositol 3 phosphate
PTI	PAMP triggered immunity
PVDF	Polyvinylidene difluoride
QoIs	Quinone Outside Respiration Inhibitors
Ra	Rapamycin
RFP	Red fluorescent protein
RNA	Ribonucleic acid
ROS	Reactive oxygen species
RT	Reverse transcription

RT-qPCR	Real-Time Quantitative Reverse Transcription PCR
S/Ser	Serine
SA	Salicylic acid
SAR	Systemic acquired resistance
SC	Synthetic complete medium
SD	Standard deviation
SDS	Sodium dodecyl sulphate
siRNA	Small interfering RNA
SNP	Single Nucleotide Polymorphism
Spp.	Species
SSC	Side light scattering
T35S	Cauliflower Mosaic Virus (CaMV) 35s terminator
TAP	Tris Acetate Phosphate medium
TBS	Tris Buffered Saline
TEM	Transmission electron microscopy
TMV	Tobacco mosaic virus
TOR/TORC	Target of Rapamycin (-complex)
Ub	Ubiquitin
UBC	Ubiquitin conjugating enzyme
UBL	ubiquitin-like
UTR	Untranslated region
V/Val	Valine
VSP	Vacuolar protein sorting
W/Trp	Tryptophan
WT	Wild type
X	Any amino acid in aminoacidic sequences
Y/Tyr	Tyrosine
Y2H	Yeast two-hybrid
α-	Antibody

Figures and Tables

Figure 1.1: Symptoms associated with *Phytophthora parasitica* infection.

Figure 1.2: Infectious cycle of *Phytophthora parasitica*.

Figure 1.3: The RxLR effector family.

Figure 1.4: Overview of RxLR effectors targets in plant cells.

Figure 2.1: Core macroautophagy machinery in *Saccharomyces cerevisiae*.

Figure 2.2: Core autophagy machinery in *Arabidopsis thaliana* compared to yeast.

Figure 2.3: Autophagy in plants.

Figure 2.4: Role of autophagy in plant-pathogen interaction.

Figure 3.1: Amino acid sequence alignment of Avh195 and PITG_04099.

Figure 3.2: Expression profile of Avh195 during the *P. parasitica* life cycle.

Figure 3.3: Schematic representation of the Avh195 protein sequence.

Figure 3.4: Avh195 transiently inhibits HR through interaction with ATG8.

Figure 3.5: Relative expression of ATG8 members during *Arabidopsis* root infection by *P. parasitica*.

Figure 3.6: Phylogenetic relationships of ATG8 sequences from green organisms

Figure 3.7: Avh195 localizes to membranes, whereas ATG8 is both soluble and membrane-associated.

Figure 3.8: Avh195 interacts with ATG8 from *C. reinhardtii* and *A. thaliana*.

Figure 3.9: The microalga *Chlamydomonas reinhardtii*.

Figure 3.10: Core autophagy machinery in *Chlamydomonas reinhardtii* compared to yeast.

Figure 3.11: Experimental strategy applied to *Chlamydomonas* experiments.

Figure 3.12: Characterization of *C. reinhardtii* transformant cell lines.

Figure 3.13: Flow cytometry analyses of *Chlamydomonas reinhardtii* WT and transgenic cell lines.

Figure 3.14: Heat shock induces lethality in *Chlamydomonas* transformant strains.

Figure 3.15: Flow cytometry analysis of *C. reinhardtii* transformant cell lines upon rapamycin treatment.

Figure 3.16: Response of *Chlamydomonas* cells to rapamycin treatment.

Figure 3.17: Subcellular phenotypes of *Chlamydomonas* cells expressing Avh195, as analyzed by TEM.

Figure 3.18: *C. reinhardtii* Avh195 transformants starch metabolism perturbation.

Figure 3.19: Overexpression of Avh195 in *C. reinhardtii* only moderately changes the accumulation of autophagy-related gene transcripts and of ATG8 protein.

Figure 3.20: Expression levels of Avh195 in two independent transgenic *A. thaliana* lines

Figure 3.21: Avh195 promotes infection and changes the timely onset of plant defense responses.

Figure 3.22: Expression of Avh195 in *A. thaliana* changes the timely onset of oomycete life style.

Figure 3.23: Overexpression of Avh195 in *A. thaliana* promotes susceptibility to biotrophic *H. arabidopsidis*.

Figure 3.24: Exogenous Avh195 is taken up by mammalian cells.

Figure 3.25: Morphological modifications induced by Avh195 treatments.

Figure 3.26: Exogenous Avh195 increases the accumulation of acidic vesicles.

Figure 3.27: Morphological effect of Avh195 transfection.

Supplementary Figure 1: Representative view of Chlamydomonas cells from the wild-type and transgenic lines expressing *Avh195*, as analyzed by TEM.

Supplementary Figure 2: Accumulation of electron-dense, lysosome-like structures in cells from Avh195-expressing Chlamydomonas lines that were not treated with rapamycin.

Table 3.1: Bioinformatic analysis of Avh195 protein sequence.

Chapter 1: Oomycetes

General Introduction

Oomycetes are one of the most economically and ecologically important class of eukaryotic microorganisms playing a fundamental role in nutrient recycling, but also representing a major threat to agriculture and natural ecosystems worldwide.

Historically, Oomycetes were considered as members of the kingdom of Mycota, as an ancient basal lineage of fungi [1]. This misconception was due to the strong similarities that fungi and Oomycetes display, such as the filamentous growth in the form of tip-growing branching hyphae, and their similar ecological role and feeding behavior [2]. However, technical advances in the 20th century suggested that Oomycetes and Fungi share less than meets the eye: Oomycetes display distinctive features both at a morphological and molecular level, which unite them with brown algae and diatoms among Stramenopiles (Straminipila) [3]. For example, the cell wall of Oomycetes is mainly composed of cellulose and glucans, and the major fungal cell wall compound chitin is only a minor constituent. Oomycetes develop mostly non-septate hyphae, they are auxotrophic for sterols, diploid for the majority of their life cycle, and disseminate mainly asexually with biflagellated zoospores [4]. Molecular phylogenies based on conserved mitochondrial and nuclear DNA sequences and more recent genome-scale phylogenetic studies further confirmed the distant relation of Oomycetes from true fungi [5–7].

It is thought that the common ancestor of the Straminipila lineages was a biflagellate photosynthetic organism that obtained the chloroplasts from endosymbiosis with a red alga. Then Oomycetes underwent repeated loss of plastids and genes for phototropism, leading to the current morphology and lifestyle [3], although some lineages still conserve photosynthesis-related genes [8].

The evolutionary history of Oomycetes is mostly inferred from molecular studies on living species and molecular clock estimates suggest that they diverged from other Straminipila in the first half of the Paleozoic era, up to 430 million years ago [9]. In addition, the existence of preserved oomycete structures in the fossil records from the Carboniferous period (300 million years ago) supports the Palaeozoic origins of this lineage [10]. Fossils also report the ancient parasitic lifestyle of Oomycetes toward plants [11]. In fact, although numerous oomycete species are saprophytic, pathogenicity evolved independently several times in different oomycete lineages [12]. The evolution of this trait

appears to be deeply rooted in the oomycete lineage [2], and was certainly facilitated by an ancient horizontal transfer of genes linked to pathogenicity from fungi and bacteria, such as hydrolytic enzymes, toxins, nutrient transporters and effectors [13,14].

Indeed, the attitude toward parasitism is widespread along the phylogenetic branch of Oomycetes. The basal-most lineage of Oomycetes comprises marine organisms which are predominantly parasites of seaweeds, nematodes or crustaceans [2]. The remaining clades can be broadly regrouped in two subclasses: the Saprolegnomycetes and the Peronosporomycetes. Saprolegnian organisms are mainly marine and freshwater saprophytes and parasites of animals such as the members of the genus *Saprolegnia* [15], with an exception for some species belonging to the *Aphanomyces* which are plant parasites [16]. Peronosporomycetes is by far the largest order of terrestrial organisms that includes the most studied species of Oomycetes, comprising downy mildews, *Albugo*, *Pythium* and *Phytophthora* and the majority of organisms belonging to those taxa are plant parasites with a wide range of hosts, including crop species, ornamental plants, and native plants and trees [12].

Overall, pathogenic Oomycetes have evolved different lifestyles. Saprophytic species can be facultative necrotrophic pathogens that kill host tissue before feeding on it; such behavior can be found among *Pythium* and *Aphanomyces* genera. On the other hand, several lineages evolved a biotrophic lifestyle, characterized by maintaining an intimate interaction with living plant cells. Species belonging to the downy mildews and the *Albuginales* display obligate biotrophy, requiring metabolic active plant tissues to complete their live cycle and developing highly specific interactions with the host [17]. By contrast, species of the genera *Phytophthora* and *Pythium* display an intermediate lifestyle called hemibiotrophy, adopting a two-step infection: the pathogen initially establishes a transient biotrophic relationship with the host, followed by necrotrophy which determines extensive cell death of host as the infection progresses [18,19].

Oomycetes are ubiquitous in natural ecosystems, ranging from marine, freshwater and terrestrial environments and are adapted to the most diverse ecosystems, reaching the cold polar regions, the arid deserts and temperate forests [17]. Unsurprisingly, this global distribution represents a problem when we have to deal with pathogenic Oomycetes that are responsible every year for enormous economic losses and damages in natural and cultured ecosystems. For example, *Saprolegnia* and *Aphanomyces* species are responsible for the decline of natural populations of salmonids and represent a threat to aquaculture of freshwater fish [20]. However, the most

notorious and devastating Oomycetes are plant pathogens, in particular those belonging to the genus *Phytophthora*. The late blight epidemics caused in Ireland by *Phytophthora infestans* in the nineteenth century is probably the most well-known devastating outbreak in cultivated crops, and still represents a threat for potato and tomato crops. Another example, among several others, is the *Phytophthora ramorum* epidemics that struck California and southern Oregon in the late 1990s that led to the destruction of Oak forests. This pathogen is presently spreading across Europe to ornamental plants [21,22].

Control of oomycete diseases relies mainly on the use of fungicides containing molecules with a high specific mode of action. This specificity permitted many *Phytophthora* species to develop resistance traits. One example is given by the phenylamide Mefenoxam, an inhibitor of RNA synthesis. The emergence of insensitive *Phytophthora infestans* isolates was documented across Europe, North America and Mexico and was associated with single nucleotide polymorphism (SNP) in the gene encoding the large subunit of RNA polymerase II [23]. Another class of molecules is represented by inhibitors of the respiratory chain called Quinone Outside Respiration Inhibitors (QoIs). Resistant isolates of *Phytophthora viticola* evolved rapidly in vineyards across Europe and once more the trait was associated with SNP in the sequence of the Cytochrome *b* gene [24]. The persisting threat by Oomycetes is made worse by the intensification of human displacements and the increase in international trading and climate warming, all factors that favor the introduction and establishment of new pathogens all over the world [25,26].

Is therefore clear that the study of these organisms is crucial for the development of novel strategies for disease management. The ongoing sequencing projects of several *Phytophthora* species already allowed to improve our understanding of oomycete origins and the molecular basis of the infectious process, and underlined the importance of molecular exchanges between the pathogen and the host [27].

1.1 The species *Phytophthora parasitica*

As described in the previous Section, the most known plant parasitic Oomycetes belong to the genus *Phytophthora* ('plant destroyer' in Greek), which includes over 140 described species [28]. In this work a particular attention will be devoted to *Phytophthora parasitica* (syn. *Phytophthora nicotianae*) which is gaining importance as a pathogen in terms of distribution, host range and economic impact. The species was first described in 1869 on tobacco plants displaying black skank, and hence the species name *nicotianae* was coined first. However, this pathogen has currently been isolated all over the world on up to 90 different plant families such as *Solanaceae*, citrus, horticultural and forest trees, ornamental plants, and medicinal herbs [29,30]. Usually, *P. parasitica* isolates display preferences for specific hosts, but some of them have a marked host flexibility and can infect numerous hosts, like the model plant *Arabidopsis thaliana* [31]. This makes the pathogen an ideal model to study the mechanisms regulating host specificity and susceptibility, and the molecular exchanges between the pathogen and the plant.

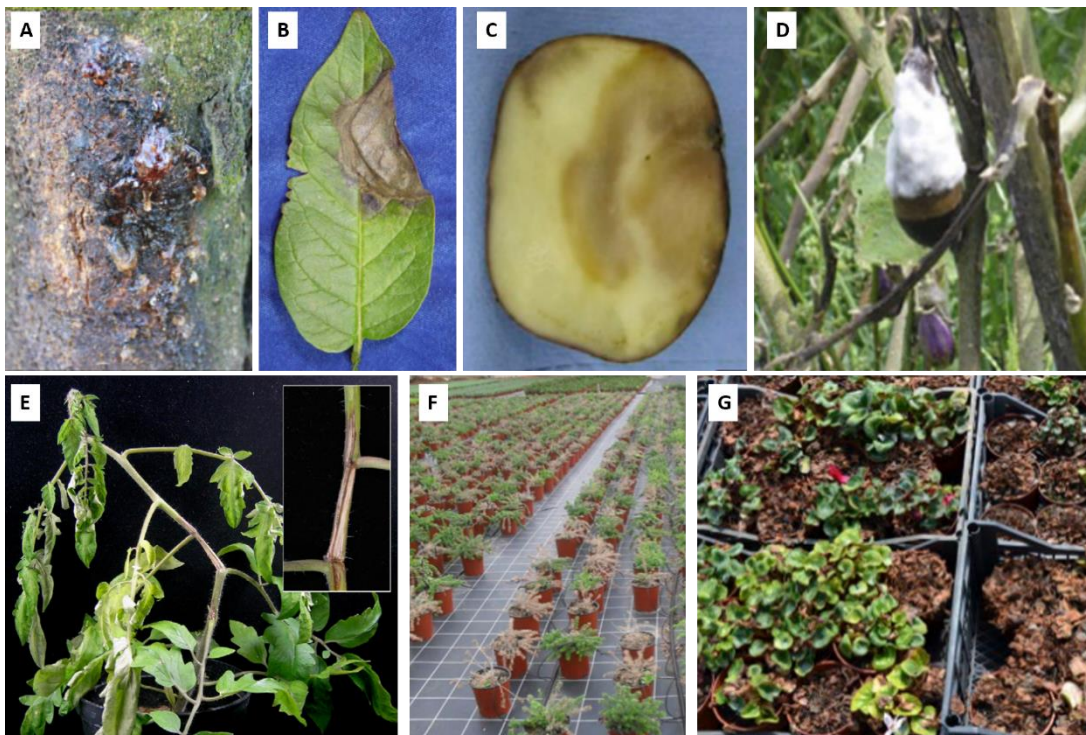


Figure 1.1: Symptoms associated with *Phytophthora parasitica* infection.

Pictures show various plant hosts and plant organs presenting the disease: (A) Citrus trunk (B) Potato leaf (C) Eggplant fruit (D) Potato tuber (E) Tomato stem. Diseased plantlets of (F) *Grevillea lanigera* (G) *Cyclamen* recovered from ornamental plant nursery. Adapted from [21,30,32].

1.1.1 P. parasitica life cycle and reproduction

As a soilborne pathogen *Phytophthora parasitica* mainly attacks the roots of host plants, but it is also able to develop on aerial parts of the plants and to survive outside hosts. The typical life cycle of this oomycete mainly relies on the asexual multinucleated sporangium which ensures long-distance dispersal of the organism according to two strategies: in warm and moist soils, the sporangium can germinate directly and produce a hypha that starts host colonization. Yet, under most other conditions, the sporangium undergoes sporulation (zoosporangiogenesis). This process happens in specialized hyphae responsible for the asexual reproduction of the organism, in which the production of spores is achieved through rapid cytokinesis leading to the release of single nucleated, wall-less cells called zoospores.

Zoospores are responsible for the infectious cycle (**Figure 1.2**): they are biflagellated motile cells that swim towards the roots of a potential host by means of a combination of several factors, including chemotaxis, electrotaxis and autotaxis [33]. When contact with the plant occurs, zoospores detach their flagella and adhere to the surface, become cysts through rapid formation of a cell wall and secrete adhesive material. The encasement leads to the formation of a germ tube that emerges close to the plant, growing on the surface towards a suitable penetration site. Here, it develops a specialized structure, the appressorium, a swollen hypha where degrading enzymes enable the penetration of the cuticle and the epidermal layer. Once inside plant tissues, the oomycete starts vegetative growth by forming hyphae that grow and branch intercellularly. During the initial biotrophic phase, hyphae break plant cell walls and develop inside the host cells specialized feeding structures called haustoria. Haustoria are surrounded by the plasma membranes from both the oomycete and the host cell, which provide an intimate contact for nutrient uptake and molecular exchanges with the host [34]. As the infection proceeds, the necrotrophic phase initiates via the release of toxic compounds that kill the host tissue, allowing invasive growth of the pathogen with a rapid increase in biomass, and culminating in the formation of new sporangia, and eventually, in the reiteration of the cycle on a new host [35,36].

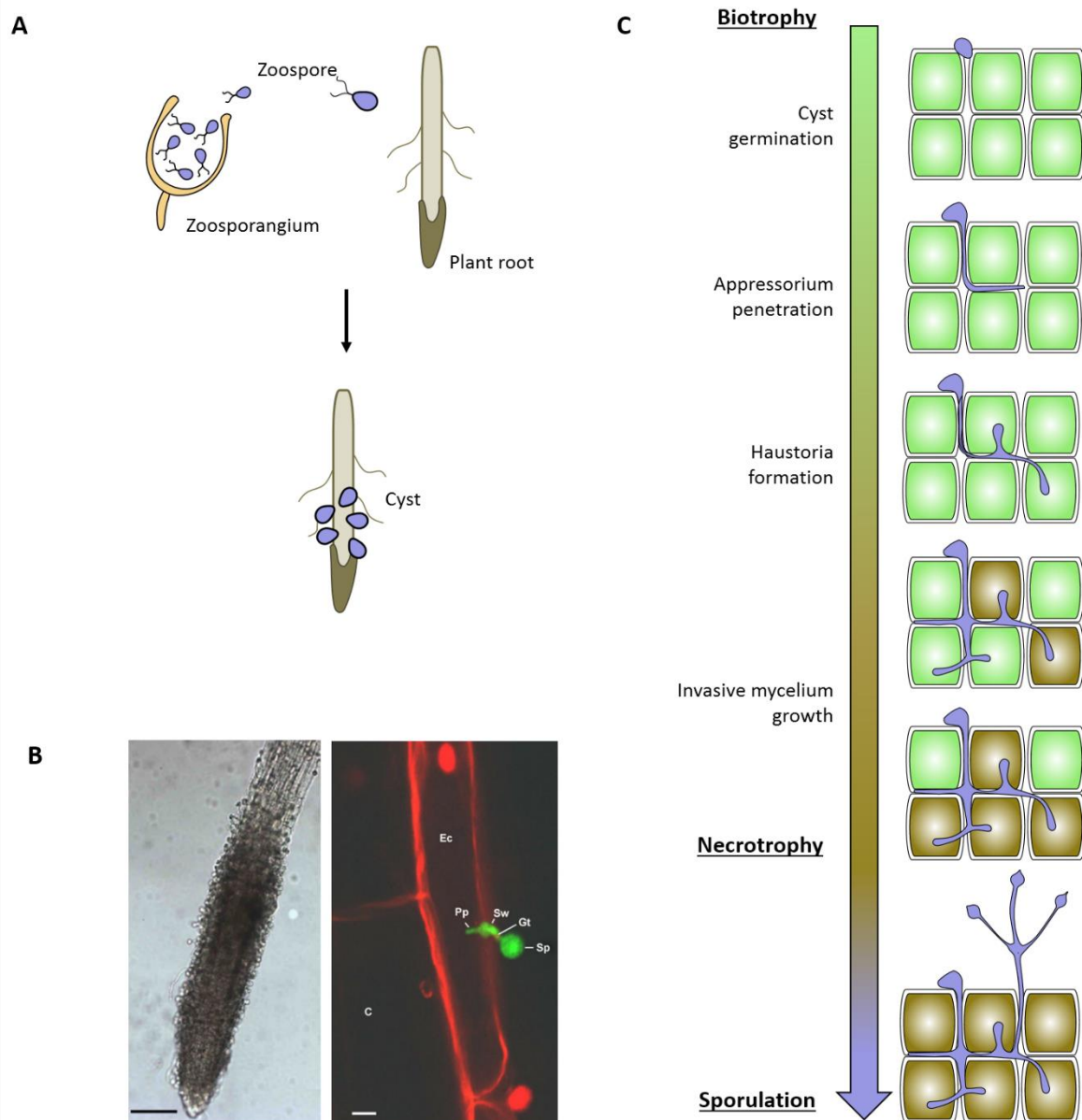


Figure 1.2: Infectious cycle of *Phytophthora parasitica*.

- A. The infectious cycle of *P. parasitica* begins with the formation of zoosporangia and the release of biflagellate zoospores that swim towards plant roots: once the contact takes place the flagella are lost, and the zoospore becomes a cyst.
- B. Left panel: Magnification of a root tip from *Arabidopsis thaliana* being attacked by *P. parasitica* zoospores. The zoospores form clumps during encystment at the elongation and differentiation zones. Scale bar represents 100 μ M. Right panel: confocal laser scanning micrograph of a GFP-expressing zoospore [38] (green fluorescence) penetrating in tomato roots stained with propidium iodide (red staining). The encysted zoospores (Sp) germinate, and the germination tube (Gt) forms an appressorium-like swelling (Sw) to push aside joined epidermal cells (Ec), and to enter a penetration peg (Pp) in between them. The absence of cytoplasmic propidium iodine stain (C) indicates that plant cells are alive. Pictures adapted from [32].
- C. At the beginning of the infection (biotrophy) the germinated cyst searches for a suitable site where a specialized structure, the appressorium, enables the penetration of the oomycete into plant tissues. Here the oomycete starts vegetative growth by forming intercellular hyphae and intracellular specialized feeding structures called haustoria. As the infection proceeds, the necrotrophic phase initiates via the release of toxic compounds that kill the host tissue, allowing invasive growth of the pathogen with a rapid increase in biomass, and culminating in the formation of new sporangia, and eventually, in the reiteration of the cycle on a new host.

Phytophthora parasitica can also produce thick walled spores, called Chlamydospores, which are believed to help the pathogen to survive in a dormant state when the temperatures are too low [37]. If humidity and temperature are not ideal for the infection process *Phytophthora* can also form haploid gametangia, the antheridia and oogonia, carrying the male and female gametes respectively, which are necessary for sexual reproduction. *Phytophthora parasitica* is not self-fertile (heterothallic) and requires the interaction between gametes belonging to different mating types. This process leads to the formation of oospores, which may persist in soil for years prior to further formation of sporangia or germ tubes directly. This reproduction strategy does not only allow the organism to overcome adverse environmental conditions but it also constitutes an important source of genetic variation, and potentially of increased virulence [29].

1.1.2 *P. parasitica* pathogenicity

The outcome of oomycete infections depends on plant immune responses that aim at blocking the pathogen, and on the ability of the microorganism to overcome these responses, to adapt, and to exploit the resources of the host. The processes leading to the success or the failure of infection are based on a complex molecular dialog between the plant and the pathogen, and many research efforts were made to understand this dialog. Until recently, most of these efforts were focused on the famous and economically important *P. infestans* species. However, *P. parasitica* gains importance as a model, since it represents the soilborne lifestyle of most *Phytophthora* species (contrary to *P. infestans*, a foliar pathogen), and due to the diversity of susceptible hosts [30]. For these reasons several resources were developed and are evolving, starting from the generation of a bacterial artificial chromosome library [39] until the public release of the genome sequence [40]. Much interest was also devoted to the profiling of gene expression during different phases of the *P. parasitica* life cycle. Expressed sequence tag (EST) libraries were generated from *in vitro*-growing hyphae [41], from zoospores and germinating cysts [39,42], as well as from different stages of the plant-pathogen interaction ranging from initial penetration to sporulation [38,39,42,43]. These activities helped to better characterize the molecular program deployed by the pathogen throughout the different stages of the life cycle, especially during the interaction with the plant. More recently, hybridization-based transcriptome experiments allowed refining the description of the events modulating the infection process, both in plant and in the pathogen [44,45].

Emerging from studies on *Phytophthora parasitica* and other *Phytophthora* species is that Oomycetes achieve their infection by modulating plant immunity through the deployment of a large repertory of effector proteins. Effectors are molecules, mainly proteins, which are secreted during infection and target plant functions to alter the normal physiology and response of the plant [46]. The genes encoding effector proteins are mostly located in plastic regions of the genome, rich in repeats and transposons that promote duplication events, shuffling, mutagenesis and silencing, thus underlining the importance of effectors in evolution and adaptation of Oomycetes, and to a wider extent, filamentous pathogens [27,47].

1.2 Molecular dialogue between plants and Oomycetes

As mentioned above, the success of oomycete infection passes through the manipulation of host defenses, metabolism and functions, overcoming the several layers of defense implemented by plants [48]. The first layer of plant defense is made of passive preformed barriers, such as the cell wall and the cuticle, and of the constitutive accumulation of antimicrobial compounds that allow plants to be protected against most attacks. However, if a pathogen succeeds in overcoming those barriers, plants deploy an innate immune system that controls most of the infection attempts. Detection of the so-called pathogen-associated molecular patterns (PAMPs) is based on the recognition of molecules, mainly proteins, or of activity-related parts of the molecules, that are generally essential for the pathogen's life cycle. PAMPs are recognized by plants when they are exposed and sensed by specific transmembrane receptors (PPRs) that recognize them. Activation of PRRs leads to the induction of defense responses, involving ion fluxes, oxidative bursts, and the activation of Mitogen-Activated Protein Kinase (MAPK) cascades, which in turn promote transcriptional regulations that aim at blocking further penetration of the pathogen [48,49]. Examples for identified *Phytophthora* PAMPs are Pep-13 and NPP1. Pep-13 is a highly conserved 13-amino acid fragment within the cell wall glycoprotein GP42 from *P. sojae* [50,51]. NPP1, necrosis-inducing *Phytophthora* protein 1, was identified in several *Phytophthora* species as a cell-wall protein eliciting immune responses in plants [52].

This second layer of plant defense can be overcome by pathogens by means of effector proteins, which can roughly be classified as extracellular (apoplastic) and intracellular effectors. Oomycetes such as *Phytophthora* secrete different type proteins that either protect the pathogen from host defenses or contribute to the process of invasion. Secreted apoplastic effectors may inhibit hydrolytic enzymes (chitinases, glucanases and proteases) that are released by the plant to block pathogen proliferation. RGD (Arginine–Glycine–Aspartic acid)-containing effectors promote entry and development of the pathogen by interfering with host signaling pathways that regulate adhesion of the plant cell wall to the plasma membrane. Other effectors are cell wall degrading enzymes as well as toxins, used by the oomycete to induce cell death when hemibiotrophic infection switches to necrotrophy [43,53,54]. A particular class of apoplastic effectors from *Phytophthora* that has been actively studied in the last decades is constituted by the elicitors. Elicitors are structurally conserved proteins that were initially described in *Phytophthora* spp. as able to elicit hypersensitive (HR) cell death and disease resistance in tobacco [55]. Elicitors are able to bind sterols and other

lipids [56]: since *Phytophthora* spp. are sterol auxotrophs, it was speculated that those molecules may serve as extractors of sterols from the plant membrane to ensure the metabolic needs of the oomycete, and consequently disrupt the membrane integrity leading to cell death [55].

Intracellular oomycete effectors are secreted proteins that carry host-translocation signals for their transport into the plant cell. Additional motifs then allow the relocalisation to specific subcellular compartments. Intracellular oomycete effectors mainly fall into two groups. The first comprises RXLR-effectors, whose typical feature is the presence of a conserved aminoacid signature at the N-terminus of the protein: Arginine, any amino acid, Leucine, Arginine (hence the name RXLR) often followed by a shorter Glutamate-Glutamate-Arginine (-EER) motif [57]. The second class is composed of the so-called Crinklers, named after the cell death phenotype they induce when overexpressed *in planta*. Similar to RxLR effectors, crinklers have a modular structure comprising conserved aminoacid motifs and seem to target the host nucleus [58].

In some cases, both apoplastic and intracellular effectors may be sensed by plants and activate a further layer of defense, called effector-triggered immunity (ETI). This immunity is provided by resistance (R) proteins, that are able to detect either directly or indirectly effectors proteins (named in this context avirulence proteins; AVR). The outcome of ETI is more rapid and stronger than PTI, and often leads to a hypersensitive response (HR), a form of localized host cell death to confine the pathogen at the infection site and to prevent further propagation into non-infected plant tissues.

This tight interaction of molecules from both the plant and the pathogen is the base of the so called “zig-zag” model postulated by Jones and Dangl [48], according to which the co-evolution of pathogen virulence determinants and plant resistance and immunity factors drives the outcome of plant-pathogen interactions.

1.2.1 The RXLR effector family

A study published in 2005 by Rhemany and colleagues compared the sequences of predicted secreted avirulence proteins from several oomycete species, and identified a conserved amino acid motif, namely the RXLR-EER motif [59]. Further searches for candidate effectors in *Phytophthora* genomes evidenced the presence of an important number of genes that potentially encode for RXLR effector proteins, many of which are part of gene families comprising numerous paralogs with marked positive selection for their C-terminal regions [60].

Proteins belonging to this class share a modular structure, characterized by an N-terminal signal peptide for secretion, the RXLR(-EER) region and a C-terminal effector domain that encodes the functional part of the protein [46,61]. While the N-terminal part of the protein seems to adopt a disordered conformation, crystallographic and *in silico* analyses of RxLR effectors showed that the C-terminal part of some of them share a conserved three alpha-helix fold, termed WY-domain after their composition in W and Y residues. WY domains probably allow oligomerization of the effectors, or modify their physiochemical properties thus leading to diversification in function [62,63].

The RXLR motif shares some similarities with a host-targeting signal (HT) conserved in proteins from malaria parasites (*Plasmodium* species), leading to the hypothesis that RXLR functions as a signal that mediates cell entry [59]. Indeed, several experiments show that this motif acts as a signal for host delivery [64,65]. Furthermore, the HT was demonstrated to be functional in *Phytophthora* to efficiently trigger effector translocation [66]. However, the mechanism used for translocation inside host cells remains unclear and is subject to controversial discussion. Published work showed that the motif is responsible for binding to host Phosphatidylinositol-3-phosphate thus triggering lipid raft-mediated endocytosis in a microbe-independent way [67–69]. Nevertheless, other studies indicate that the motif alone is not sufficient to produce this translocation [53].

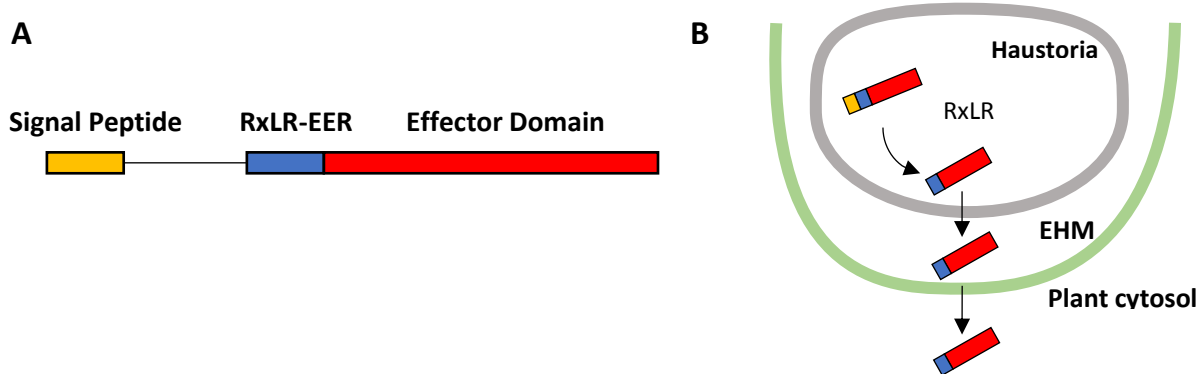


Figure 1.3: The RxLR effector family.

- A. The general structure of RxLR effectors includes a N-terminal domain containing a signal peptide for secretion (yellow box), followed by a RxLR-EER motif (blue box), which allows the translocation of the effector into the host cell. The effector domain (red box) is localized at the C-terminus of the protein.
- B. RxLR effectors are synthesized with a signal peptide for secretion and are assumed to follow the canonical ER/Golgi secretory pathway. Prior secretion the signal peptide is cleaved, and the mature effector is secreted from Haustoria in the extra-haustorial matrix (EHMx). From here the effector is translocated through the extra-haustorial membrane into plant cytosol with a mechanism that is not yet clarified. Adapted from [70].

Due to the great number of putative RxLR effectors revealed by genomic screens, a lot of work still needs to be done to define their activities and functions. Up to now most screens were based on the avirulent activity of a given putative effector, possibly leading to the activation of plant immunity and the HR. More recently different “-omics” approaches showed that the pathogen rather deploys an array of virulence activities that help suppressing plant immune responses to maximize the infection potential. For example, transcriptional profiling of *P. sojae* during infection of soybean showed that the expression of effectors is finely orchestrated over the different stages of infection. This work evidenced that early expressed effectors are predominantly able to suppress ETI and are followed by a wave of effectors that suppress (PAMP)-triggered immunity (PTI) [71]. In addition, the SNE1 effector from *P. infestans*, expressed during the early stages of infection, was shown to suppress host plant cell death, but also to counteract the activity of necrosis-inducing proteins released by the pathogen in later stages of the infection, thus providing a regulation for the transition from biotrophy to necrotrophy [72].

To sustain the association with the plant, pathogens have to suppress virtually any step of the immune response machinery. This can rely on the subcellular localization of effector activity in the host. Transient expression screens with effector genes from the oomycete *Hyaloperonospora*

arabidopsidis showed that RxLR effectors accumulate either in the nucleus, in the membranes or both in the nucleus and the cytoplasm [73]. In line with this finding, *in silico* analysis of effector localization predicted that few oomycete RxLR effectors may target chloroplasts or mitochondria, but that a good proportion may target the host's nucleus [74].

Indeed, some characterized RxLR effectors from *Phytophthora* species were shown to subvert host defenses by interfering with transcriptional and post-transcriptional regulation. For example, the *P. infestans* effector Pi03192 binds to a host transcription factor localized in the endoplasmic reticulum (ER), thus preventing its relocalisation to the nucleus [75]. Two effectors from *P. sojae* (PSR1 and PSR2 - Phytophthora suppressors of RNA silencing 1 and 2 respectively) were shown to bind to a host's RNA helicase involved in processing and accumulation of miRNA and siRNA, thus interfering with RNA silencing and leading to increased plant susceptibility [76].

Other effectors interfere with defense-related phytohormone signaling. The *P. infestans* effector Pi0431 interferes with the induction of jasmonic acid (JA)- and salicylic acid (SA)-responsive genes [77], and the *P. sojae* effector Pslsc1 triggers a decrease in the amount of available SA in the host cell [78]. The *P. parasitica* PSE1 is predominantly expressed during penetration of host roots, and modulates the local auxin content to favor infection, by altering the distribution of auxin efflux carriers [79]. Other oomycete effectors target PTI signaling pathways. For example, a group of effectors from *P. infestans* (called SFI, Suppressor of early Flg22-induced Immune response) act upstream or downstream of the MAPK signaling cascade, which is activated in response to PAMP perception, interfering with signal transduction events at the plasma membrane or suppressing defense gene upregulation, respectively [80].

1.2.2 The Endomembrane system as a target for RxLR effectors

Another important target for RxLR effectors is the endomembrane system of plant cells. In fact, this complex network of membranes, which includes the plasma membrane, membranes of the ER, the Golgi apparatus, vacuoles and endosomes, is essential for the life of a cell and the exchanges within this network are essential for the maintenance of cell homeostasis during development and immune responses.

When pre-existing barriers cannot prevent pathogen ingress, the plants respond to penetration by specifically rearranging the cytoskeleton, organelles, and compartments around a spatially confined area where the invasion occurs. One of the earliest events is a rearrangement of actin microfilaments at the penetration site, together with an aggregation of the ER and Golgi bodies that provide material for secretion, such as callose, phenolic compounds, phytoalexins and PR proteins, to block pathogen entry [81–83].

However, this dramatic reorganization can be targeted and rerouted by the pathogen to facilitate infection. For example, the formation of haustoria for feeding and trafficking of effectors requires important subcellular rearrangements of the host plasma membrane, which accommodates and envelops pathogen haustoria thus forming the so called extrahaustorial membrane (EHM). Formation of EHM is driven by biogenesis of new membranes and the relocalisation of resident proteins that are selectively excluded from this newly formed area [84,85]. These rearrangements seem to be partially due to apposition of host vesicles, which are redirected to the haustorial interface. The pathogen particularly redirects late endosomes, which are emerging as modulators of immune responses by balancing the degradation or recycling of PRRs [86].

Unsurprisingly, several oomycete RxLR effectors were shown to target different processes of the host endomembrane traffic. The well-studied effector AVR3a from *P. infestans* was initially identified as a cell death suppressor, but it was also shown to reduce internalization of the activated PPR-receptor FLS2 by binding DRP2, a plant GTPase involved in receptor-mediated endocytosis, thus perturbing PTI responses [87]. Effectors can also block plant exocytosis, such as *P. infestans* AVR1 that was shown to interact with Sec5. This protein is a component of the plant exocyst protein complex, which is required for tethering vesicles and their fusion with the plasma membrane. Binding of AVR1 to Sec5 thus disturbs an essential process in plant immunity [88]. Finally, RxLR effectors were also shown to target processes involving intracellular trafficking of vesicles, in particular autophagy. An example is the PexRD54 effector from *P. infestans*, which interferes with

complex formation between ATG8, a ubiquitin-like protein required for the formation of autophagosomal membranes, and Joka2, an autophagic cargo receptor. This interference leads to the pathogen-driven stimulation of autophagosome formation, which is supposed to favor elimination of plant defense-related compounds [89].

Although the examples for oomycete effectors are limited, research in recent years revealed an important role of endosomes and autophagy-related membrane trafficking in plant-pathogen interactions. The next chapter will focus on the process of autophagy and its role in plant immunity, pointing out how pathogens can manipulate this plant function for successful infection.

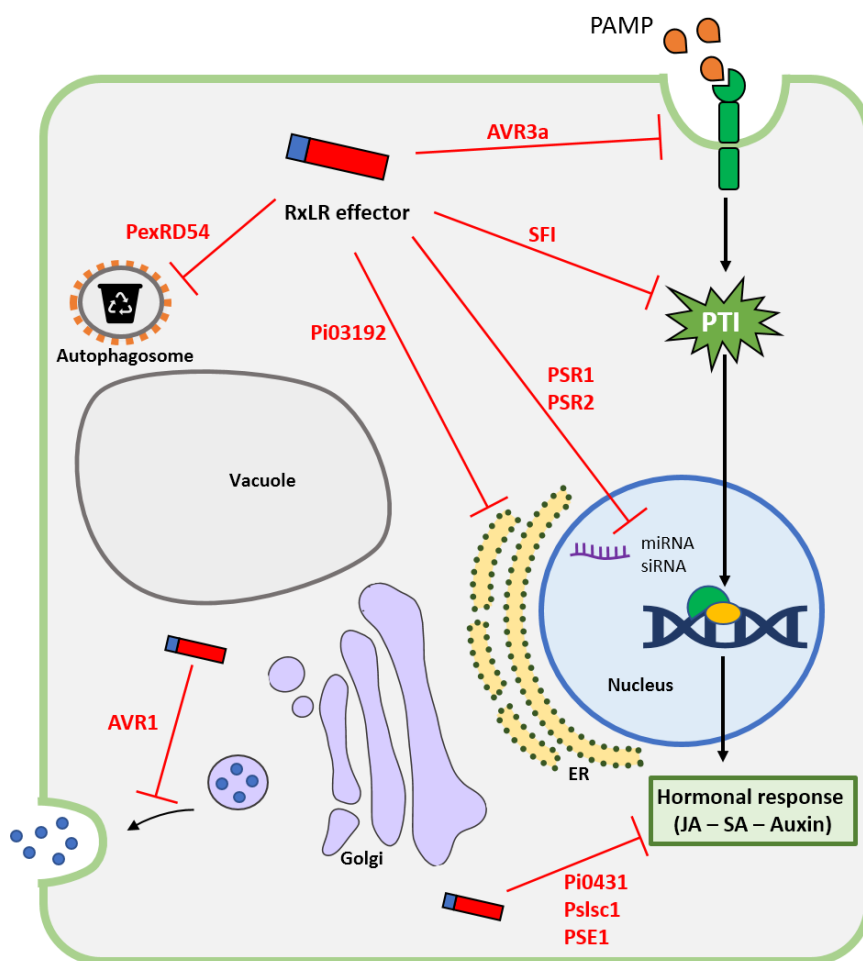


Figure 1.4: Overview of RxLR effectors targets in plant cells.

Effector proteins are known to subvert and manipulate plant defenses: among the identified targets are several steps of the PTI responses, starting from receptor internalization (AVR3a [87]) and MAPK signaling cascade (SFI [80]). Other effectors have been shown to deregulate defenses at a transcriptional level by preventing the relocalisation of transcription factors from the ER to the nucleus (Pi03193 [75]) or to interfere with miRNA and siRNA-dependent RNA silencing (PSR1 and PSR2 [76]). Other targets are represented by defense hormones: effectors have been shown to deregulate their downstream signaling (Pi0431 [90]), their availability (Pslsc1 [78]) or their redistribution (PSE1 [79]). Finally, effectors have been shown to target the endomembrane system and affect plant exocytosis (AVR1 [88]) and plant autophagic machinery (PexRD54 [89]) to prevent release of defense-related compound or to favor their elimination respectively.

Chapter 2: Autophagy

General Introduction

Autophagy, meaning “self-eating” (from ancient Greek “auto-“, self and “-phagía” eating), describes a complex and highly conserved biological process, which allows eukaryotic cells to degrade and recycle material and to dispose of damaged organelles or toxic compounds. The term was coined by Christian de Duve to describe a mode of protein degradation involving their delivery to lysosomes, which was observed mainly by transmission electron microscopy of mammalian cells [91]. Indeed, during canonical autophagy, portions of the cytoplasm are sequestered within a double-membraned vesicle, which fuses with lysosomes or vacuoles where the engulfed material is degraded to simple molecules such as amino acids.

Since the discovery of autophagy, research focusses on understanding the physiological role and regulation of the process. Initially, progress was hindered by the lack of specific markers allowing to follow the evolution of autophagic flux, both at a biochemical and morphological level [92]. A huge advance in autophagy research was accomplished when the Nobel Prize Yoshinori Ohsumi first described genes regulating this process in *Saccharomyces cerevisiae*. The use of a simple model system led to the first morphological description of autophagy [93,94]. Few years later, the generation of autophagy-defective mutants allowed the definition of genes composing the core machinery of autophagy [95,96]. At present, we know that autophagy is executed through the coordinated action of more than 30 core Autophagy-related (ATG) proteins, together with other important players such as the members of the Vacuolar Protein Sorting (VPS) protein family [97].

Autophagy likely evolved first in unicellular organisms as a survival mechanism to overcome the scarcity of nutrients, and as a basal function for quality control and clearance of long-lived proteins and organelles. In fact, by digesting portions of the cytoplasm, cells can increase the likelihood of survival in hostile conditions by obtaining nutrients and metabolic precursors when they are not available from the environment. Moreover, autophagy is important to remove superfluous and damaged organelles, pathogens or toxic material, such as misfolded proteins that could endanger cell survival.

After the early works on yeast, autophagy has been identified and described in all higher eukaryotes, pointing out how this process is important and conserved across the tree of life. In multicellular

organisms, autophagy is essential during embryonic development and its activity appears to determine lifespan and tissue homeostasis [98]. Work on human cells evidenced the role of autophagy in cell survival and metabolism, and dysfunction of the process leads to pathologic conditions such as neurodegenerative diseases and cancer [99]. In plants, too, autophagy is involved in developmental processes, and in events such as the regulation of programmed cell death (PCD) during immune responses [100].

2.1 A focus on macroautophagy

Due to its fundamental role in cell homeostasis, autophagy seems to be constitutively activated in cells at a basal level. Nonetheless, it can be transiently induced during conditions that require rapid nutrient supply or extensive cell remodeling, such as starvation, abiotic and biotic stress, or switches in physiological programs (development, senescence, cell death) [98].

Autophagy (synonymous for “macroautophagy”) is a coordinated process, in which cellular components are non-selectively engulfed in a double membrane vesicle and delivered to the lytic compartment for degradation. This contrasts to “microautophagy”, which describes the selective direct engulfment of cytoplasm into lysosomes or vacuoles. Under particular conditions, macroautophagy specifically removes whole organelles, such as mitochondria and peroxisomes, regions of the Golgi and the ER, and even plant chloroplasts [101]. Specific proteins might also be delivered to the lytic compartment for degradation via the cytosol-to-vacuole-targeting or CVT in yeast and by chaperone-mediated autophagy in higher eukaryotes [102]. Finally, specific cargoes can be bound by specific adaptor proteins called autophagy receptors and degraded by the macroautophagic machinery via the so-called “Selective autophagy” [103].

During stress responses, autophagy can also mediate programmed cell death. In plants, autophagic components are involved in developmental cell death that is required for the formation of xylem [104]. The role of autophagic cell death in developmental morphogenesis was also described in *Drosophila melanogaster* and *Caenorhabditis elegans* [105]. Other work evidenced a strong interplay between autophagy and apoptosis since some autophagic components are also hubs for the regulation of caspase-dependent or -independent apoptosis, and of non-apoptotic cell death [106].

2.1.1 The autophagic machinery in yeast

As mentioned before, the earliest studies on autophagy in the 1960s were mainly based on Transmission Electron Microscopy, which allowed the morphological description of events leading to autophagic degradation. Several independent screens of yeast mutants allowed then to describe the molecular actors of autophagy and the identification of 31 *ATG* genes (autophagy-related genes) that encode the essential machinery of the process [97,107]. Functional analyses of these genes defined five protein groups, which act in a hierarchical way. These protein groups form the ATG1 complex, the Phosphatidylinositol 3-kinase complex, the ATG9 complex, and two conjugation systems involving ATG12 and ATG8 as key players (**Figure 2.1**).

The following paragraphs describe in detail the molecular autophagic machinery, according to the description for *S. cerevisiae*.

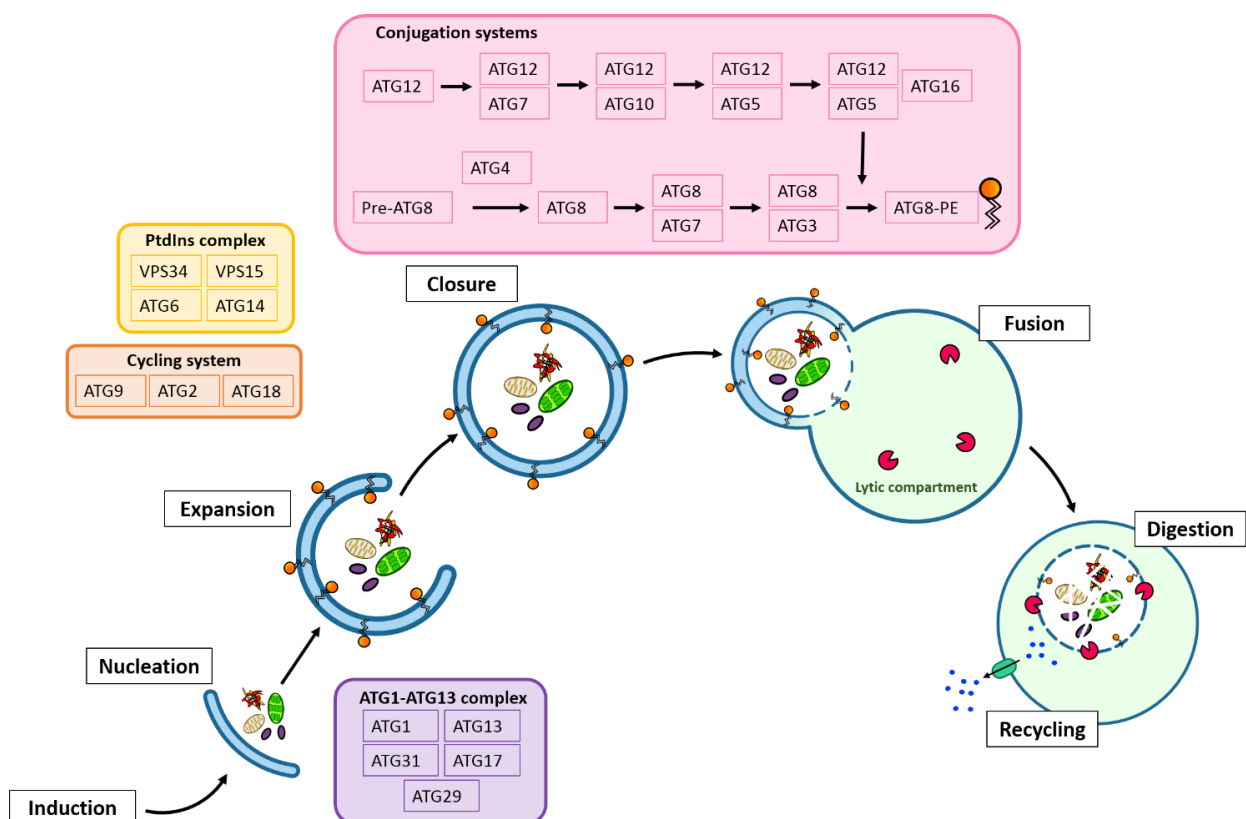


Figure 2.1: Core macroautophagy machinery in *Saccharomyces cerevisiae*.

Following autophagy induction, a double-membrane vesicle begins to nucleate and to expand, randomly enclosing cytoplasmic material which can include organelles and aggregated proteins. The formed vesicle then fuses with the cell's lytic compartment where hydrolases drive the digestion of the enclosed cargo. This process releases amino acids and lipids that are recycled back to the cytoplasm by specific transporters. Colored boxes present the core functional groups of proteins that participate to autophagosome formation: the ATG1-ATG13 complex, The PtdIns complex, the ATG9 cycling system and the two conjugation systems for ATG12 and ATG8. Adapted from [108].

Initiation of autophagy

Autophagy is tightly regulated by the integration of signals coming from the environment as well with signaling pathways regulating cell cycle, metabolism, and programmed cell death. Stimuli coming from the different pathways often converge in a complex including the serine/threonine protein kinase TOR1 (Target Of Rapamycin), which is considered as one of the master regulators of autophagy. As the name of the protein suggests, TOR1 can be inhibited by chemicals such as the bacterial metabolite Rapamycin, isolated in 1965 in Rapa Nui from a soil sample. In *S. cerevisiae* two isoforms of this protein intervene in the complex: TORC1 integrates extra- and intra-cellular signals coming from nutrient levels, growth factors, and the energy balance, whereas TORC2 is mainly involved in cytoskeleton polarization during cell growth [109]. Under normal conditions, TORC1 phosphorylates several substrates, including the initiation complex of autophagy thus determining a negative regulation of the process. Under unfavorable conditions, TORC1 activity is inhibited thus determining a stop of the cell cycle in G0, and the release of autophagy [110]. In addition to the inhibition of TORC1, autophagy can be activated by alternative signaling pathways such as those involving the cAMP-dependent protein kinase (PKA) pathway [111], or by soluble and membrane-associated receptors to induce the selective degradation of misfolded proteins and organelles [112,113].

ATG1-ATG13 complex and the pre-autophagosomal structure

In yeast, the initiation of autophagosome formation is controlled by a multimeric complex composed of the 5 main proteins, ATG1, ATG13, ATG17, ATG29 and ATG31, which may be supported by specific regulators for targeted degradation of cargos such as ATG11 [114].

The protein ATG1, a serine threonine kinase, and its regulator ATG13, interact constitutively under nutrient-rich and -deprived conditions via a specific region called the FV-motif [115]. Under nutrient-rich conditions, ATG13 is hyperphosphorylated by multiple kinases including the TORC1 complex [116]. These phosphorylations cause conformational changes that prevent the activation of the ATG1 kinase activity, and the formation of the multimeric complex mentioned above. Upon starvation, dephosphorylation of both ATG1 and ATG13 leads to a stabilization of ATG1, thus enhancing its kinase activity, promoting autophosphorylation, and allowing the interaction with ATG29, ATG31 and ATG17, the latter being specifically recruited in response to starvation [117,118]. The formation of this multimeric complex marks the beginning of nucleation of the Phagophore

Assembly Site (PAS). In yeast, this site has been identified as a perivacuolar region [119] where the core machinery proteins will assemble and function either as scaffold, or as regulators for the nucleation of the phagophore, a double membrane-enveloped vesicle that will eventually mature into an autophagosome [120].

The Phosphatidyl-Inositol 3-kinase (PtdIns3K) Complex

Biogenesis and maturation of the phagophore relies on membrane trafficking converging at the PAS. Membranes involved in this traffic have a unique composition, but their origin remains elusive. However, both the ER and the Golgi were identified as contributors to the nucleation of the phagophore [121]. A characteristic of phagophore membranes is the over-representation of Phosphatidyl-Inositide (PtdIns) and Phosphatidyl-Inositide-3-phosphate (PtdIns3P) [122]. The enrichment of these lipids is enabled by the PtdIns3K complex. The complex is associated to membranes and includes the PtdIns3K VPS34, the Ser/Thr kinase VPS15, and VPS30 (aliases: ATG6, Beclin1), which promotes kinase activity. These three proteins participate in both vacuolar protein sorting (regulating intracellular protein trafficking) and autophagy. To accomplish autophagy, the complex requires an additional factor, ATG14, which supports localization at the PAS. The enzymatic activity of the complex is the phosphorylation of PtdIns, leading to accumulation of PtdIns3P, which is essential for the subsequent steps of phagophore elongation and maturation [122,123].

The Cycling system ATG9 and the ATG2-ATG18 complex

The presence of PtdIns3P at the PAS triggers the recruitment of other protein complexes. One of them is the ATG2-ATG18 complex, composed of ATG2, which associates with the lipid at the PAS, and of ATG18 which in turn recruits and regulates the recycling of another actor in phagophore nucleation, ATG9 [124]. ATG9 is a six-transmembrane domain protein that, unlike other ATG proteins, localizes both to a peripheral reservoir of vesicles located at the PAS and to the close proximity of mitochondria [125]. ATG9 cycles between the two pools, and its transport toward the PAS is supported by ATG11, ATG13 and ATG27. At the PAS, ATG9 self-interacts and tethers upcoming vesicles, thus contributing to membrane supply for the forming phagophore, and facilitating the recruitment of downstream complexes. The regulatory activity of ATG18 together with ATG1-ATG13 and the PtdIns3K complexes relieve the retention of ATG9 at the PAS, thus allowing its shuttling back to the peripheral sites [126].

Vesicle expansion: the UBL complexes ATG12 and ATG8

The interaction of the complexes described above eventually promotes the recruitment of two ubiquitin-like (UBL) conjugation systems [124], which include an important fraction of the ATG protein core machinery. The two complexes are named after the key players of the reaction, ATG12 and ATG8, two proteins whose crystal structure revealed the presence of a conserved ubiquitin fold [127,128]. During autophagy, both proteins undergo a covalent modification, similar to the process of ubiquitin activation, which is operated by modifying enzymes analogous to the E1-E2-E3 enzymes involved in ubiquitination.

ATG12 was the first UBL-like protein that was identified as an essential component of the autophagic machinery [129]. This protein is first activated by an E1-like enzyme, ATG7, by the formation of a thioester bond between a C-terminal glycine of ATG12 and Cys507 of ATG7. Then ATG12 is transferred to ATG10, which acts as an E2-enzyme and operates the conjugation of ATG12 to its target, ATG5. The ATG12-ATG5 complex can interact with ATG16, a small protein that promotes the formation of a multimeric complex. Homo-oligomerization of ATG16 and binding to the lipid PtdIns localizes the ATG12-ATG5-ATG16 complex to the phagophore membrane [130,131], which in turn promotes the activity of the second UBL- complex, the ATG8 conjugation system [119].

ATG8 is synthesized as a precursor, which is immediately cleaved at its C-terminus by the cysteine protease ATG4 [132]. This cleavage exposes a Glycine residue, which becomes the target of the E1-like enzyme ATG7. Similarly to what happens for ATG12, ATG7 forms a thioester bond with ATG8 before ATG8 is transferred to the E2 enzyme ATG3. This transfer leads to the formation of an amide bond between ATG8 and the lipid Phosphatidyl-Ethanolamine (PE) [132]. The ATG8-PE conjugate then integrates on both sides of the double layer of the elongating vesicle, where it is essential for the fusion of membranes converging at the crescent phagophore. It was shown that the asymmetric distribution of ATG8-PE between the inner and outer face of the phagophore determines the curvature and the closure of the autophagic vesicle, thus defining mean radius and size of the autophagosome [133,134].

ATG8 has additional functions as a recruiter and selector of autophagic cargoes by virtue of its interaction with cargo receptor proteins. It tethers selective cargoes bridged by the receptor ATG19 and leads them to specific degradation. The interaction of proteins with ATG8 is mainly driven by the conserved aminoacidic motif W/YxxL/I/V, called AIM (ATG8 interacting motif) [135]. Importantly, the conjugation of ATG8 with PE is reversible, and the protein can be released from the

phagophore by a second cleavage operated by ATG4. This restores the pool of non-lipidated cytosolic ATG8 ensuring a reservoir for the formation of new autophagosomes when needed [136].

Autophagosome maturation and fusion with the lytic compartment

The elongated, curved phagophore encloses the cargo and eventually matures into the autophagosome, which is bordered by a doubled membrane bilayer. The completion and closure of the double membrane strongly relies on the action of ATG8. Recent work shows that ATG1 phosphorylates ATG4 and inhibits its cysteine protease activity to protect the pool of available ATG8-PE from cleavage until completion of phagophore closure [137]. When the autophagosome is established, release of the ATG1-ATG13 complex from the membranes allows ATG4 to operate the cleavage of the PE anchor from ATG8, and thus to initiate the subsequent steps of maturation. The hydrolase Ymr1 is a phosphoinositide phosphatase that removes phosphate from the PtdIns of the autophagosome membrane. This event disrupts PtdIns3P-dependent signaling, which is essential for the recruitment of several ATG proteins to the forming phagophore, thus causing the release of the autophagic protein complexes from the membrane. Several proteins then regulate the fusion of the autophagosome with the lytic compartment (lysosome or vacuole). In yeast, this fusion is mediated, among others, by specific members of the HOPS tethering complex, the SNARE complex and the RAB GTPase YPT7 [138]. After the fusion, several hydrolases such as the proteinases A, Pep4, and B, Prb1, and the lipase ATG15 participate in the degradation of the cargo, which requires acidification of the compartment [139]. Eventually, molecules released by the lytic activities are exported from the vacuole back to the cytoplasm by means of aminoacid effluxers such as ATG22, and the vacuolar permeases Avt3 and Avt4 [140].

2.2 Autophagy in plants

The morphology of plant autophagy was first described in the late 1970s using electron microscopy, leading to a first description of autophagic vesicles and their role in vacuole biogenesis [141]. In the following decades, genome sequencing programs allowed to confirm for photosynthetic organisms the conservation of the autophagic machinery in higher eukaryotes. Most of the genes encoding the yeast autophagic core machinery have a corresponding ortholog in photosynthetic organisms that range from algae to monocots and dicots [142,143]. Even though plant autophagy gene sequences rather diverge from their yeast orthologs, the residues that determine protein function are conserved. Important advances in the characterization of ATG proteins in plants were made possible by the generation of loss-of-function mutants, in particular in the model plant *Arabidopsis thaliana* [141]. Since, it appears confirmed that the general mechanism and the functional complexes of autophagy are conserved in plants [144,145]. However, it is important to note that genes encoding some members of the ATG core family including *ATG4*, *ATG8* and *ATG12* diversified in plants, and are encoded by small gene families. Individual members of these families might exhibit specific expression patterns, and the encoded proteins might diverge in subcellular localization and function [143,146].

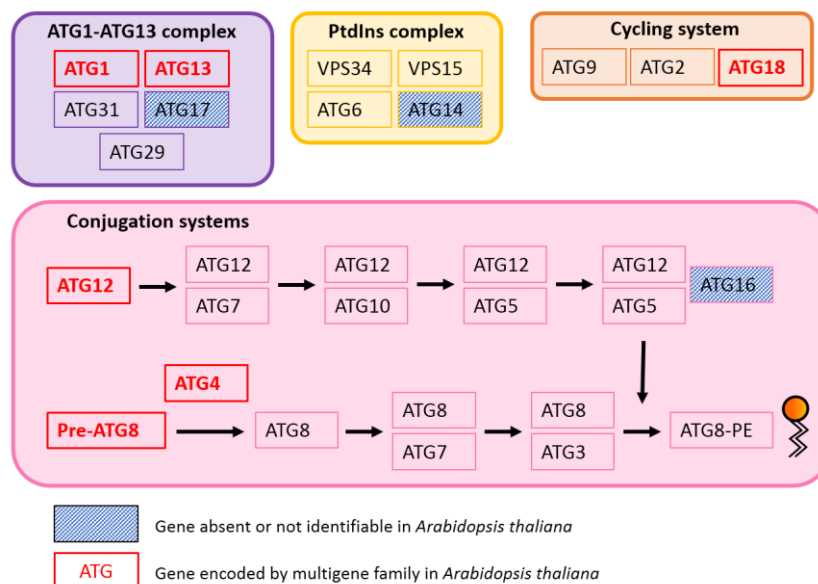


Figure 2.2: Core autophagy machinery in *Arabidopsis thaliana* compared to yeast.

The four main complexes constituting the core autophagy machinery are conserved in plants. The figure illustrates the core machinery of *Arabidopsis thaliana*: pattern-filled boxes stand for genes that are missing or that are still not identified whereas red boxes indicate genes that underwent expansion in plant and are now encoded by gene families.

Under nutrient-rich growth conditions, plants, which have mutations in genes, or are down-regulated for genes encoding proteins of the autophagic core machinery such as those involved in induction (ATG13 [147]), nucleation (ATG9 [148], ATG6 [149], ATG18 [150]), conjugation (ATG7 [151] ATG4a4b [152] ATG5 [153], ATG10 [154]), and fusion (VTI1 - [155]) achieve a normal life cycle and produce viable seeds (except plants lacking ATG6 [156]), but display accelerated leaf senescence and reduced fertility. However, when those plants grow under challenging conditions different phenotypes emerge. The plants exhibit senescence markers prematurely, and react hypersensitive to stress such as starvation with an overall reduced growth and compromised survival ([157] for review).

Autophagy is essential for several developmental processes in plants. For example, autophagy participates in developmental cell death programs that are required for the biogenesis of the vacuole [158], and, in *Arabidopsis thaliana*, for the differentiation of tracheary elements [104] and the germination of pollen [156].

Another aspect emerging from the studies on autophagy-defective mutants is the role of autophagy in plant nutrient recycling. As for other organisms, basal autophagy in plant cells contributes to control the availability of carbon and nitrogen, among others by means of upstream signaling converging in the regulator TORC1. However, the role of autophagy for nutrient remobilization in plants becomes evident during nutrient deprivation, and during certain developmental stages such as seed germination and senescence. For example, autophagy was shown to be active during the night and contributes to the degradation of starch, probably assuring its breakdown and subsequent carbon availability [159]. Moreover, autophagy is involved in nitrogen turnover, as ATG mutants are less efficient in the remobilization of nitrogen from senescing leaves to seeds [160].

In addition, plant autophagy was shown to be essential for responses to various abiotic stress such as oxidative stress, salt, drought and heat [161–163]. Related to this, several forms of selective autophagy in plants were reported that aim at disposing of damaged organelles and protein aggregates, whose formation increases under certain conditions. Examples for this phenomenon are the degradation of peroxisomes during seed germination [164] and the removal of aggregated peroxisomes following oxidative stress [165], the partial or complete degradation of chloroplasts in senescing leaves as well as under carbon starvation [166,167]. Autophagy was also shown to be a sensor for ER-stress and to provide a pathway for the degradation of aggregated and misfolded proteins [168,169]. The study of the relation between the ER and autophagy also evidenced that

plant autophagy contributes to the intracellular trafficking of proteins and membranes from the ER to the autophagosome and the vacuole [158,170,171]. Furthermore, there is increasing evidence of a crosstalk between autophagy and other endocytic pathways ([172,173] for review).

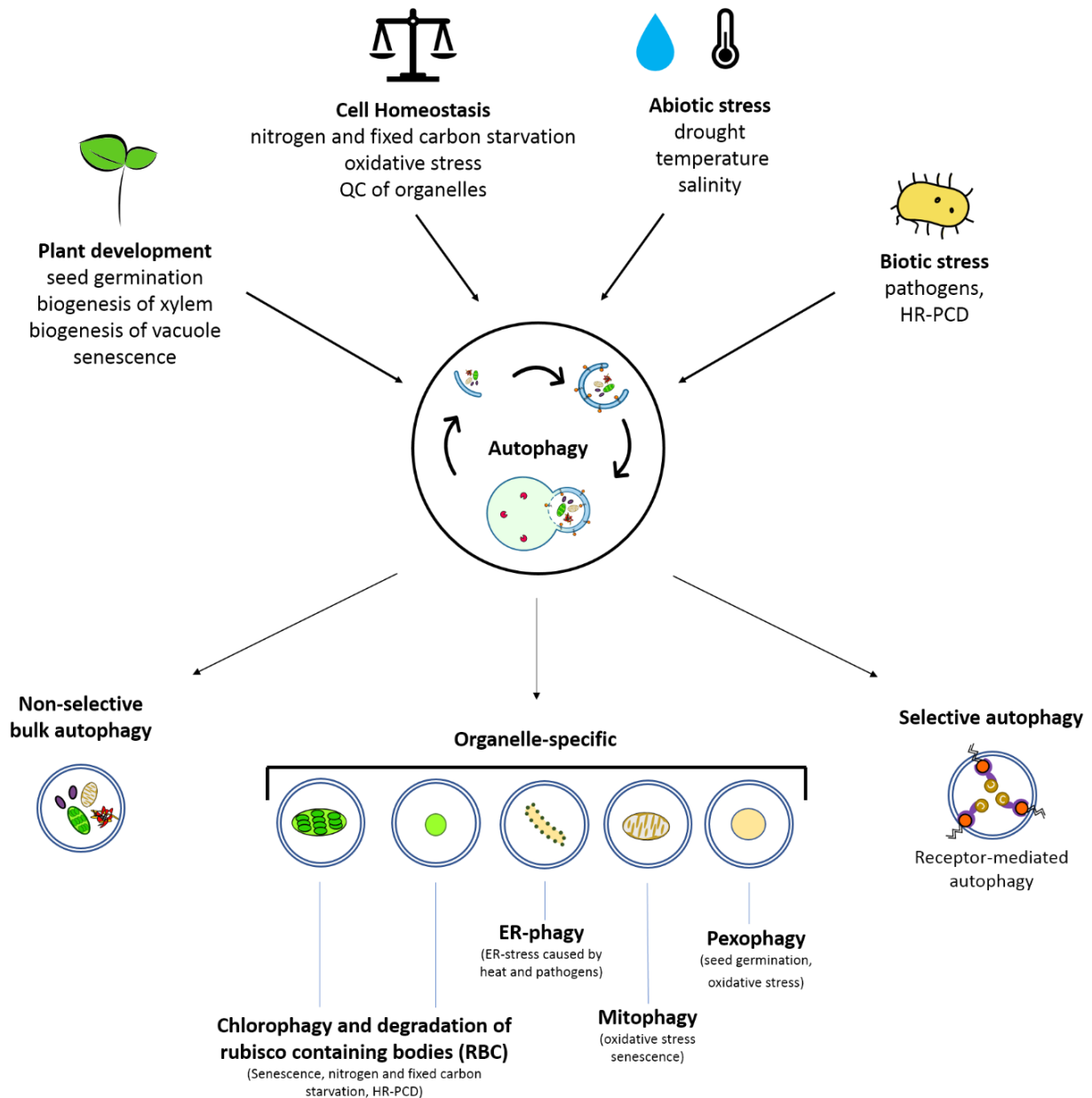


Figure 2.3: Autophagy in plants.

Similarly to what reported in yeasts and mammals, autophagy is induced in plants by several stimuli ranging from developmental processes, internal regulation of cell homeostasis but also environmental cues such as abiotic and biotic stresses (top of the figure). Some of those stimuli are unique to plants, especially those related to plant development and the response to pathogens. The autophagic digestion in plants happens with the fusion of an autophagic vesicle with the plant lytic compartment: the central vacuole. Those autophagic vesicles can engulf material either in a non-selective manner or target specific cell compartments (organelles specific) and cargoes (selective autophagy mediated by cargo receptors). Among the different modalities, the degradation of organelles often responds to specific stimuli (bottom of the figure): the degradation of chloroplasts and rubisco containing bodies is unique to green organisms and is triggered by stimuli such as senescence and HR-PCD that unique to plants [174].

2.2.1 Autophagy in plant-pathogen interactions

As discussed in the previous chapter, autophagy contributes to endocytic trafficking and appears to be significantly involved in the outcome of biotic interactions. For example, autophagic components belonging to the PI3K-complex were shown to be essential for the mutualistic interaction between common bean (*Phaseolus vulgaris*) and both rhizobial bacteria and mycorrhizal fungi, since the impairment of this complex strongly compromised the formation of root nodules and of arbuscular structures that are necessary for symbiosis [175].

Beside this example, most of the research on biotic interaction focused on the role of autophagy in plant defense and the interaction with pathogens. Over the years, autophagy has been suggested to play both a “pro-survival” or a “pro-death” role in plant immunity-related cell death, depending on at least two main factors: the lifestyle of the pathogen and the age of the plant.

Concerning the first aspect, findings involving *ATG* mutants revealed that autophagy has a double-edged role in pathogen-triggered PCD. In fact, when the plant is faced to a necrotrophic pathogen such as *Alternaria brassicicola* or *Botrytis cinerea*, autophagy acts as a pro-survival mechanism, as it contributes to removing both toxins released by the pathogen, and damaged and potentially toxic cellular constituents generated during the response to infection. Indeed, the impairment of the autophagic machinery results in extensive pathogen growth and pathogen-induced plant cell death [176,177].

On the other hand, autophagy acts both as a regulator and executor of PCD during the HR, when the plant is challenged with (hemi)biotrophic pathogens, thus contributing as a pro-death mechanism to resistance. *Nicotiana benthamiana* infected with tobacco mosaic virus displays an activation of autophagy in both infected and uninfected tissues. As a response to the virus, the plant develops an HR-PCR, which localizes to the site of infection and limits the virus replication of the virus. In *ATG6*-, *ATG4*-, and *ATG7*-deficient plants, virus replication is no longer restricted [178]. Similarly, the immunity-associated cell death response of *Arabidopsis thaliana* to *Pseudomonas syringae* strain DC3000 relies on the activation of autophagy [179]. Cells undergoing HR-PCR were reported to accumulate autophagosome-like structures during the early stages of infection [180]. It is important to note that in both systems (*N. benthamiana* - TMV and *A. thaliana* - *P. syringae*) autophagy might have a pro-survival role, since it prevents the diffusion of the HR-PCR to uninfected areas, as demonstrated by *ATG* mutant plants displaying unrestricted PCD [149,178,181]. Other

reports present contrasting results, indicating that autophagy deficiency enhances the resistance to *P. syringae* and powdery mildew rather than decreasing it [180,182].

This apparent contradiction may be explained by the second factor determining the role of autophagy in immunity: plant age. As mentioned, the phytohormone SA plays an important role in disease resistance responses to biotrophic pathogens, and it has been shown to promote developmental senescence [183]. *A. thaliana* ATG mutants display increased levels of SA, which lead to premature senescence, hypersensitivity to oxidative stress, and increased susceptibility to necrotrophic pathogens (increased SA levels antagonize the hormone JA, which mediates immunity to necrotrophs) [176,182,184]. The early senescence phenotype and premature cell death in ATG mutants can be partially reverted by impairing SA signaling, indicating that these phenotypes are mainly due to SA accumulation, and only an indirect effect of autophagy deficiencies. However, the findings show that autophagy is induced by SA accumulation, which in turn is regulated by autophagy through negative feedback loop [141]. Consequently, differences in the accumulation of SA, which are also dependent on plant age and growth conditions, might explain the contrasting findings of pro-survival and pro-death roles of autophagy during the interaction with (hemi)biotrophic pathogens.

Considering the dual role of autophagy in cell survival and cell death, it is not surprising that microbial pathogens developed the ability to either inhibit or stimulate plant autophagy to their own advantage.

For example, the necrotrophic pathogen *Sclerotinia sclerotiorum* secretes the phytotoxin oxalic acid (OA) to promote tissue invasion [185]. By using combinations of OA-deficient strains and *Arabidopsis* plants defective in autophagy, the authors show that pathogen uses oxalic acid to suppress autophagy and autophagy-dependent HR-PCD, and to promote pathogen-induced necrotic cell death.

Other pathogens instead use plant autophagy for the success of infection. For example, the *Ralstonia solanacearum* effector, AWR5, was shown to be an inhibitor of TOR in *A. thaliana* and thus an activator of autophagy. The resulting activity mimics the effects of starvation in infected tissues, possibly determining a remodeling of the host metabolism favoring the development of the pathogen [186]. Recent work showed that the effector HopM1 from *P. syringae* stimulates autophagy for selective removal of proteasomes, which are involved in immune responses and the degradation of pathogen-derived compounds. Interestingly, plants counteract this activity by

activating simultaneously a distinct selective autophagy pathway mediated by the cargo receptor NBR1, which targets pathogen immunity suppressors [187].

NBR1-mediated autophagy was also shown to be the target of other pathogens. PexRD54, an effector of the RxLR family from *Phytophthora infestans*, contains AIMs that promote its binding with high affinity to the potato ATG8CL protein. This binding prevents the interaction of ATG8CL with JOKA2, the potato homolog of NBR1, which is involved in plant resistance to *P. infestans* infections. PexRD54 also appears to stimulate autophagy and to redirect autophagosomes towards the EHM, redistributing membrane for EHM biogenesis and possibly nutrients to favor pathogen growth [89,188]. A different study shows that NBR1 can target proteins of the Cauliflower mosaic virus capsid and promote their degradation via autophagy. However, the virus protects itself from degradation by forming inclusion bodies and maintains host autophagy in an active state to promote survival of infected cells [189].

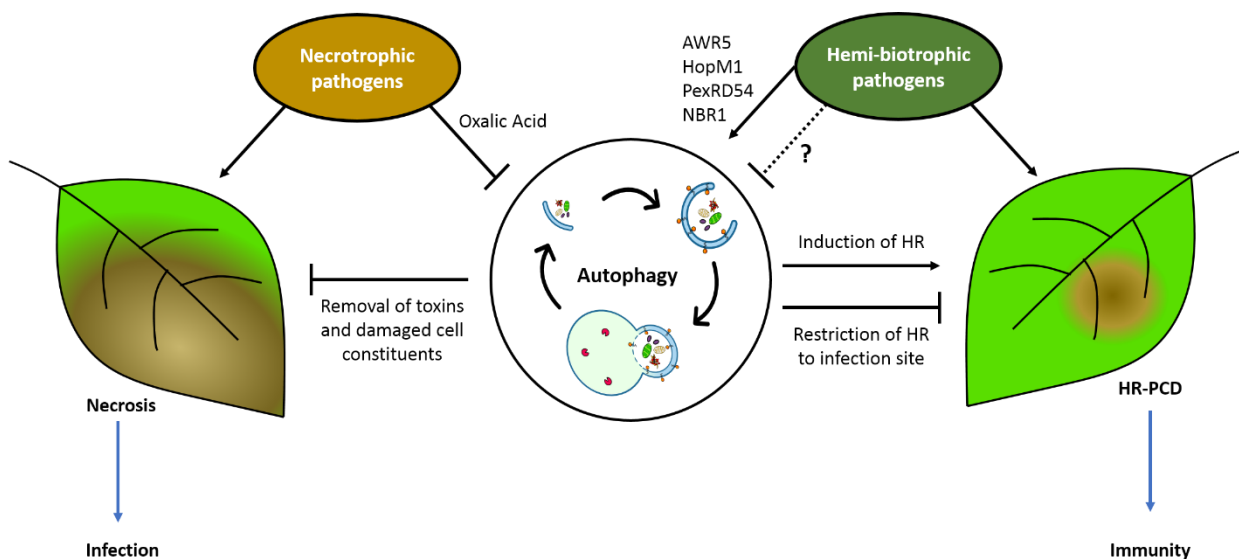


Figure 2.4: Role of autophagy in plant-pathogen interaction.

Autophagy has a pivotal role in the outcome of interactions with pathogens. It has been shown that it can either promote or restrict different forms of cell death and this action appears to be dependent on the lifestyle of the pathogen. Autophagy was shown to suppress the necrosis induced by necrotrophic pathogens (left side) via the removal of pathogenic toxins and damaged cell constituents [176,177]. In turn some necrotrophic pathogens such as *S. sclerotium* have been reported to inhibit autophagy with Oxalic Acid to promote infection [185]. On the other hand autophagy promotes HR-PCD in response to (hemi-)biotrophic pathogens and, in parallel to prevent the diffusion of this response in non-infected tissues [178,180]. Various biotrophic pathogens have been reported to hijack or promote autophagy to escape this response [186–189] however the employment of inhibitory strategies remains to be discovered. Adapted from [100].

Objectives of the PhD project

As described in the first chapter, the plant pathogen *Phytophthora parasitica* is gaining importance from an economical and a scientific point of view. In fact, the oomycete is establishing as a model organism to understand the mechanisms regulating plant-pathogen interactions and the molecular exchanges between them.

The hosting laboratory, where this thesis work has been carried out, is interested in deciphering those mechanisms on different levels. A previous project led to the production of two cDNA libraries from *P. parasitica* infecting onion epidermal layers and tomato plants in early [1] and late [2] stages of infection. This work has allowed to identify several ESTs representing transcripts from genes encoding potential effectors proteins, in particular those from the RxLR family. One of the genes encodes a protein of 195 amino acids belonging to the RxLR family. Since the sequence did not correspond to any known Avr protein, it was denominated avirulence-homologue 195 or Avh195. Interestingly, the bioinformatic analysis of the effector revealed the presence of five Atg8 interacting motifs in the effector domain of the protein, which could indicate that PpAvh195 is potential perturbator of autophagy.

Due to the importance of both RxLR proteins and autophagy in the infectious process, this PhD project has focused on the **molecular and functional characterization of the *Phytophthora parasitica* effector Avh195 and on the elucidation of its role in autophagy perturbation.**

In **Chapter 3** I will present the results obtained during my PhD thesis, which focused on the following objectives:

- To infer the general function of Avh195 from its sequence and its pattern of expression during infection.
- To validate the interaction between Avh195 and Atg8.
- To characterize the molecular mode of action of Avh195 and its effect on plant autophagy machinery.
- To characterize the role of Avh195 during Plant-pathogen interaction.
- To validate the selectivity of Avh195 action on a non-photosynthetic model.

Chapter 3: Results

This chapter is dedicated to the presentation of the results obtained during my PhD thesis: it is articulated in five main sections, each of which will deal with the objectives of the work presented in the previous chapter.

3.1 Molecular characterization of Avh195

3.2 Avh195 interacts with ATG8

3.3 Characterization of Avh195 in *Chlamydomonas reinhardtii*

3.4 Role of Avh195 during the host-pathogen interaction

3.5 Trans-kingdom activity of Avh195

3.1 Molecular characterization of Avh195

The interaction between pathogenic oomycetes and host plants is a process that strongly relies on fine-tuned exchanges between the two partners. The study of the molecular mediators of this communication is improving and helping to shed a light on the mechanism by which the pathogen suppresses the host defenses and hijacks the host machinery to promote infection. A part of this area of research focuses on effector proteins: soluble mediators secreted by the oomycete that target various functions in plant cells in order to divert host machinery.

On this line, the present work has based on a previous project aimed to identify the determinants of pathogenicity via the generation of two EST libraries obtained from *P. parasitica* infected plant tissues [38,43]. In the arsenal of molecules deployed by the oomycete during the penetration and infection of the host tissue, those works allowed the identification of cDNA belonging to effector proteins, thus potentially implicated in the outcome of infection. One of them was found to encode a putative effector protein, designated as **PpAvh195** (Alias **Avh195**). The sequence of this gene corresponds to a transcript of 588 pb, which is predicted to encode a 195-amino acid protein with the typical structure of an RxLR effector.

BLASTp search for homologs of *Avh195* in other organisms revealed that this gene is unique to *P. parasitica* species and is not present in other oomycetes, except the 202 amino acid related sequence PITG_04099 in the potato late blight pathogen *P. infestans*, which presents 66.7% identity to PpAvh195 **Figure 3.1**.

```

. . . .10 . . . .20 . . . .30 . . . .40 . . . .50 . . . .60
PpAvh195  MRLPYVLLLAVCIIIASCNALSAYEQEAVVAQNAQRWSSVTHSVAAEETGDTSGRLLRSD: 60
PITG_04099 MRLPYVLLLAVSIATIEFCTAAAS.EQEAAVTLQAKRWGSLHPATAPGYRDTSGRLLRSD: 59

. . . .70 . . . .80 . . . .90 . . . 100 . . . 110 . . . 120
PpAvh195  .SIPVTD.....AERATPGMTKLTETIKKWISARSKLSNKKLWVWNYQKLGKQKLSDDL:114
PITG_04099 DSIPIVDDDDVNTTEERGLASFKNEMIKKGSASAKASNKMLWLKYQKLLGQKLSDDL:119

. . . 130 . . . 140 . . . 150 . . . 160 . . . 170 . . . 180
PpAvh195  ITGWLKNGKSYDDLFRWIRLDKSPRQAANKLLNHGTTTNDLYKVLRRKRNMNLETIRP:174
PITG_04099 ITGWLKNGKSAIDLFRWIRLSKSPRQAATNLLNHGTTTANDLYKVLRRKRNMNLETIRP:179

. . . 190 . . . 200 .
PpAvh195  WKEVGLTEYQLRAARHAAS..AL:195
PITG_04099 WIKVGLTEELQLRAARAKAINSVL:202

```

Figure 3.1: Amino acid sequence alignment of Avh195 and PITG_04099.

The amino acid sequences were aligned using ClustalO and the alignment was edited using Matchboxshade for Macintosh. Shading indicates blocks of identical (black) or similar (gray) amino acids.

3.1.1 *Avh195* is expressed during biotrophy of *P. parasitica*

To support the hypothesis that the encoded protein may act as a pathogen-specific virulence factor, we investigated the presence of *Avh195* EST in libraries generated from additional developmental stages of *P. parasitica*. This analysis showed that the gene is neither expressed in germinated cysts, zoospores, nor during vegetative growth [39,41,42] suggesting that it is specifically expressed during infection.

To validate this hypothesis, we investigated the expression pattern of *Avh195* using RT-qPCR in roots of *Arabidopsis* plantlets at 3, 10, 30 and 48 hours post inoculation (hpi) with *P. parasitica* zoospores. This test was first designed to follow the progression of the infection starting from the beginning of biotrophy then going through necrotrophy. To describe the infection process we monitored the expression of two transcripts: *PpHMP1* (the ortholog of *P. infestans* Haustorial Membrane Protein 1 [7]) a gene specifically expressed in haustoria during biotrophy, and Nep1-like protein 1 (*PpNpp1*) [8] a necrotizing factor expressed during necrotrophic stages of *Phytophthora* infection [190].

This kinetics showed that the biotrophic stage of the infection is characterized by a rise in *PpHMP1* with a maximum corresponding to the switch from biotrophy to necrotrophy at 10hpi [6]. In turn *PpNPP1* shows an increment after this point indicating the onset of the necrotrophic stage (**Figure 3.2 A**).

In this context, expression of the *Avh195* transcript was detected in the early steps of the infection, displaying a maximum at 10hpi then slowly decreasing during later steps, and becoming barely detectable at 48hpi (**Figure 3.2 A**).

Thus, based on their respective mRNA levels **we could conclude that *Avh195* is expressed during *P. parasitica* infection.** We also determined that the transcript **preferentially accumulates during the biotrophic step of the *P. parasitica* infection cycle.** Therefore, we considered the effector a specific, biotrophy-associated pathogenicity factor.

Since *P. parasitica* has a broad host range, being able to attack more than 255 plant genera in 90 families [30] we also assessed the expression of *Avh195* during infection of tomato, another common host of this pathogen to confirm its pattern of expression. Similarly to what showed for *Arabidopsis thaliana*, we analyzed the level of mRNA for *PpHMP1* and *PpNPP1* in roots of *Solanum lycopersicum* (tomato Var. Marmande) in interaction with *P. parasitica* zoospores. In this pathosystem we could identify a progressive increase in both *PpHMP1* and *PpNPP1* transcript levels

until 30hpi, followed by a decrease in the mRNA level of *PpHMP1*, corresponding to the switch from biotrophy to necrotrophy. The relative expression of *Avh195* showed to be parallel to the one of the biotrophy marker, further confirming the accumulation in this specific stage of the infection (**Figure 3.2 B**).

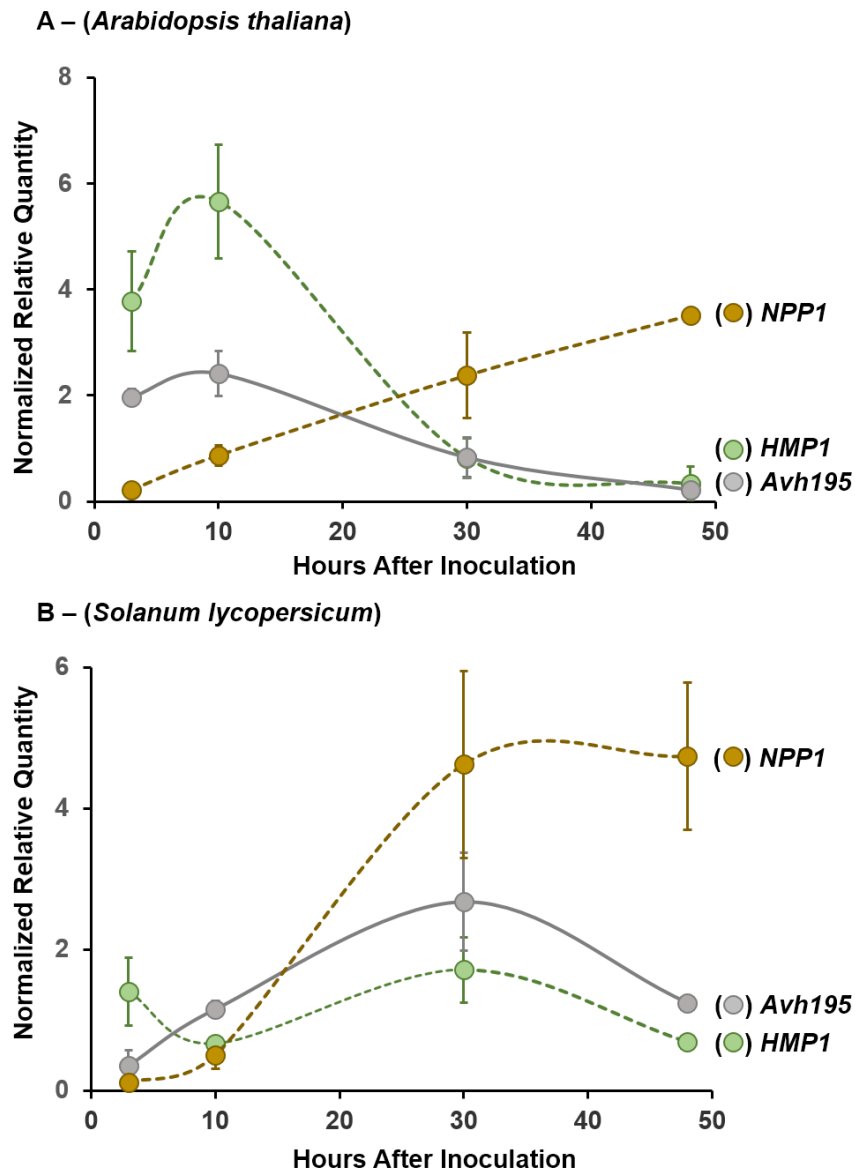


Figure 3.2: Expression profile of *Avh195* during the *P. parasitica* life cycle.

Relative mRNA levels of *Avh195* were quantified by quantitative RT-PCR in samples corresponding to *A. thaliana* (Panel A) or *S. lycopersicum* (Panel B) plantlets collected at different time-points after infection with *P. parasitica* zoospores. Data are presented as expression ratios relative to the *UBC*, *WS21* and *WS41* reference genes. Error bars represent standard error of the mean. The expression profiles of *PpHMP1* (green) and *PpNpp1* (brown) are also presented, as representative of the biotrophic and necrotrophic stages of the infection, respectively.

3.1.2 *Avh195* potentially interferes with autophagy

As anticipated in the previous Section, *Avh195* encodes a protein of 195 amino acids with the typical structure of a RxLR effector. Indeed, the sequence includes a 20 amino acid signal peptide, the canonical RxLR-EER motif harbored by this class of proteins, followed by an effector domain (**Figure 3.3**).

The computation of physical and chemical parameters of the encoded effector domain highlighted a marked abundance of positively (Arginine and Lysine) charged residues, accounting for 20% of the amino acid sequence, compared to 8.80% of acidic (Aspartic and Glutamic acids) residues. This composition leads to an elevated theoretical isoelectric point of the protein (pI: 10.31) which might be relevant to the function of the protein (**Table 3.1**).

Further *in silico* analysis of *Avh195* indicated that the polypeptide contains 5 putative ATG8 interacting motifs (AIMs), alternatively known as LC3-Interacting regions, or LIRs. This motif consist of 6 amino acids with a typical core consensus sequence [W/F/Y]xx[L/I/V], which can be found in proteins across the phylogenetic tree of life, and which is crucial for interactions with ATG8-family proteins [135,191]. The identification of AIMs in *Avh195* was performed by comparison with a collection of LIR motif-containing proteins (LIRCPs) from various organisms that are hosted at the iLIR autophagy database. The AIMs of LIRCPs are defined by a position-specific scoring matrix (PSSM) score which is derived from the alignment of experimentally verified AIM/LIR motifs [192,193]. The AIMs identified for *Avh195* were located in the effector domain of the protein and their PSSM score ranged from 7 to 16 (**Table 3.1**). As shown in [192], reliability of the PSSM score as a predictor of genuine AIM/LIR motifs can be set in the range of 13-17, not excluding however lower or higher values: for this reason we decided to set a cut-off of 10 on the score, and retained 3 candidate AIMs for further analyses.



Figure 3.3: Schematic representation of the Avh195 protein sequence.

The signal peptide and RxLR-EER motif characteristic of this class of effector are shown as yellow and blue boxes, respectively. The effector domain, in red, contains five ATG8 interacting motifs indicated as hexagons. The identified ATG8 interacting motifs displayed different PSSM scores (as indicated in Table 3.1); the motifs retained for further investigation in this study are indicated by an asterisk.

Amino acid composition of Avh195.

Only the effector domain was retained for analysis.

Amino Acid	Occurrence	Relative abundance (%)
Ala	9	7.20
Cys	0	0.00
Asp	7	5.60
Glu	4	3.20
Phe	1	0.80
Gly	6	4.80
His	2	1.60
Ile	6	4.80
Lys	15	12.00
Leu	19	15.20
Met	3	2.40
Asn	8	6.40
Pro	3	2.40
Gln	4	3.20
Arg	10	8.00
Ser	7	5.60
Thr	9	7.20
Val	2	1.60
Trp	6	4.80
Tyr	4	3.20

Identification of ATG8 interacting motifs on Avh195

Motif	Start	End	PSSM Score*
WNYQKL	100	105	7
KSYDDI	124	129	12
DRWIRL	131	136	16
DLYKVL	156	161	9
PIWREV	173	178	10

* PSSM Scores < 10 were discarded from the study

Theoretical pI: 10.31

Table 3.1: Bioinformatic analysis of Avh195 protein sequence.

The tables illustrate the physical and chemical parameters of the Avh195 coding sequence (left side) and the prediction of ATG8 interacting motifs in the effector domain of the protein (right side).

3.1.3 Avh195 transiently antagonizes HR-associated induced cell death in tobacco

The heterologous transient expression of proteins in *Nicotiana tabacum* leaves is a frequently used preliminary screen to analyze the capacity of an effector protein to induce or repress the HR. The method is based on the capacity of *Agrobacterium tumefaciens* to transfer a defined portion of DNA into plant cells, and to integrate it into the host genome [194]. We thus assessed the possible contribution of Avh195 to HR phenotypes by transient expression in *N. tabacum* leaves through *A. tumefaciens*-mediated transformation.

Firstly, several variants of mature Avh195 (without signal peptide) were tested alone for their ability to produce visible symptoms on plants *Nicotiana* leaves, notably cell death. The variants included the native version of Avh195 and a version deleted of the whole effector domain (**Avh195 Δ ED**). In addition, by the means of site-directed mutagenesis, we generated a mutant version of the effector in which the hydrophobic residues of the three AIM sites displaying the highest scores were changed into alanines, thus creating a triple mutant disabled for the three AIMs (**Avh195 Δ AIM**). Since at 72hpi no cell death was observed for the native construction (**Figure 3.4 A**), this first assay revealed that **Avh195 has no toxic effect and/or does not trigger a hypersensitive response in tobacco**. Similarly, no cell death was observed upon expression of the recombinant variants, indicating their suitability for subsequent tests (**Figure 3.4 A**).

We then assessed the ability of the effector to suppress plant defense responses by simultaneous agroinfiltration of a construct expressing cryptogein: an elicitor secreted by *P. cryptogea* that induces a strong HR-associated cell death symptom on tobacco [55].

Co-infiltrations of cryptogein with Avh195 display an initial delay in the evolution of necrotic lesions compared to the co-infiltrations of the truncated version Avh195 Δ ED, as observed at 36hpi (**Figure 3.4 B**). Similarly, this delay in the evolution of symptoms was visible also when compared against Avh195 Δ AIM. Yet all the differences were abolished at 72hpi when the lesions reached their maximum for all the tested combinations (**Figure 3.4 B**).

To evaluate the extent of the delay observed at 36hpi, we scored the necrotic lesions produced on the same leaf by cryptogein and co-infiltrated with Avh195 and its variants. The scoring system was designed to evaluate the reduction of HR-associated cell death while not being influenced by the natural variability of plants linked to both plant and leaf ages, parameters, which greatly influence the manifestations of HR and frequently leading to deceptive results. For each analyzed leaf, a first score of 1 was attributed to the infiltrated patch presenting the weakest symptoms. We then

compared the symptoms observed in the two neighboring patches and gave them a score ranging from 1 to 4 with 1 indicating absence of difference and 4 greatest difference.

An analysis conducted over 62 leaves is presented in (**Figure 3.4 C**). Overall, the native form of Avh195 was more frequently the patch presenting the lowest degree of necrosis, when compared to the variants Avh195 Δ ED and Avh195 Δ AIM. Infiltrations with Avh195 Δ ED frequently resulted in more necrotized areas than infiltrations with Avh195 Δ AIM, indicating that the abolition of three out of five AIMs does not completely disrupt the activity of Avh195.

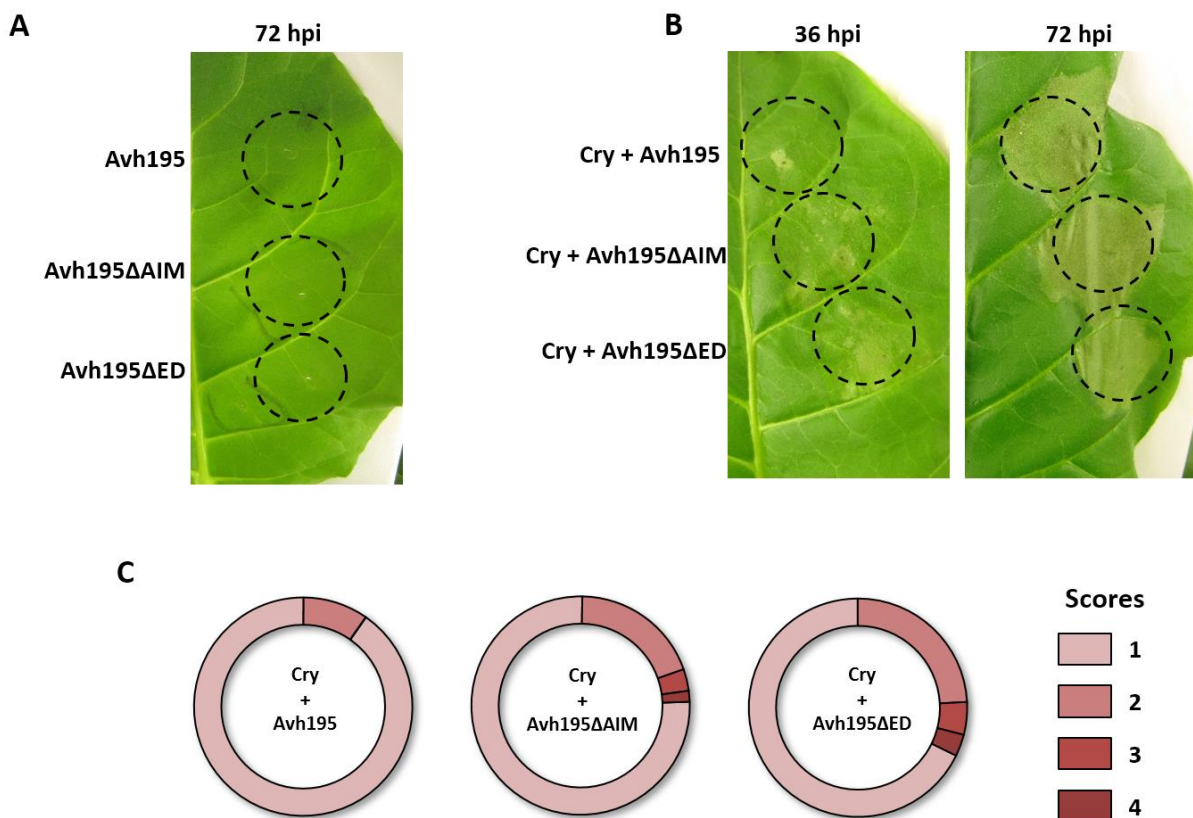


Figure 3.4: Avh195 transiently inhibits HR through interaction with ATG8.

- A. Responses of *Nicotiana tabacum* leaves 72 hours after agroinfiltration of native Avh195 (Avh195) and its derived variants, namely Avh195 deleted of the effector domain (Avh195 Δ ED) or mutated in AIMs (Avh195 Δ AIM). The absence of lesions indicates that the proteins do not have toxic or HR-inducing effect on tobacco leaves.
- B. Response of tobacco leaves to co-agroinfiltration of cryptogein (Cry) and the various forms of the effector: Avh195, Avh195 Δ ED, Avh195 Δ AIM. Pictures were taken at 36hpi (left) and 72 dpi (right).
- C. Evaluation of cryptogein-induced necrosis extent. Differences in symptom intensity were scored from 1 to 4 with 1 indicating absence of difference and 4 greatest difference among the compared infiltrated patches (see Results). Experiments were performed three times with a total of 14 plants and 62 infiltrated leaves per construct.

Taken together, these results indicate that ***Avh195* transiently reduces HR**: it appears that **the activity resides in the effector domain of the protein and that it is dependent of AIMS**. Thus, **the physical interaction with ATG8 seems a prerequisite for the biological activity of Avh195**.

3.2 Avh195 interacts with ATG8

Based on the results introduced in the previous Section we decided to further analyze if Avh195 physically interacts with ATG8.

As mentioned in the introduction, ATG8 is a ubiquitin-like protein with a pivotal role in autophagy: it promotes recruitment of autophagy-related protein complexes, cargoes and is involved in vesicle trafficking and vacuolar fusion of autophagosomes. This protein is highly conserved across the phylogenetic tree, but underwent gene expansion in higher eukaryotes, including plants. The number of gene family members varies among plant genera: for example it accounts for 7 members in tomato and 9 members in *Arabidopsis* [195]. Phylogenetic analysis of *Arabidopsis* ATG8 sequences show that the gene diverged into three subfamilies or clades. Although some of the paralogs are closely related, this expansion led to diversification of function and specificity [146]. The members of the ATG8 gene family display differential expression in plant organs, tissues, and in response to various environmental cues [143,196,197].

To evaluate whether ATG8 expression is modulated during infection, we exploited data generated in our lab on the root transcriptome of *Arabidopsis* upon infection with *P. parasitica* [45]. We evaluated the expression profile of each ATG8 member over a 30-h time course using an Affymetrix array. As shown in (**Figure 3.5**) the global expression of individual ATG8 members was relatively stable upon infection, but hybridization values greatly varied among biological replicates. So, we could anticipate that data interpretation and subsequent functional analyses would be difficult to conduct.

We then decided to assess the potential binding of ATG8 by Avh195 by choosing the coding sequence of ATG8 issued from a reduced-complexity model: the unicellular photosynthetic alga *Chlamydomonas reinhardtii*. Indeed, the *Chlamydomonas* ATG machinery is encoded by single-copy genes [143] that are related to plant homologs. Phylogenetic alignment of ATG8 shows that the gene in *Chlamydomonas* is close enough to plant ATG8 members belonging to clades I and II to be considered as a sister (**Figure 3.6**). For this reason, the *Chlamydomonas* ATG8 gene (hereafter CrATG8) appears as a valid representative of the plant gene family. In addition, this model organisms presents several other advantages for the present work, which will be presented in more detail in Section 3.3 of this chapter. With these assumptions in mind, we designed a series of targeted protein-protein interaction studies aimed to confirm the possibility of a physical interaction between Avh195 and ATG8.

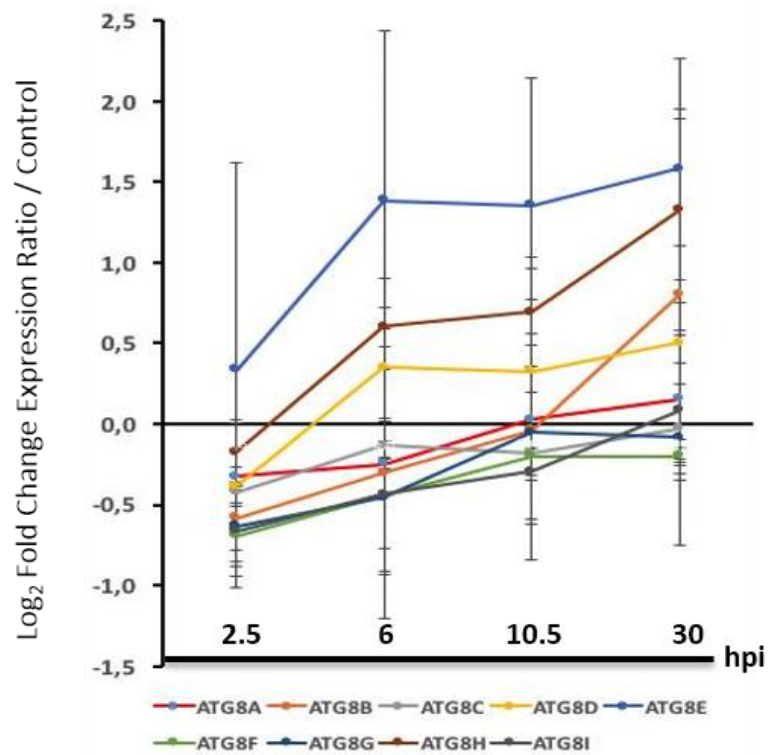


Figure 3.5: Relative expression of ATG8 members during Arabidopsis root infection by *P. parasitica*.

A. thaliana roots were inoculated with *P. parasitica* and a time-course analysis was performed using the Affymetrix ATH1 array for four sets of conditions: transcripts of roots 2.5hpi, 6hpi, 10.5hpi, 30hpi. Expression profiles were K-mean clustered as previously described [45].

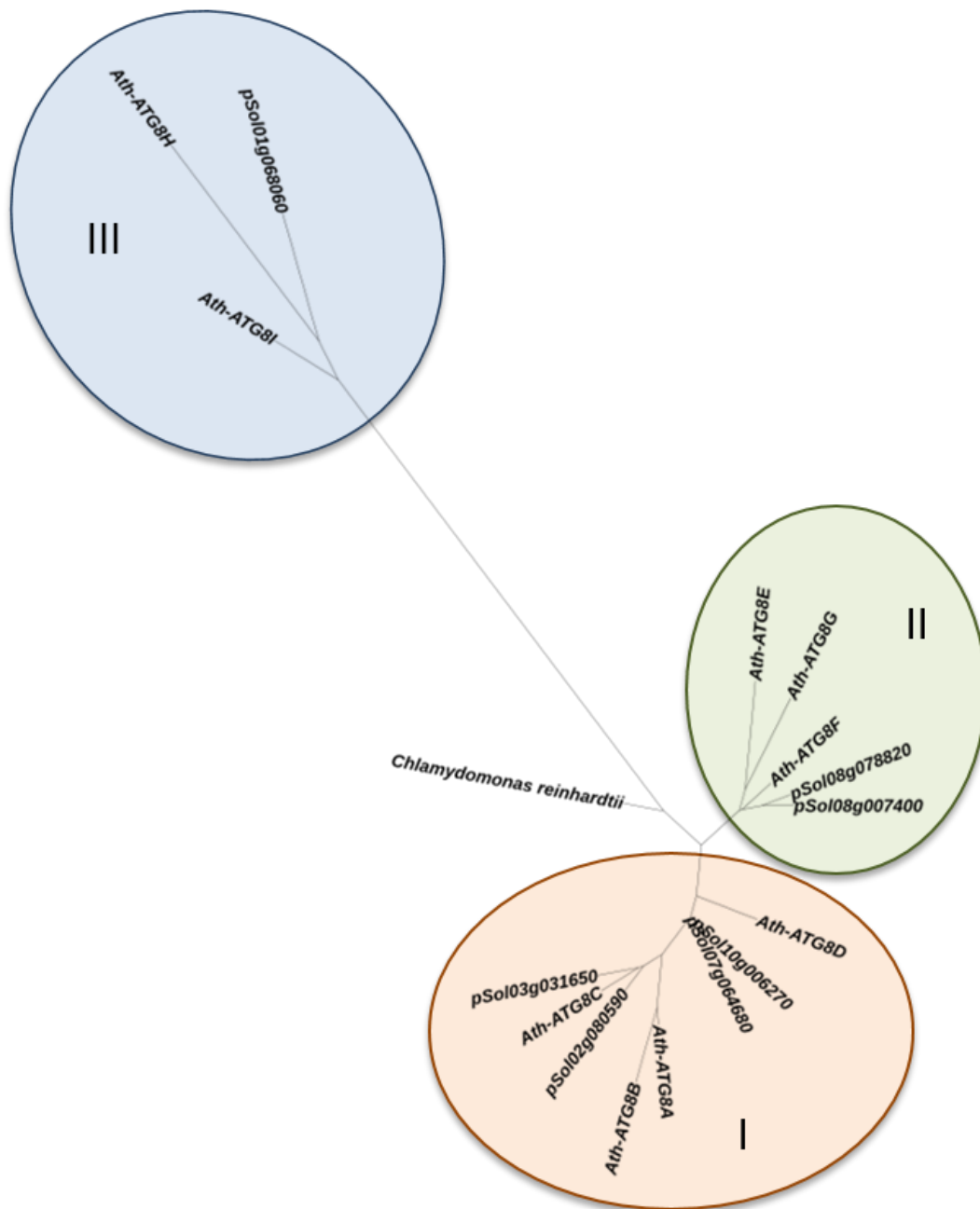


Figure 3.6: Phylogenetic relationships of ATG8 sequences from green organisms

The analysis was performed on ATG8 sequences from *C. reinhardtii*, tomato (pSolxxgxxxxxx) and *A. thaliana* (Ath-ATG8A-I). The tree has been constructed using the Maximum Likelihood (ML) method based on the LG model with a gamma rate of heterogeneity. Three clades (I-III) are defined, in agreement with other reports [146].

3.2.1 *Avh195 physically interacts with ATG8 in a non-specific manner*

Avh195 co-localizes on membranes with CrATG8 *in planta*

Since subcellular co-localization is a prerequisite for the study of protein-protein interaction, a first series of experiments was designed to identify the distribution of Avh195 and its candidate partner, CrATG8 in living cells. To this aim Avh195 carrying a N-terminal Green Fluorescent Protein (GFP)-tag (GFP-Avh195) was co-expressed with N-terminal RFP-tagged CrATG8 (RFP-CrATG8) in leaves of *Nicotiana benthamiana*. Observation of leaf explants via confocal microscopy 72h after *Agrobacterium*-mediated co-infiltration showed that the GFP-Avh195 fluorescence was restricted to membranous structures, while ATG8-associated RFP fluorescence localized to the cytoplasm and to membranes, arguably corresponding to the soluble and the membrane-associated forms of this protein, respectively (**Figure 3.7 A**). In some cases, the fluorescence of the two proteins was detected in vesicle-rich, membrane-surrounded cytoplasmic filaments (**Figure 3.7 A**).

These localization studies suggest that **both proteins interact *in planta* at membranous structures**.

In order to obtain biochemical validation of the co-localization of Avh195 and CrATG8 and their association with membranes, samples of *N. benthamiana* leaves were co-infiltrated with the same constructs presented above and samples were collected 72 hours later. Membrane-associated proteins were separated from soluble proteins by ultracentrifugation. Proteins from both fractions were then separated on electrophoresis gels, prior to Western blot analysis. Detection with an anti-ATG8 antibody showed that RFP-CrATG8 accumulates in almost equal amounts in both soluble and microsomal fractions (**Figure 3.7 B**). In contrast, immunodetection of Avh195 with an anti-GFP serum showed accumulation of the protein exclusively in the membrane-associated protein fraction (**Figure 3.7 B**).

This result, in line with what we observed by confocal microscopy, further indicates that potential interactions between CrATG8 and Avh195 occur at membrane layers.

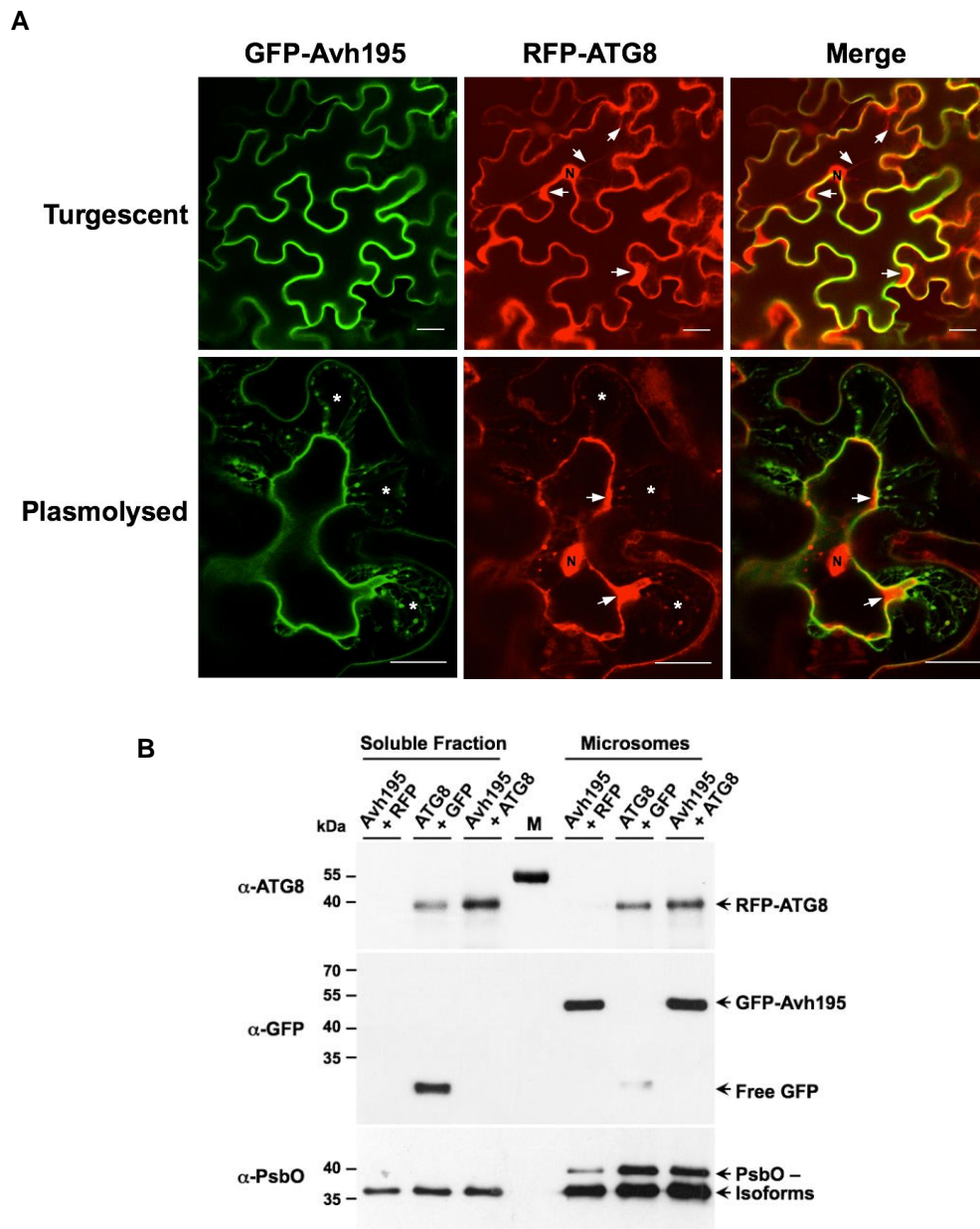


Figure 3.7: Avh195 localizes to membranes, whereas ATG8 is both soluble and membrane-associated.

- A.** Optical sections of *N. benthamiana* epidermal cells transiently co-expressing Avh195 and ATG8 from *C. reinhardtii*, as analyzed by confocal laser-scanning microscopy. In fully turgescent cells (upper lane) the N-terminal GFP-tagged Avh195 protein (left panel) outlines the cell border and does not appear in the cytoplasm. N-terminal RFP-tagged ATG8 (middle panel) localizes to the same border structure, but appears also in the cytoplasm, cytoplasmic threads passing the vacuole, and in the nucleus. This localization pattern becomes more evident in plasmolyzed epidermis cells (bottom lane). Here, green Avh195 labels the plasma membrane, and vesicle-rich, membrane-surrounded cytoplasm filaments (asterisks in middle and right panels) that attach to the cell wall. Red ATG8 (middle panel) labels the cytoplasm and the nucleus. Similar to Avh195, it localizes to the plasma membrane, to cytoplasm filaments, and to some, but not all, of the enclosed vesicles. Yellow color in the merged channel micrographs (right panels) shows co-localization of both proteins. Arrowheads point to cytoplasmic localization of ATG8. N = nucleus. Bars represent 20 μ m.
- B.** Immunoblot analysis of Soluble and Microsomal fractions prepared from *N. benthamiana* leaves transiently co-expressing GFP-tagged Avh195 with free RFP, RFP-tagged ATG8 with free GFP, and GFP-tagged Avh195 with RFP-tagged ATG8. Detection of antigens was performed with antisera directed against ATG8 and GFP. An antibody recognizing the photosystem II PsbO protein, which exists in soluble and membrane-associated forms, was used for loading control.

Avh195 interacts with ATG8 proteins in yeast

To identify an interaction between Avh195 and CrATG8, we used a yeast two-hybrid (Y2H) system. Considering that Avh195 is associated with membranes, we used the mating-based split-ubiquitin system (mbSUS), which has been developed to detect interactions between membrane proteins or between a membrane protein and a soluble partner [198]. This technique relies on the reassembling of N-terminal and C-terminal domains of a ubiquitin protein fused to bait and prey proteins. Physical proximity between bait and prey at the membrane reconstitutes a functional cytoplasmic ubiquitin. This last is recognized by ubiquitin specific proteases, which release the artificial transcription factor “PLV” (ProteinA-LexA-VP16) that is linked to the C-terminus of the bait. The released PLV translocates to the nucleus and binds lexA-regulated promoters of the reporter genes ADE2 and HIS3, which confer autotrophy for adenine and histidine to the yeast cells. Growth in the absence of adenine and histidine indicates interaction between bait and prey proteins.

When we used Avh195 as a bait and CrATG8 as a prey, mated yeast transformants expressing both proteins readily grew on selective medium. In contrast, Avh195 did not interact with the various negative controls that were integrated in the experiment as shown by the absence of growth on selective media (**Figure 3.8**).

In order to analyze whether Avh195 also interacts with plant ATG8 homologs, we used three members of the ATG8 family from Arabidopsis as baits. We selected AtATG8D, AtATG8G and AtATG8H as representatives of the clades I, II and III, respectively (**Figure 3.6**) Avh195 interacted with each of these ATG8 preys, leading to growth on selective media (**Figure 3.8**).

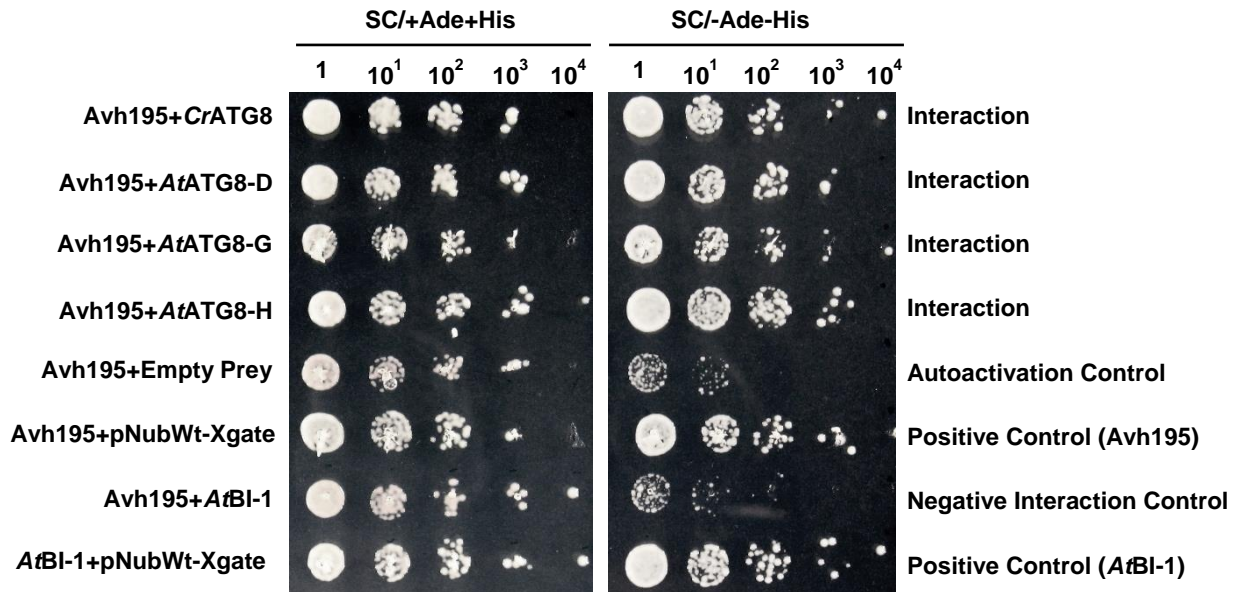


Figure 3.8: Avh195 interacts with ATG8 from *C. reinhardtii* and *A. thaliana*.

The mating-based split-ubiquitin system (mbSUS) was used to monitor the interaction of membrane-anchored Avh195 with ATG8 from *C. reinhardtii* and with 3 different ATG isoforms from *A. thaliana*. Serial dilutions of yeast cells expressing bait and prey constructs (labelled on the left) were assayed for growth on synthetic complete (SC) medium without adenine and histidine. Positive and negative controls, as well as the auto-activation control are indicated. SC/+Ade+His = synthetic complete medium including all amino acids; SC/-Ade-His = synthetic complete medium without adenine and histidine. For negative control, the membrane-associated Arabidopsis Bax Inhibitor 1 (AtBI-1) was used.

Taken together these results show that **Avh195 interacts with ATG8 proteins from organisms of the green lineage in a non-selective manner, and that this interaction involves membrane-associated ATG8. These findings further support the hypothesis that the effector exerts its biological action through perturbation of the host's autophagic machinery.**

3.3 Characterization of Avh195 in *Chlamydomonas reinhardtii*

As anticipated in Section 3.2 we selected *Chlamydomonas reinhardtii* as an alternative system to plants to facilitate the study of a complex process such as autophagy. This organism is a eukaryotic green microalga belonging to the phylum of chlorophyte, which diverged from land plants over a billion years ago and is adapted to live in soil and fresh water worldwide [199]. *Chlamydomonas* are motile, unicellular photosynthetic organisms: the cells have a round shape with two flagella in the anterior part, mitochondria and a cup-shaped chloroplast that allows the cells to obtain energy from the light (**Figure 3.9**). The efficiency of this process is guaranteed by two specialized structures: the eyespot that allows the alga to sense and follow the light: and the pyrenoid, an organoid where CO₂ is concentrated to improve the electron transport chain. Nonetheless *Chlamydomonas* has also the ability to grow in the dark and use acetate as a carbon source to obtain energy and in certain condition such as nutritional stresses it can accumulate energy rich compounds like lipids and starch.

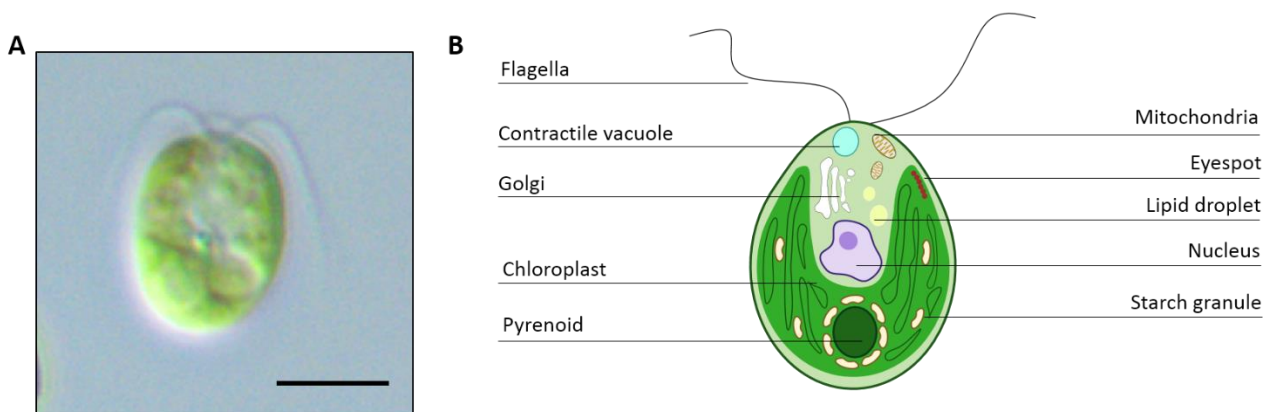


Figure 3.9: The microalga *Chlamydomonas reinhardtii*.

- A. Light microscope image of *Chlamydomonas reinhardtii*. Scale bar represents 5 μm .
- B. Schematic representation of the cell structure of *Chlamydomonas*.

The nuclear genome of *C. reinhardtii* is composed of 17 chromosomes with a total size of ~120 Mbp [200] (data: Joint Genome Institute 2015). Comparative genomic analyses revealed that many *Chlamydomonas* genes are derived from the last plant-animal common ancestor, particularly, genes related to photosynthesis and plastid functions. Other genes such as those encoding the flagellum or regulatory proteins that are critical for survival under changing nutrient conditions, like Na⁺/SO₄ transporters, were instead lost by land plants but maintained in this lineage [200].

Additional investigations in *C. reinhardtii* led to the identification of orthologs of ATG genes from yeast. Genome-wide analysis of ATG genes revealed that most of the core machinery genes are conserved in *Chlamydomonas*. Unlike plants, the microalga only possesses single copy ATG genes. When compared to yeast, plants and the algae miss 4 and 7 ATG proteins, respectively. However, both plants and algae are able to achieve functional autophagy (**Figure 3.10**) [143,201,202].

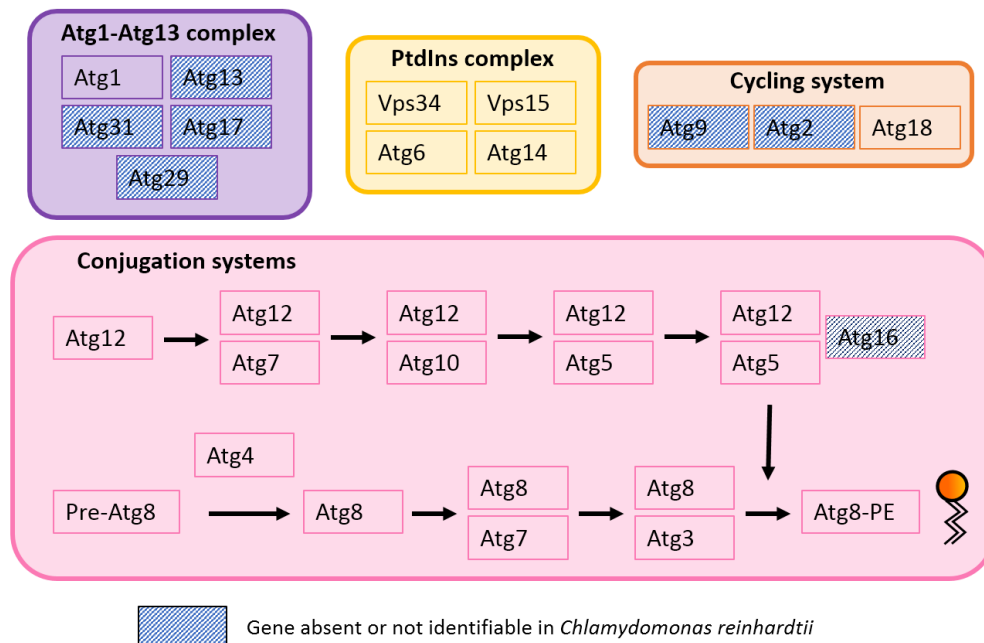


Figure 3.10: Core autophagy machinery in *Chlamydomonas reinhardtii* compared to yeast.

The four main complexes constituting the core autophagy machinery are conserved in *Chlamydomonas reinhardtii*. Pattern-filled boxes stand for genes that are missing or that are still not identified in the microalga [201].

Chlamydomonas is sensitive to a range of factors that induce autophagy in higher plants, like nutrient limitation, oxidative stress, ER stress, or entry into the stationary phase of the cell cycle [203]. In addition, *Chlamydomonas* also responds to the treatment with the macrolide rapamycin, which exerts a direct action on TORC1 pathway determining arrest of cell growth and the induction of autophagy [204].

Numerous techniques and molecular tools are available for analyzing this organism, and in recent years specific methods were developed to monitor autophagy and autophagic flux (among others: immunodetection of ATG8 and ultrastructure imaging of autophagic vacuoles). These methods greatly improved our knowledge on the regulation of autophagy in *Chlamydomonas* [205]. Moreover, *Chlamydomonas* is amenable to genetic transformation, and the creation of stable

transformants is faster than in the case of plants [206]. From the perspective of this work, this model was joining a reduced genetic complexity, the possibility to obtain Avh195 overexpressing lines and the availability of tools to study autophagy. All those reasons determined the choice of *Chlamydomonas* as a support to study the manipulations operated by a pathogen effector on the host autophagic machinery.

As discussed in the introduction, plant-pathogen interactions are strongly intertwined with the multifaceted role of autophagy in plant physiology and immunity. Effector-mediated stimulation or inhibition of autophagy might *per se* provide an advantage to the pathogen (e.g. for nutrition), or selectively lead to the degradation/accumulation of regulatory compounds that interfere with other (defense-related) pathways. The use of *Chlamydomonas reinhardtii* provides here an excellent model to analyze the effector-mediated inhibition or the induction of autophagy, which are probably not related to multicellularity and complex emergent properties that are typical for higher (green) organisms.

3.3.1 Selection and characterization of *Chlamydomonas transgenic lines*.

Having validated the interaction between Avh195 and CrATG8 we sought to investigate the outcome of this interaction on the autophagic process through heterologous expression of the effector protein in *Chlamydomonas reinhardtii*.

Since the *C. reinhardtii* nuclear genome has an overall GC content of approximately 65% due to a bias in codon usage [200] we needed to adapt the open reading frame of *Avh195* to this requirement. We designed a synthetic *Avh195* coding region (after deletion of the signal peptide) adapted to the codon bias of the alga in order to facilitate the expression of the foreign gene [207]. The synthetic gene was then cloned into the pChlamy_3 plasmid (Thermo Fisher®) by the group LB3M of the CEA (Atomic Energy Commission - Cadarache). This plasmid is a nuclear integrative vector that provides random integration of the construction across the genome. The gene was placed under the control of the *Heat Shock Protein 70/RUBISCO small chain 2* chimeric promoter (Hsp70A / RbcS2). The vector also includes a 5'-end of the transcript where the first intron of the RBCS2 gene acts as a transcriptional enhancer [208] and a 3'-UTR sequences from RbcS2 gene for proper termination of transcription. The same laboratory performed the transformation of the *Chlamydomonas reinhardtii* strain *dw15.1* via electroporation of linearized plasmids and the selection of transgenic strains on selective media. The strain was selected, because it is deficient of a cell wall and thus more accessible to uptake of exogenous stimuli such as autophagy inducers and inhibitors.

Transgenic alga lines were then analyzed to confirm the successful integration and correct expression of the cassette containing *Avh195*. At first, 101 independent clones were validated for the presence of the gene via PCR of genomic DNA using primers internal to the *Avh195* coding sequence. The quality of the DNA preparation was assessed with the amplification of the housekeeping gene Guanine nucleotide-binding protein beta subunit-like (*CBLP*). Among the validated transgenic lines ($n = 62$), 33 were analyzed for proper integration and expression of *Avh195*. A further step of selection was performed on 15 lines to verify the correct processing of the transcript (splicing of the intron RBCS2). Finally, 8 lines were selected, which express the correctly spliced and validated version of *Avh195* mRNA.

The validated lines were then analyzed for the level of expression of *Avh195* via RT-qPCR: the relative mRNA level of *Avh195* greatly varied from one transformant to another. We retained three independent lines for further analysis, on the basis of their high, average, and low expression of the transgene relative to reference genes: these lines are hereafter designed as **N15**, **N26** and **C40**, respectively (**Figure 3.12**). In all following experiments, the transgenic lines will be compared to the non-transformed wild-type strain *dw15.1*, hereafter designed as **WT**.

In order to minimize the dependency from circadian variations and the nutritional status of cells (parameters known to have an impact on autophagy) all experiments were performed in mixotrophic conditions, with a light-dark cycle to obtain synchronization of cell divisions [209]. For the same reason, the beginning of the light period was assessed as time $t = 0$ for both chemical treatments and sample collection, as exemplified in **Figure 3.11**.

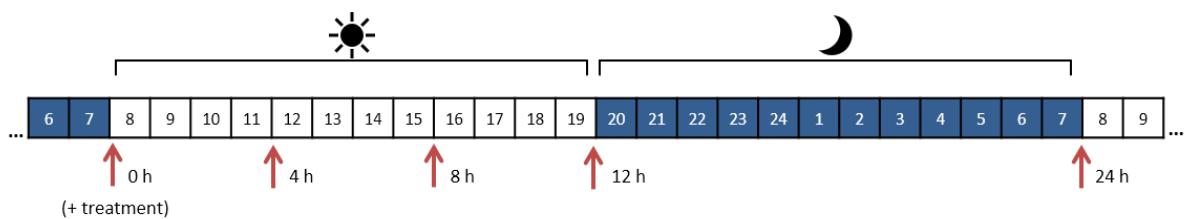


Figure 3.11: Experimental strategy applied to *Chlamydomonas* experiments.

The Diagram represents the conditions that were applied to *C. reinhardtii* cultures. Cells were grown under a 12/12 light-dark cycle to obtain synchronization of cell divisions. Red arrows represent the time points used during experiments for chemical treatments and samples uptake.

3.3.2 Heterologous expression of Avh195 does not affect physiology and fitness of *Chlamydomonas*

To gain knowledge on the function of Avh195 we first checked for a putative impact of transgene expression on the global fitness of the transformants. As a first analysis determined growth and biomass increase of the selected isolates by measuring optical density at 600 nm (OD₆₀₀) of liquid cultures. Over a period of three days of culture at 23°C with a 12/12 light-dark cycle the increase of OD₆₀₀ was reduced in transgenic strains, when compared to the WT (**Figure 3.12**), possibly indicating that the expression of the transgene alters cell physiology.

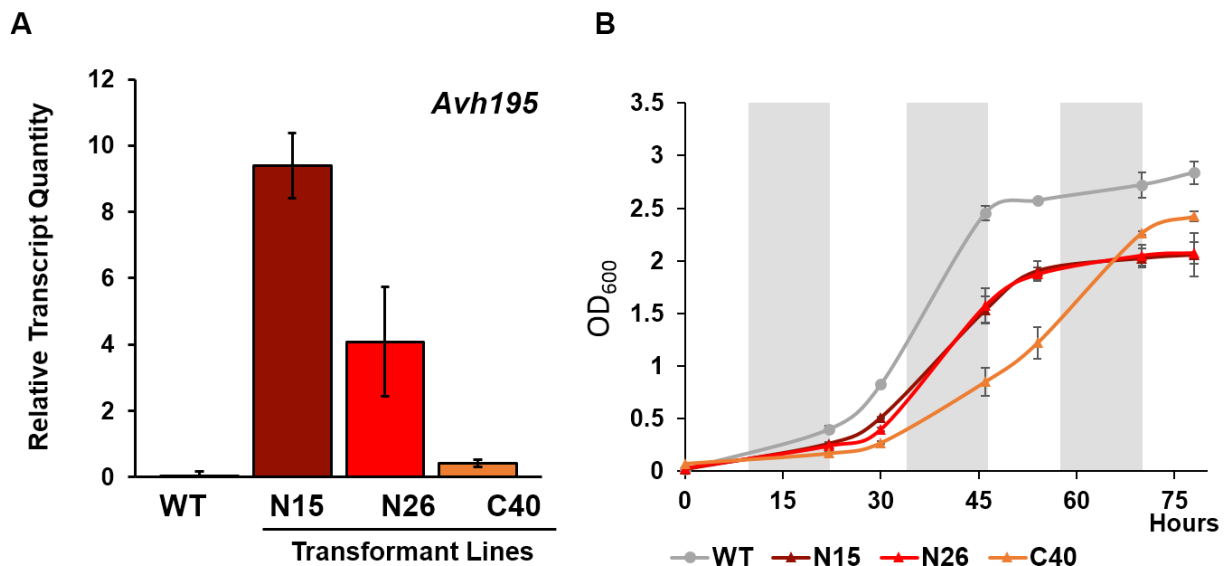


Figure 3.12: Characterization of *C. reinhardtii* transformant cell lines.

- Overexpression of *Avh195* in *C. reinhardtii*. RT-qPCR analysis of transcripts encoding Avh195 in the wild-type line DW15-C2 (WT), and in 3 selected transformant lines (N15, N26 and C40). RT-qPCR data were normalized with the constitutive *C. reinhardtii* genes *Cre02.g106550*, *Cre04.g227350* and *Cre05.g232750* [210]. Shown are means \pm SD from 3 biological replicates.
- Mixotrophic growth of cultures of *C. reinhardtii* over a period of 72 hours. Liquid cultures of the WT and transformant lines N15, N26 and C40 were inoculated with equal number of cells (10^5) and OD₆₀₀ was measured over time. Each time point indicated by the marker (● for WT, ▲ for transformant lines) represents the means \pm SD from three biological replicates. Shaded areas represent the periods of darkness of the 12/12 light-dark cycle.

To further verify a potential impact of transgene expression on the global fitness of the transformant lines, we analyzed *Chlamydomonas* cultures by flow cytometry over a period of 24 hours. Several parameters were taken into account: physical parameters, chlorophyll content, cell viability and cell proliferation.

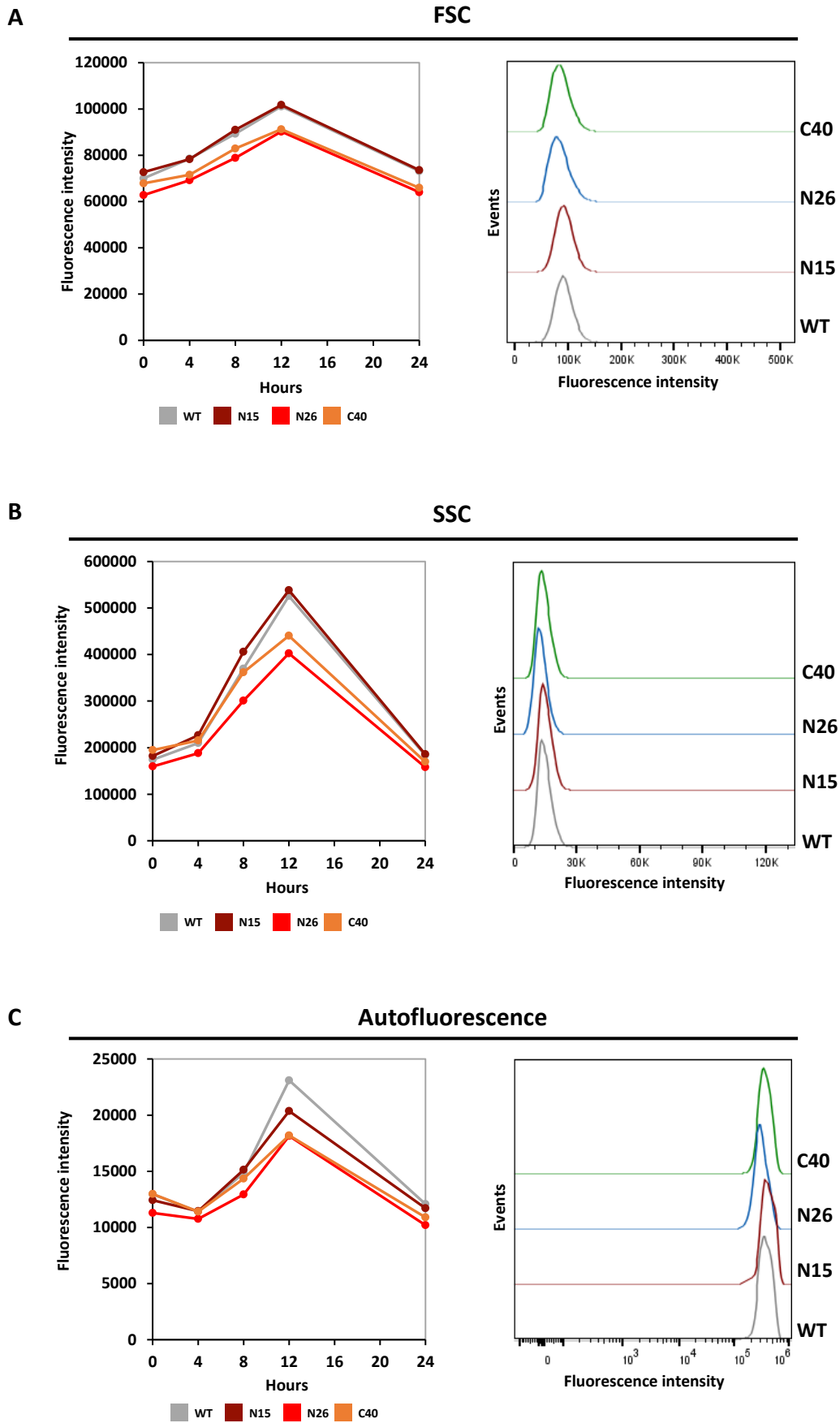
Physical parameters of the cells were determined by measuring forward light scattering (FSC), which is proportional to cell size, and by determining side light scattering (SSC), which reflects cell structure complexity. Transformants and wild type strains displayed similar FSC and SSC parameters, which changed in tight connection with the light/ dark cycle (**Figure 3.13 A and B**). For both parameters, values increased progressively from time point 0h to 12h reaching a mean increase of 29% for FSC and 37% for SSC but returned to the initial values at time point 24 h. Over the 24 hours analyzed, WT and transgenic cells displayed an increase of the same magnitude. Considering the central time point of the kinetics (measure at 8 h), the histograms for FSC and SSC presented in **Figure 3.13 A and B** clearly show that the distribution of **size and complexity within the population of algae is similar for cells from the WT and transformant lines**.

The second parameter taken into account was the chlorophyll content, which can be deduced by measuring autofluorescence intensity of cells: it presents a spectrum of emission in the range of $\lambda = [660 \text{ nm} - 750 \text{ nm}]$, mainly corresponding to the spectra of chlorophyll emission. As observed for physical parameters, also chlorophyll content was strongly influenced by the diurnal cycle, increasing progressively during the light period and decreasing back to the starting values at the end of the dark period (**Figure 3.13 C**). Median values of fluorescence intensity did not differ obviously between WT and transgenic cells all along the analyzed period (**Figure 3.13 C**): once more, the histogram of these values at time point 8h highlights that **distribution of chlorophyll content is not altered in the population of transformant cells, when compared to the WT**.

Viability of cells was estimated by staining with 4'-6-diamino-2 phenylindole dihydrochloride (DAPI), an impermeant DNA dye that is widely used to mark dying and dead cells. Throughout the 24h analyzed, only a very small ratio of cells stained positively with DAPI and this proportion never exceeded 6% of the total population (**Figure 3.13 D**). **These results indicate a similar rate of cell death within cultures of WT and transformant cells**.

We then examined the proliferation rate of WT and transgenic cells, based on the dilution of the fluorescence intensity of carboxy-fluorescein succinimidyl ester (CFSE) upon cell division [211]: Commonly used for measurements in animal cell populations, this technique has also been successfully applied to the microalgae [212]. As expected for synchronized cultures, the values for CFSE fluorescence intensity slightly decreased during the light period but were strongly reduced at 24 h, indicating that several cell divisions (mainly) occur during the dark period. In addition, analysis of this staining over time did not reveal relevant differences in proliferation rate between the WT culture and the three transformants (**Figure 3.13 E**). This result, in agreement with data collected on the evolution of cell size and complexity, indicated that **the cell cycle is not affected in transformants overexpressing Avh195**.

The apparent discrepancy with the result obtained for optical density of cultures might result from the reduced accuracy of OD₆₀₀ measurements, which is influenced by the presence of debris in the suspension, the formation of cellular aggregates and interference with chlorophyll absorption. For this reason, despite the fact that a reduction of OD₆₀₀ in transgenic cultures was obtained systematically, we did not investigate any further this aspect.



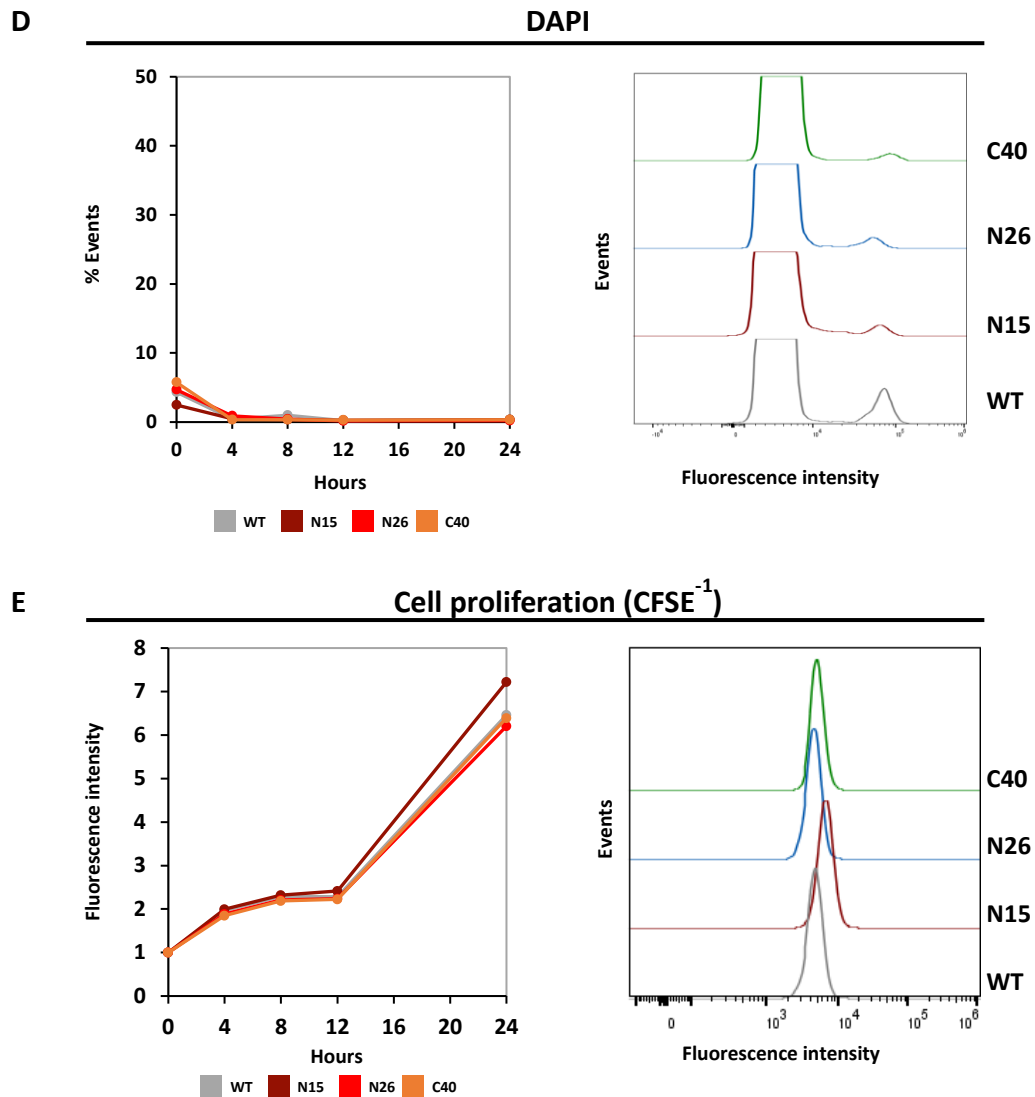


Figure 3.13: Flow cytometry analyses of *Chlamydomonas reinhardtii* WT and transgenic cell lines.

Chlamydomonas cultures of the WT and the transformant lines were analyzed on a SP6800 spectral cytometer (SONY Biotechnologies®) over a period of 24 hours. For each time point, at least 80.000 cells (Events) were analyzed for the following parameters: Forward Light Scattering - FSC (A); Side Light Scattering - SSC (B); Autofluorescence of cells (C) that is indicative of chlorophyll content; DAPI staining (D) to assess cell death; CFSE repartition into daughter cells (E), here presented as CFSE⁻¹ to highlight cell proliferation.

Panels A, B, C, E: left plot represents median values of fluorescence intensity (arbitrary units) over a 24 hours period, shaded areas represent the periods of darkness of the 12/12 light-dark cycle. Right plot presents the distribution of fluorescence intensity within the indicated population of cells collected at time point 8 h.

Panel D: left plot reports the proportion of cells positively stained with DAPI over a 24 hours period; shaded areas represent the periods of darkness of the 12/12 light-dark cycle. Right plot presents a magnification of the distribution of fluorescence intensity within the population of DAPI stained cells collected at time point 8 h.

3.3.3 Heat shock induction of Avh195 leads to lethality of Chlamydomonas

As presented above, the *Hsp70A/RbcS2* promoter controlling the expression of *Avh195* is a chimeric promoter: the sequence elements belonging to the *Hsp70* portion are responsive to heat shock and can be used to further induce the expression of the downstream gene [213]. We decided to apply a 40°C heat-shock for 1h on WT and transformant cell cultures and analyzed the level of expression of *Avh195* by RT-qPCR in samples collected 4h after heat-shock. The accumulation of transcripts was highly increased after the heat shock for the three selected transformants. In all three lines, the mRNA abundance was about 800- to 1,000-fold higher after heat shock, when compared with the amount detected in non-induced conditions.

Starting from the end of the heat shock, cell cultures were also observed over time and analyzed for their optical density. The transgenic cultures displayed different levels of bleaching and decrease in optical density, which in some cases led to the complete loss of the culture (**Figure 3.14 A**). This phenomenon was further investigated with the viability fluorescent dye SYTOX[®] that penetrates death cells: staining of cultures 2h after the heat shock revealed the presence of extensive cell death in transformant strains compared to the WT (**Figure 3.14 B**). These results suggest that **excessive amounts of Avh195 are lethal for Chlamydomonas**.

We thus decided not to exploit heat shock-induced overexpression of the transgene, as lethality of excessive *Avh195* overexpression would certainly interfere with autophagy and mask subtle effects of the effector on this mechanism.

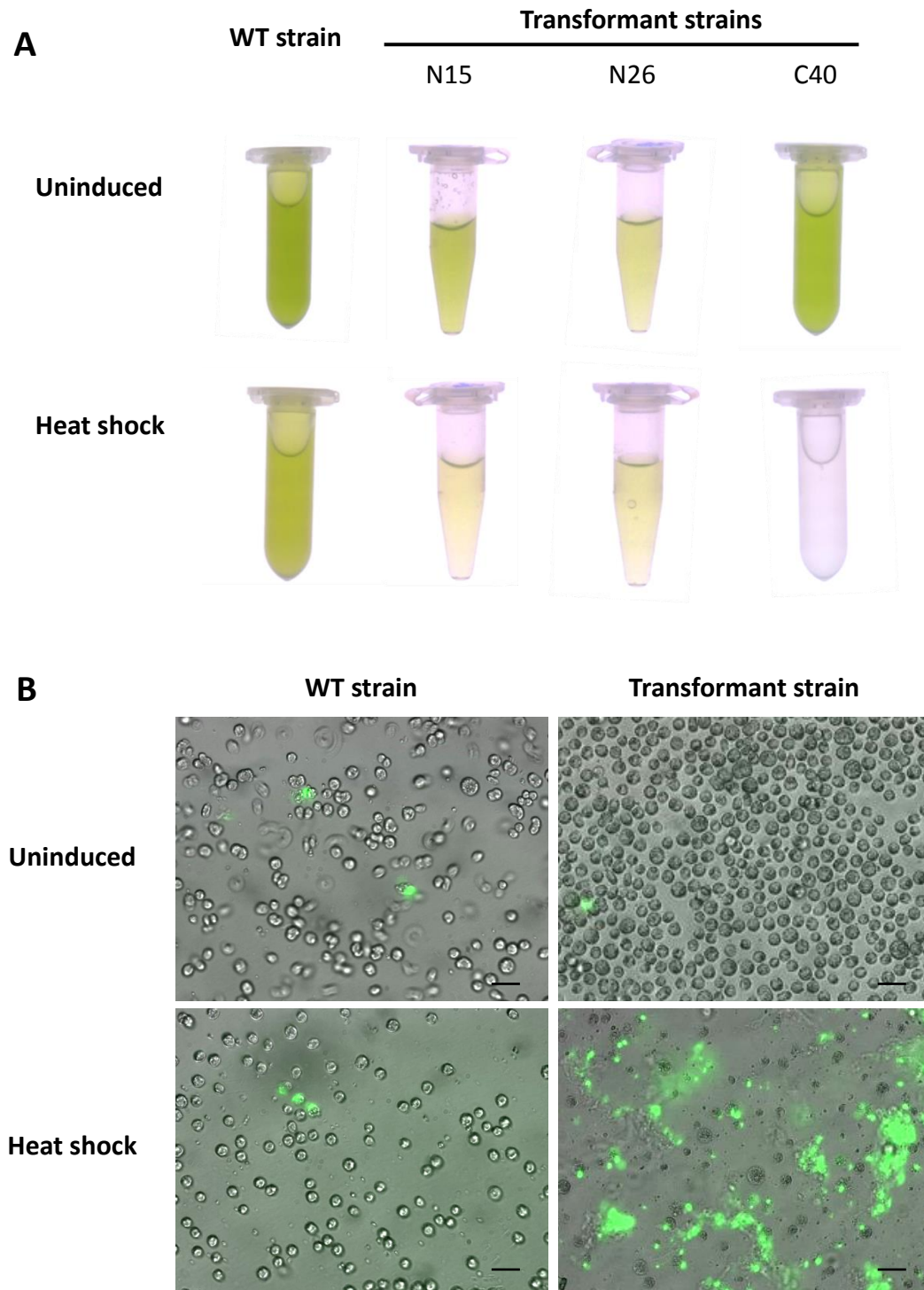


Figure 3.14: Heat shock induces lethality in *Chlamydomonas* transformant strains.

- A.** *Chlamydomonas reinhardtii* WT and transformant cultures were exposed to heat shock (40°C for 1 h) to induce expression of the transgene *Avh195*. 24 hours later, transformant strains show an important decrease in cell content as it can be observed by the bleaching of cell cultures.
- B.** Light and epifluorescence micrographs of *Chlamydomonas* cells belonging to WT and transformant cultures exposed or not to heat shock. Two hours after heat shock, samples were stained with SYTOX® Green Dead Cell Stain to identify dying and dead cells. Scale bar represents 25µm.

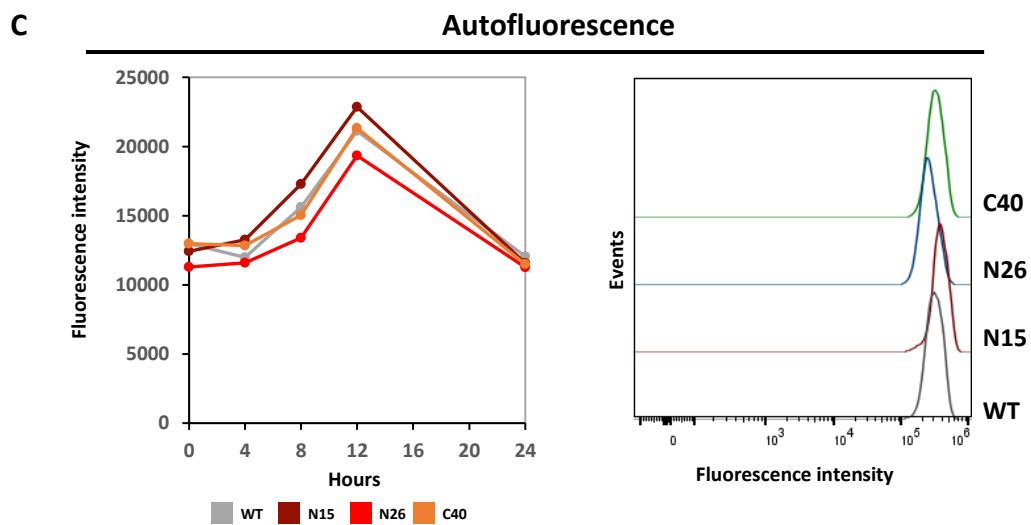
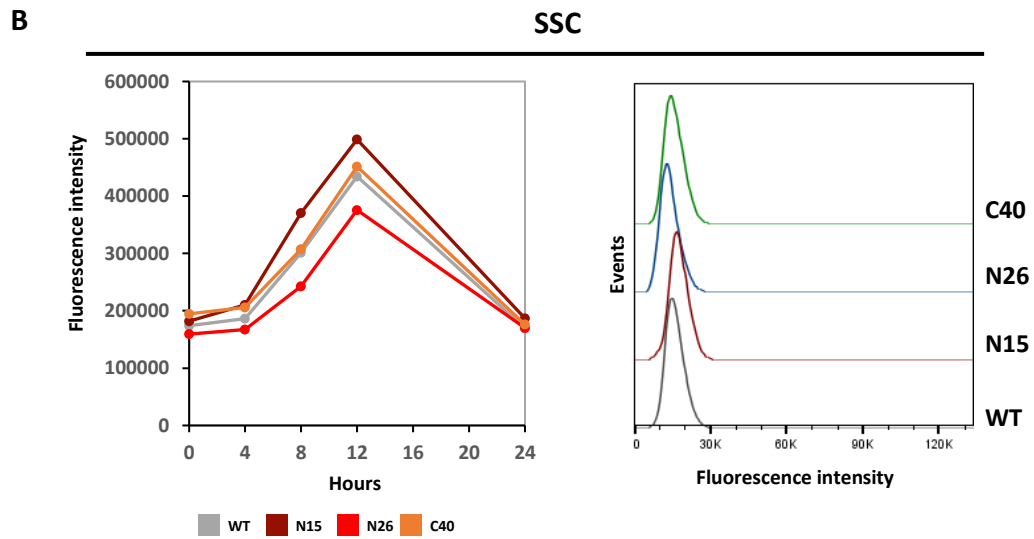
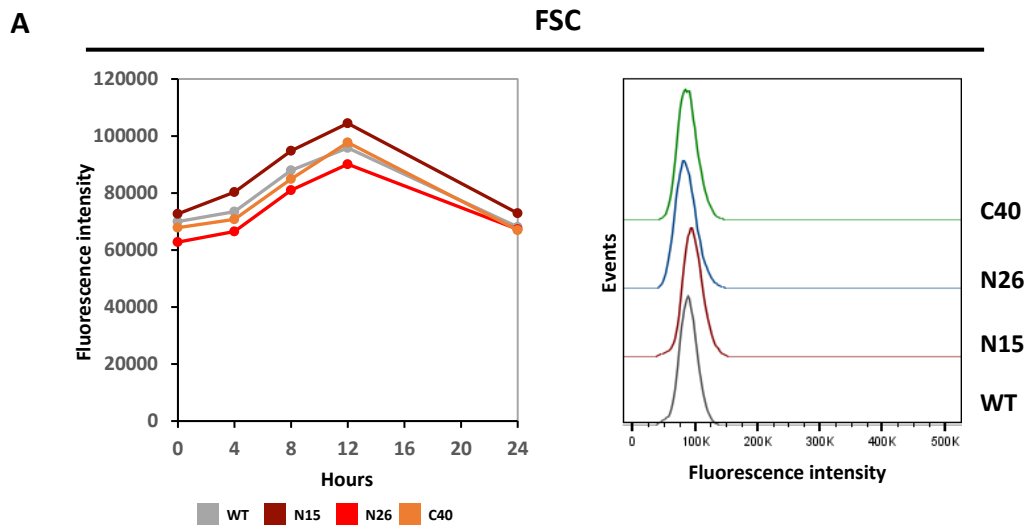
3.3.4 Characterization of autophagy perturbation in *Chlamydomonas*

To investigate the possible interaction of *Avh195* with the autophagic process in *C. reinhardtii* we first analyzed the responses of WT and transgenic cells to rapamycin, a molecule that induces autophagy through the inhibition of the TOR kinase.

Rapamycin treatment does not affect *Chlamydomonas* fitness

TOR kinase is an essential and conserved protein that integrates nutritional and environmental cues and regulates cell growth in lower and higher eukaryotes. The activity of TOR is central to metabolic pathways by promoting anabolic processes while antagonizing catabolic ones [214]. TOR is the target for the drug rapamycin, which inhibits the kinase and stimulates autophagy. Due to its strong impact on cell physiology, we decided to use relatively low concentrations of the drug (0.5 μ M) for treatments, and to assess if this concentration affects somehow the global fitness of the culture under the experimental conditions that were applied throughout the work. A recent report showed that high doses of rapamycin (5 μ M) have strong impacts on cell proliferation [215]. We thus analyzed by flow cytometry the evolution of cells from WT and transgenic cultures that were exposed to 0.5 μ M of rapamycin for a period of 24 hours. The parameters analyzed, presented in Section 3.3.2 did not show significant differences between rapamycin-treated and untreated cultures. Moreover, we only detected slight differences in the responses between WT and transformant cells (**Figure 3.15 A-E**), which likely reflect individual variations rather than a global trend.

We thus concluded that **the concentration of rapamycin that we used throughout this work does not affect viability and fitness of both WT and *Avh195*-expressing *Chlamydomonas* cell lines.**



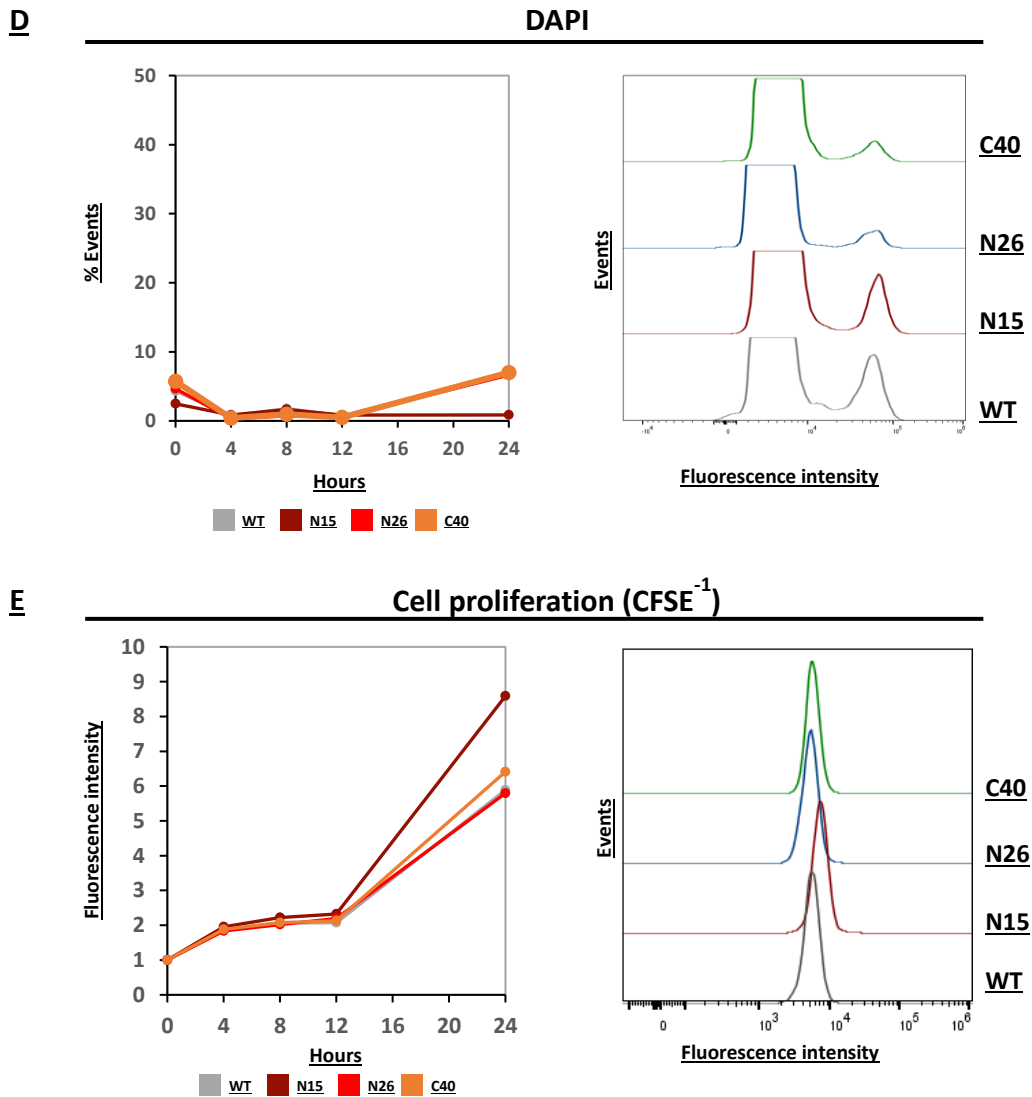


Figure 3.15: Flow cytometry analysis of *C. reinhardtii* transformant cell lines upon rapamycin treatment.

Chlamydomonas cultures of WT and transformant strains were analyzed on a SP6800 spectral cytometer (SONY Biotechnologies®) over a period of 24 hours following treatment with 0.5 μ M rapamycin. For each time point, at least 80,000 cells (Events) were analyzed for the following parameters: Forward Light Scattering - FSC (A); Side Light Scattering - SSC (B); Autofluorescence of cells (C) that is indicative of chlorophyll content; DAPI staining (D) to assess cell death; CFSE repartition into daughter cells (E), here presented as CFSE⁻¹ to highlight cell proliferation.

Panels A, B, C, E: left plot represents median values of fluorescence intensity (arbitrary units) over a 24 hours period; shaded areas represent the periods of darkness of the 12/12 light-dark cycle. Right plot presents the distribution of fluorescence intensity within the indicated population of cells collected at time point 8h.

Panel D: left plot reports the proportion of cells positively stained with DAPI over a 24 hours period; shaded areas represent the periods of darkness of the 12/12 light-dark cycle. Right plot presents a magnification of the distribution of fluorescence intensity within the population of DAPI stained cells collected at time point 8h.

3.3.5 Chlamydomonas transformant strains respond to rapamycin by autophagy induction

TOR inhibition by rapamycin was reported to activate autophagy in *Chlamydomonas* [204]. To test whether induction of autophagy is impaired in cells overexpressing *Avh195* we monitored the formation of autophagosomes using the acidotropic dye LysoSensor® Green DND189. This staining is designed to enter cells and to be retained in acidic organelles, including acidified autophagosomes. WT cells exposed to rapamycin for 24h display accumulation of fluorescent foci indicating accumulation of acidic compartments: overall, we observed an increase in the ratio of cells presenting fluorescence when compared to untreated cultures (**Figure 3.16 A and B**). We then verified the ability of transgenic cells to respond to the same chemical treatment. Cells from all lines showed an accumulation of fluorescent foci and the ratio of cells presenting acidic compartment increased upon rapamycin treatment (**Figure 3.16 B**). Since the magnitude of this accumulation is comparable to the one obtained for wild type strain we concluded that the **overexpression of *Avh195* does not affect the ability of cells to respond to rapamycin treatment and the inhibition of TOR signaling pathway**. Moreover, the accumulation of acidic compartments in transgenic cells suggest that **activities, which are related to autophagy induction and vesicle nucleation, are not affected by *Avh195***.

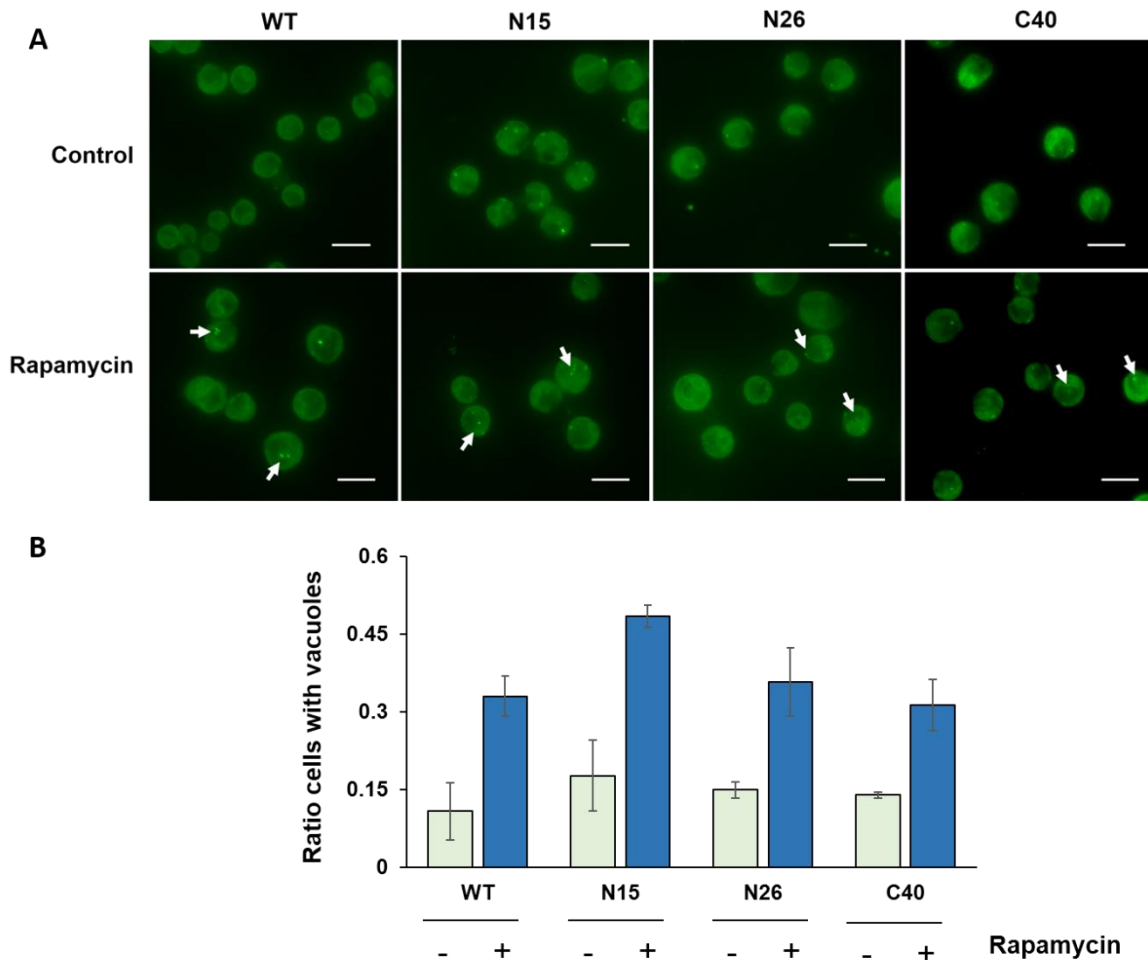


Figure 3.16: Response of *Chlamydomonas* cells to rapamycin treatment.

- A.** Fluorescence microscopy images of WT and transgenic cells of *Chlamydomonas reinhardtii* in control condition (upper lane) or exposed for 24h to Rapamycin (lower lane). Cells were stained with 2 μ M of the acidotropic dye LysoSensor® Green DND189 and analyzed for the presence of fluorescent spots corresponding to acidic compartments. Some of the analyzed spots visible in the pictures are pointed by the arrowhead. Scale bar represents 10 μ m.
- B.** The number of cells presenting spots was analyzed for cells in control and treated conditions. The bars represent the mean ratio of cells presenting a spot +/- SD of two independent experiments.

For the detection of autophagy, and the analysis and quantification of autophagy-associated events, electron microscopy remains one of the most accurate methods [216]. To monitor autophagic flux in response to rapamycin treatment, we analyzed WT and transgenic cells via transmission electron microscopy (TEM). In a first experiment, we used untreated or rapamycin-treated WT cells that were collected over a period of 24 hours. The morphology of untreated cells does not change over time, with the only exception that starch accumulated progressively during the 12 hours light period (**Figure 3.17** and **Supplementary Figure 1**). In the absence of rapamycin treatment, cells present

several small vacuoles that increase in volume upon rapamycin treatment. This increase in volume is readily visible since the first time point analyzed (4h) and is accompanied by convergence of more vacuoles in a unique central vacuole (8h) that occupies the whole cell at 12h and 24h after treatment, eventually causing swelling of the whole cell (**Figure 3.17 B**). In parallel, we observed the accumulation of material, that we assume to be autophagic bodies, at the interior of the vacuole and its progressive clearance until time point 24h (**Figure 3.17 A** and **C**).

We conducted the same analysis with cells from the transgenic lines overexpressing *Avh195*. As observed for the WT, the morphology of cells does not present changes over the 24 hours period (**Figure 3.17** and **Supplementary Figure 1**). A close observation of transgenic cells in non-induced conditions highlights the presence of several small vacuoles containing electron dense material, previously described in literature as lysosome-like structures (**Figure 3.17 D** and **Supplementary Figure 2**) [217,218]. These structures are rarely observed in WT cells, whose vacuoles are mostly empty, and we speculate they may represent cargoes that accumulate during basal autophagy. When exposed to rapamycin, transgenic cells show a response similar to that observed in the WT, namely an increase in vacuole volume and convergence into a unique central vacuole. However, analysis of the mean vacuole surface over time reveals that the fusion of vacuoles is delayed in transformant strains and is significantly reduced at time points 8h and 12h compared to the WT (**Figure 3.17 B**). However, the formation of the large vacuole is achieved by time point 24h indicating that the process is not completely blocked (**Figure 3.17 A** and **B**). Indeed, in several vacuoles of *Avh195*-overexpressing cells it is possible to observe fusing autophagosomes (**Figure 3.17 D**). Similar structures were previously described in *Chlamydomonas* cells treated with concanamycin A, an inhibitor of autophagic flux [219]. Inside the vacuole it is also possible to identify cellular constituents among the digested cargoes such as membranous structures possibly originating from thylakoid fragments (**Figure 3.17 D**). Nonetheless, vacuoles of cells from the transgenic lines are heavily loaded with material during the whole analyzed period and are still not cleared at time point 24h (**Figure 3.17 D**).

Taken together our observation suggest that **cells overexpressing *Avh195* display a slowdown of autophagic flux and an impaired degradation of autophagic cargoes.**

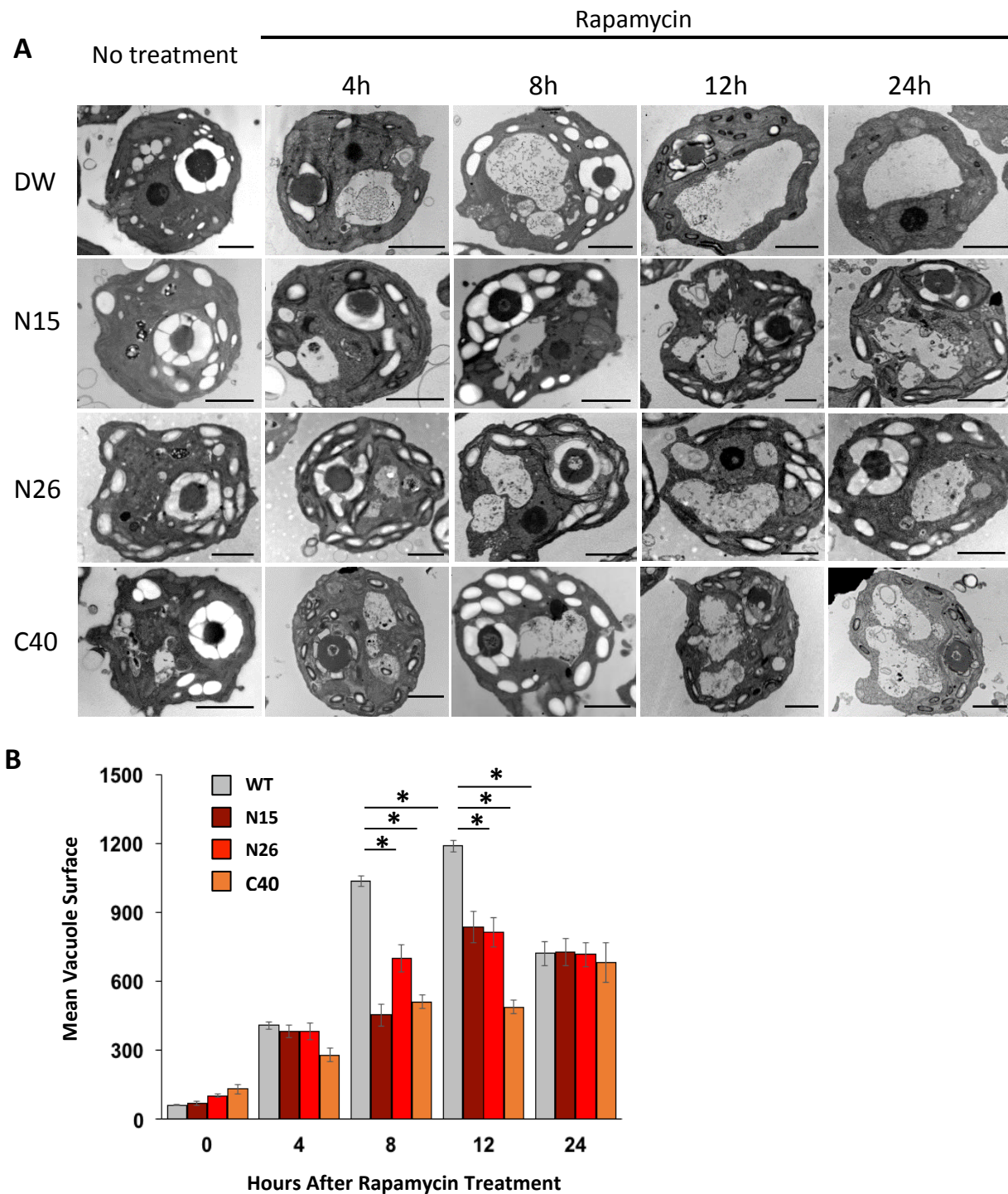


Figure 3.17: Subcellular phenotypes of *Chlamydomonas* cells expressing *Avh195*, as analyzed by TEM.

- A.** TEM micrographs of *Chlamydomonas* recorded at different time points after onset of light over a 12h-day/night cycle. Under non-induced conditions, WT cells (upper lane) contain several empty vacuoles that fuse upon the addition of rapamycin to form a predominant, large vacuole 4h after onset of treatment. Cells overexpressing *Avh195* display delay in central vacuole fusion, as well as accumulation of non-digested materials and starch. No obvious other modifications in the subcellular organization are related to effector expression. The bars represent 2 μ m.
- B.** Rapamycin-induced vacuole swelling is impaired in *C. reinhardtii* transformants expressing *Avh195*. For each line and time point of treatment, 4-5 independent TEM sections were analyzed for the presence of vacuoles. The surface of the biggest vacuole in each cell was determined using the ImageJ software. Shown are means (+/- SE) from n=30 vacuoles per line and time point of treatment. The asterisks indicate significant differences with p<0.05, as determined by Student's t-test. A.U. = Arbitrary Units.

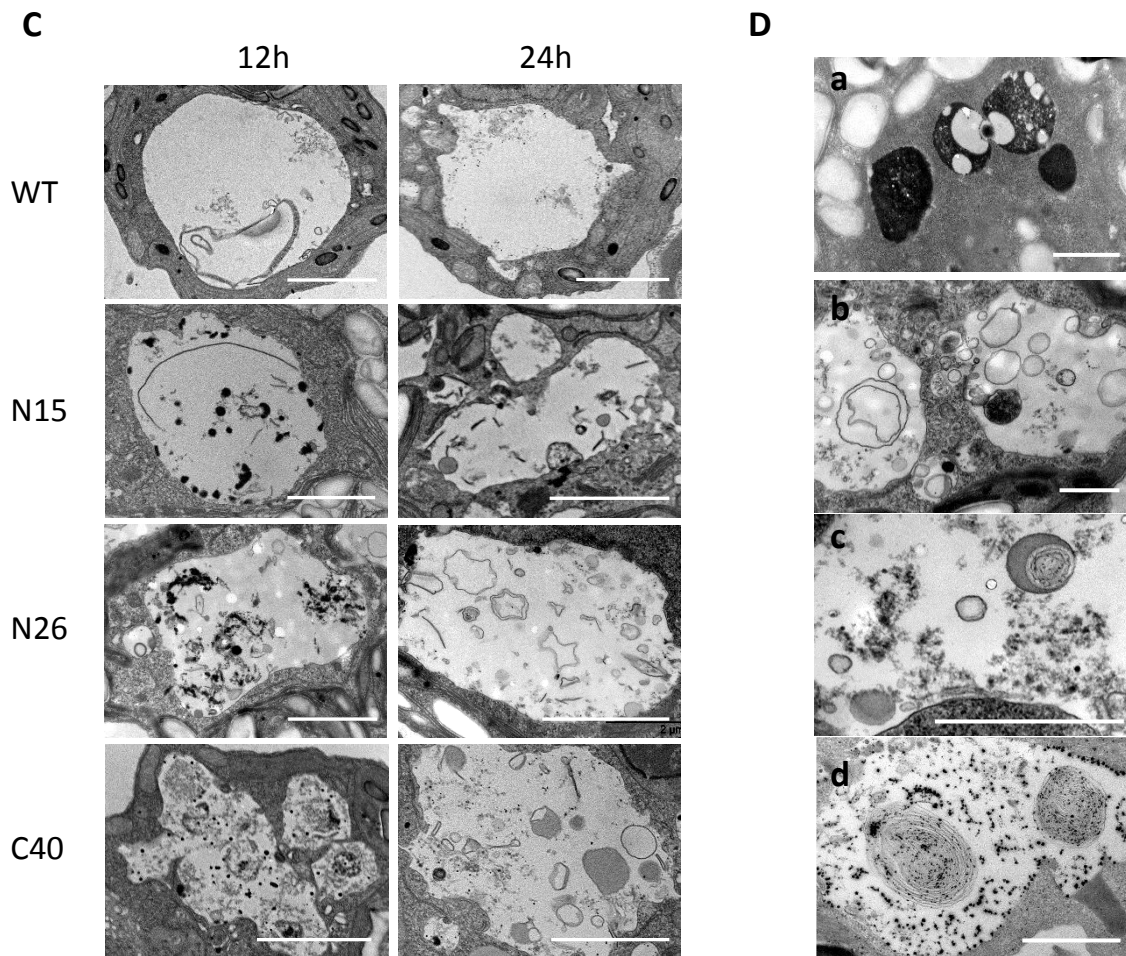


Figure 3.17: Subcellular phenotypes of *Chlamydomonas* cells expressing Avh195, as analyzed by TEM (continued).

- C. Enhanced views of vacuoles of WT and Avh195-expressing cells. Upon rapamycin treatment vacuoles start fusing and accumulate cargoes. At later time points (12h to 24h after rapamycin treatment), vacuoles are cleared in WT strain whereas in transformant strains still contain their undegraded cargo. Bars represent 2 μm .
- D. Enhanced view of vacuoles observed in *Avh195-overexpressing* strain N26. Without rapamycin treatment transformant strains contain several electron-dense, lysosome-like vacuoles rarely observed WT strain (a – 12h after the onset of light). Upon rapamycin treatment it is possible to recognize autophagosomes fusing to the central vacuoles (b, c – 4h and 12h after rapamycin treatment respectively) and cellular constituents such as membranous structures possibly originating from thylakoid fragments (c, d 12h and 8h after rapamycin treatment respectively). Scale bars represent 1 μm .

***Avh195* perturbrates starch metabolism in *Chlamydomonas* cells**

TEM observations of *Avh195*-expressing *Chlamydomonas* cells also revealed massive accumulations of starch granules in chloroplasts, when compared to the WT (**Figure 3.17 A**), suggesting that *Avh195* also influences starch metabolism.

Starch accumulation is considered as a major feature of photosynthetic organisms [32]. This form of sugar storage is synthesized during the day and degraded through respiration at night. Autophagy was shown to participate in starch degradation at night in plants, and starch accumulation was shown to be a consequence of autophagy inhibition both in *Arabidopsis atg* mutants and in plants treated with 3-methyladenine, an autophagy inhibitor [159]. In addition, high doses of rapamycin were recently shown to lead to an accumulation of starch during the light stage of the diurnal cycle [215].

We investigated the apparent starch accumulation by counting the number of starch granules per cell in the WT and the transgenic lines at 4 and 8 hours after the onset of the light period. We observed that the average number of granules per cell was higher in *Avh195*-expressing cells, reaching about 2 to 3-fold the amount determined in cells from WT cultures at time point 8h (**Figure 3.18 A**). In addition, we observed that rapamycin treatment did not significantly affect the number of starch granules (**Figure 3.18 A**).

This global starch accumulation might result from either enhanced starch synthesis or reduced starch degradation, or both. We thus assessed the relative mRNA level encoding of a subset of enzymes involved in both branches of starch metabolism. The targeted genes relevant to starch synthesis were *STA2*, which encodes GBSSI, the starch granule bound isoform of starch synthase, which is responsible of the synthesis of the minor amylose in *Chlamydomonas* [220] and *PGM1* encoding phosphoglucomutase, an enzyme that constitutes the first committed step of starch biosynthesis [221] and whose expression was found to be associated with over-accumulation of starch in *Chlamydomonas* [222]. Concerning starch degradation, we analyzed the expression of alpha-amylase 1 (*AMYA1*) a key enzyme involved in degradation of storage starch granule that was found to be downregulated in high-starch mutants of *Chlamydomonas*, and α -Glucan, water dikinase 1 (*GWD1*) a phosphorylating enzyme that promotes remobilization of starch from granules in plants [223].

For the analysis of transcript levels, synchronized cells from the WT and from lines expressing *Avh195* were harvested 4h and 8h after onset of the light period. Expression of genes related to starch biosynthesis was overall increased in transformant strains (**Figure 3.18 B**). When compared

to the WT, transcript levels of *PGM1* were higher in cells from the three transgenic lines at 4h after the onset of the light period, and higher for two out of three transformants at 8 h. Concerning *STA2*, expression was higher for two out of three transformants at 4h but not significantly increased at 8 h. On the other hand, expression of genes related to degradation of starch was moderately decreased compared to the WT (**Figure 3.18 B**). mRNA levels were significantly lower at 4h and 8h for both *AMYA1* and *GWD1* in cells from the transgenic line N15, whereas statistical significance was not reached for the two other strains, with the only exception of transcript levels of *AMYA1* in N26 cultures at time point 8h.

Taken together, these results **show that overexpression of *Avh195* leads to starch accumulation in *Chlamydomonas reinhardtii*, and that this phenotype likely results from a combination of an increase in starch biosynthesis and a slight decrease in starch degradation.**

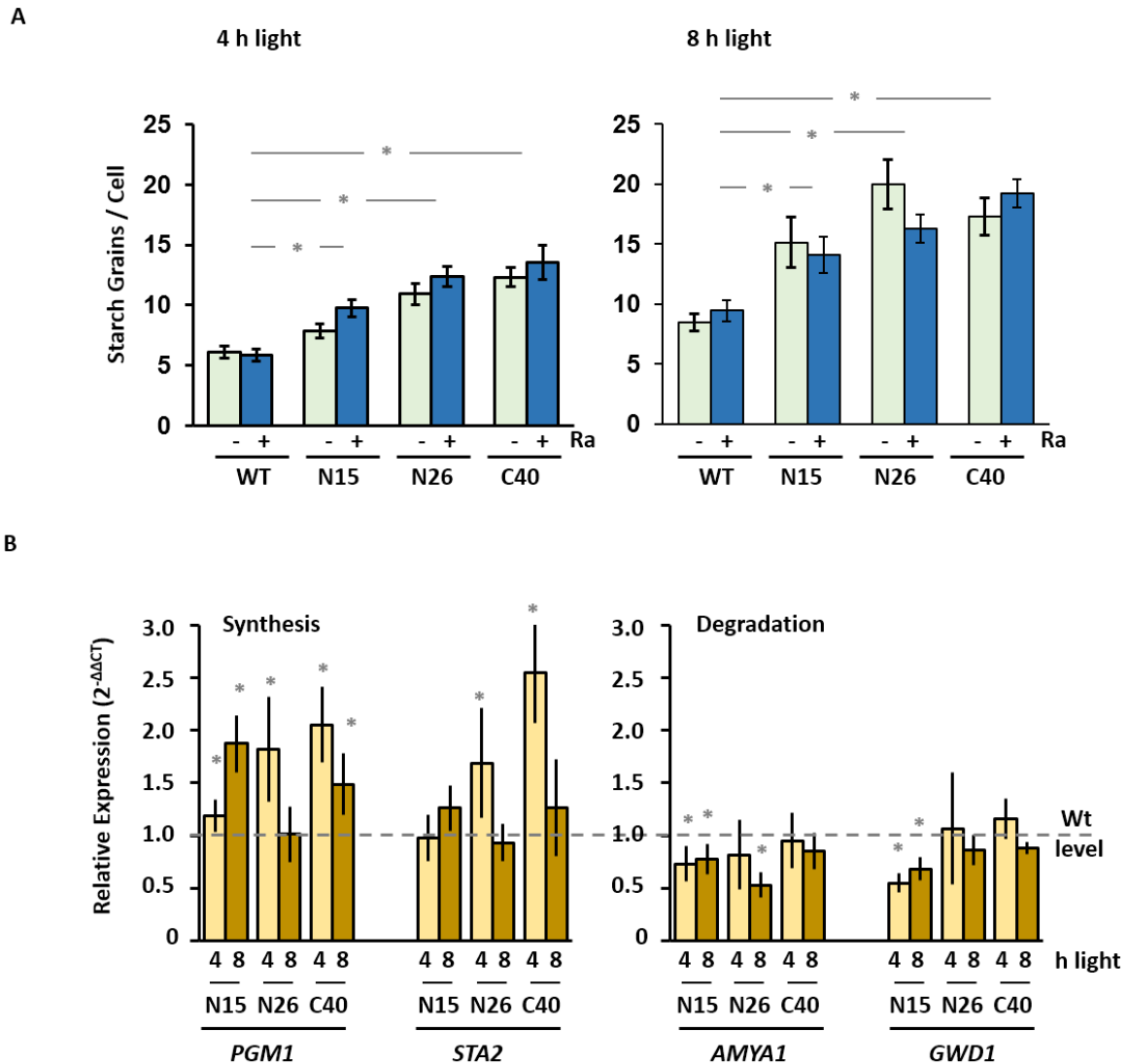


Figure 3.18: *C. reinhardtii* Avh195 transformants starch metabolism perturbation.

- A.** *Chlamydomonas* transformants expressing *Avh195* accumulate starch grains to significantly higher amounts than the WT, independent of rapamycin treatment. The number of starch grains was determined on micrographs from 5 independent TEM sections representing each 10-12 untreated cells, or cells that were treated for 8h with rapamycin (Ra). Shown are means (\pm SE) from $n=50$ cells per line and treatment. The asterisks indicate significant differences with $p < 0.05$, as determined by Student's t-test.
- B.** Expression of genes encoding the enzymes phosphoglycerate mutase 1 (PGM1) and starch synthase 2 (STA2) involved in starch synthesis, and alpha-amylase 1 (AMYA1) and alpha-glucan, water dikinase 1 (GWD1) required for starch degradation, was analyzed by RT-qPCR with cell samples collected at 4h and 8h after onset of the light period. Data were normalized with the constitutive *C. reinhardtii* genes *Cre02.g106550*, *Cre04.g227350*, and *Cre05.g232750*, and analyzed using the $\Delta\Delta C_t$ method, with wild-type expression as the reference. Shown are means (\pm SD) from 3 biological replicates. * indicates significant differences with $p \leq 0.05$, according to Student's t-test.

Avh195 moderately alters the accumulation of ATG8.

To further explore the Avh195-induced effects on Chlamydomonas autophagy, we analyzed whether the deceleration of autophagic flux observed in transgenic lines results from a transcriptional deregulation of the core machinery. We selected three genes associated to different steps of the process: *ATG6*, which participates in the early vesicle nucleation step [224], *ATG8*, because of its interaction with Avh195, and the SNARE *Vti1*, which mediates autophagosome docking and fusion to the vacuole, and therefore may reflect late steps of autophagy [225]. Compared to the WT, two out of three transformant lines display a slight but significant decrease in levels of *ATG6* transcripts, whereas all of them show increased levels of *VTI1* mRNA accumulation (**Figure 3.19 A**). This increase in mRNA levels was also observed for *ATG8* in all three *Avh195*-overexpressing lines (**Figure 3.19 B**).

To verify if this accumulation in *ATG8* transcripts reflects increased synthesis of ATG8 protein, we performed immunodetection of ATG8 in cells from the WT and the transgenic lines (**Figure 3.19 B**). Measurement of spot densities indicate 2.5-, 1.7-, and 2.5-fold increases of ATG8 protein levels in cells from lines N15, N26, and C40, respectively, when compared to the WT. We were not able to detect accumulation of lipidated ATG8, which has been widely used to monitor autophagy in a range of organisms. This post-translational modification is indicative of the covalent binding of ATG8 to phosphatidylethanolamine (PE), which is required to fulfil its function, and which can be experimentally monitored as the accumulation of a lower apparent molecular mass on SDS PAGE, corresponding to ATG8-PE [214,226]

Taken together those results indicate that **the overexpression of Avh195 in *C. reinhardtii* has slight impacts on the transcriptional regulation of autophagy-related genes, and on the accumulation of ATG8.**

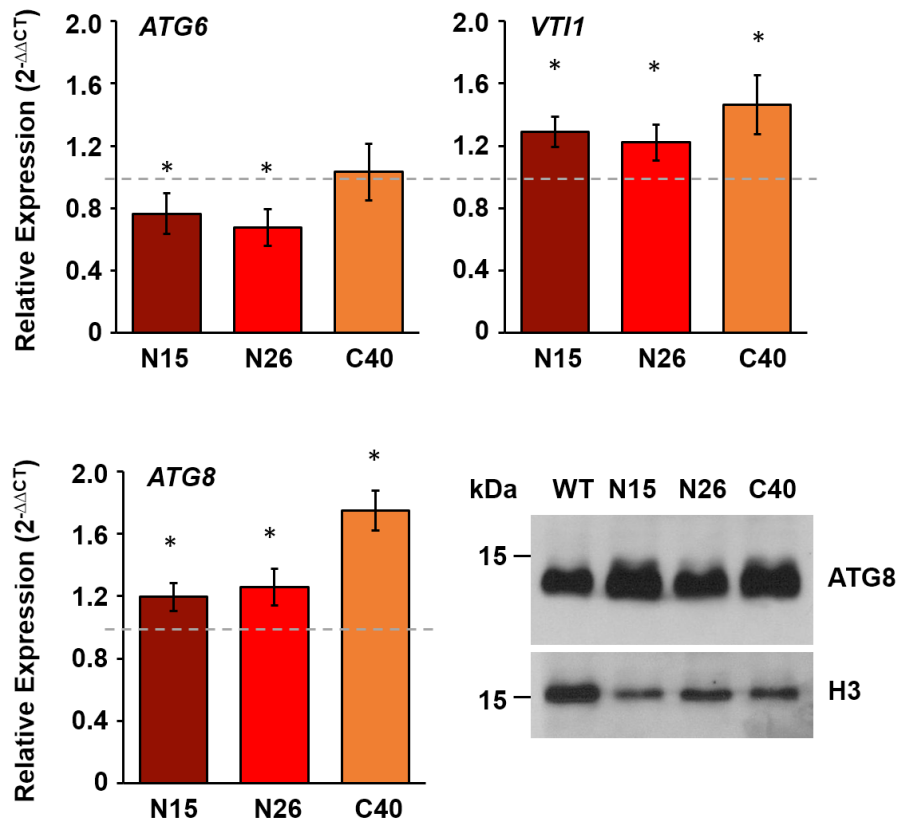


Figure 3.19: Overexpression of Avh195 in *C. reinhardtii* only moderately changes the accumulation of autophagy-related gene transcripts and of ATG8 protein.

- A.** RT-qPCR analysis of transcripts encoding ATG6, a protein of the membrane-associated PI3K complex, and VTI1, a SNARE protein involved in autophagosome fusion with the vacuole, in transgenic *C. reinhardtii*. ATG6 transcripts (left) show a rather reduced accumulation in the *Avh195*-overexpressing lines, N15 and N26, but not in line C40. Transcripts encoding VTI accumulate to slight but significantly higher extents in all 3 transgenic lines.
- B.** RT-qPCR analysis of transcripts encoding ATG8 (left) and immunoblot analysis of ATG protein accumulation (right) in transgenic *C. reinhardtii*. ATG8 mRNA accumulates weakly, but to significantly higher amounts in all transgenic lines. This is reflected by moderately increased ATG8 protein accumulation in the *Avh195*-overexpressing lines. An antibody directed against histone H3 was used as loading control. Measurements of spot densities indicate 2.5-, 1.7-, and 2.5-fold increases of ATG8 accumulation in lines N15, N26, and C40, respectively, when compared to the wild-type line DW.

RT-qPCR data were normalized with the constitutive *C. reinhardtii* genes *Cre02.g106550*, *Cre04.g227350* and *Cre05.g232750* [210], and analyzed using the $\Delta\Delta C_t$ method, with wild-type expression (line DW) as the reference. Shown are means \pm SD from 3 biological replicates. * indicates significant differences with $p \leq 0.05$, according to Student's t-test.

The results presented in this part of the work show that overexpression of *Avh195* in *C. reinhardtii* does not affect cell physiology and fitness but leads to a slowdown of the autophagic flux. This effect of *Avh195* is not related to a loss in responsiveness of cells to autophagic stimuli (here represented by inhibition of TOR signaling pathway), but rather affects autophagosome formation and subsequent degradation steps. This leads to the observed delay in the coalescence of vacuoles and the long-lasting accumulation of cellular debris within the central vacuole. The effect of *Avh195* also correlates with an accumulation of starch granules, which appears mainly related to a stimulation of biosynthesis. Furthermore, *Avh195* only moderately impacts the transcription of autophagy-related genes and the accumulation of ATG8 protein.

Taken together, our results indicate that *Avh195* acts as transient restrainer of autophagic flux, rather than an inhibitor of autophagy.

3.4 Role of Avh195 during the host-pathogen interaction

To elucidate the role of Avh195 in the plant-pathogen interaction, we generated transgenic Arabidopsis lines (ecotype Col-0) harboring the *Avh195* coding region under the control of the constitutive Cauliflower Mosaic Virus (CaMV) 35S promoter. We selected 2 independent transgenic lines (Avh195-OE6 and Avh195-OE9) that accumulate significant amounts of Avh195 transcripts (**Figure 3.20**).

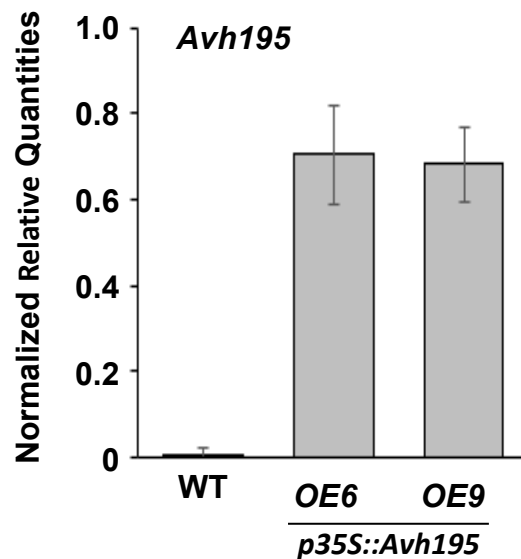


Figure 3.20: Expression levels of Avh195 in two independent transgenic *A. thaliana* lines

The expression of *Avh195* in plants from the WT and 2 transgenic lines was analyzed by RT-qPCR. Data were normalized with transcripts from the constitutive Arabidopsis gene At5g11770. Shown are the means (\pm SD) from 2 replicates.

3.4.1 Avh195 increases plant susceptibility to *P. parasitica* infection

The two lines were used to evaluate whether overexpression of *Avh195* has direct consequences on pathogen development. Seeds from homozygous transgenic lines and from the WT were inoculated with zoospores from *P. parasitica*. The development of the oomycete within plant tissues, and the evolution of different stages of the *P. parasitica* infection cycle were determined by RT-qPCR using samples of infected plants that were collected 10h, 20h, 30h, 48h, 96h, and 144h after inoculation.

For evaluating oomycete growth, we evaluated the expression of the *P. parasitica* gene *WS41*, which is widely accepted as being constitutively expressed during plant infection [44,227], and correlated the levels of transcript accumulation with the evolution of oomycete biomass. Transcripts of *WS41* became clearly detectable at 48hpi and accumulated to significantly higher levels in the two

transgenic lines, when compared to the WT (**Figure 3.21 A**). The differences in biomass increase between the transgenic lines and the WT were still detected at 144hpi. We thus concluded **that plants expressing *Avh195* were significantly more susceptible to *P. parasitica* than WT plants.**

3.4.2 *Avh195* does not repress plant defenses

To analyze whether this increased susceptibility results from an *Avh195*-mediated repression of plant defense responses, we evaluated the expression profiles of genes encoding Pathogenesis-Related protein 1 (*PR1*), a salicylic acid (SA) responsive gene that is associated with responses to biotrophic pathogens, and encoding the plant defensin *PDF1.2* which is regulated by ethylene and jasmonate signaling and is thus associated with responses to necrotrophs [228].

The RT-qPCR experiments revealed that the amounts of transcripts of both genes were not reduced in the transgenic lines (**Figure 3.21 B**). The analysis furthermore indicated that *PR1* expression follows a biphasic curve in both transformants, with a first discrete peak occurring at 10hpi, followed by a second wave of expression reaching a maximum at 30hpi (**Figure 3.21 B** left panel) By contrast, *PR1* was expressed in the WT with a single peak occurring at 48h. We also noted that the expression level of *PR1* dropped more rapidly in plants expressing *Avh195* than in the WT. A similar situation was observed when we compared the expression of *PDF1.2* between the transgenic lines and the WT. Here, too, expression showed a biphasic profile in the transgenic lines with a first peak of *PDF1.2* transcripts accumulating at 10hpi. A second wave of expression in the infected transgenic lines was reflected by a strong accumulation of *PDF1.2* transcripts at 30 to 48hpi, preceding and exceeding the highest levels of expression in the WT occurring at 48h (**Figure 3.21 B** right panel).

Upon infection, plants overexpressing *Avh195* thus exhibit an acceleration and, in the case of *PDF1.2*, an intensification of defense responses, rather than a repression. **This indicates that the increased susceptibility to *P. parasitica* of the transgenic lines is not related to an *Avh195*-triggered impairment of defense responses.**

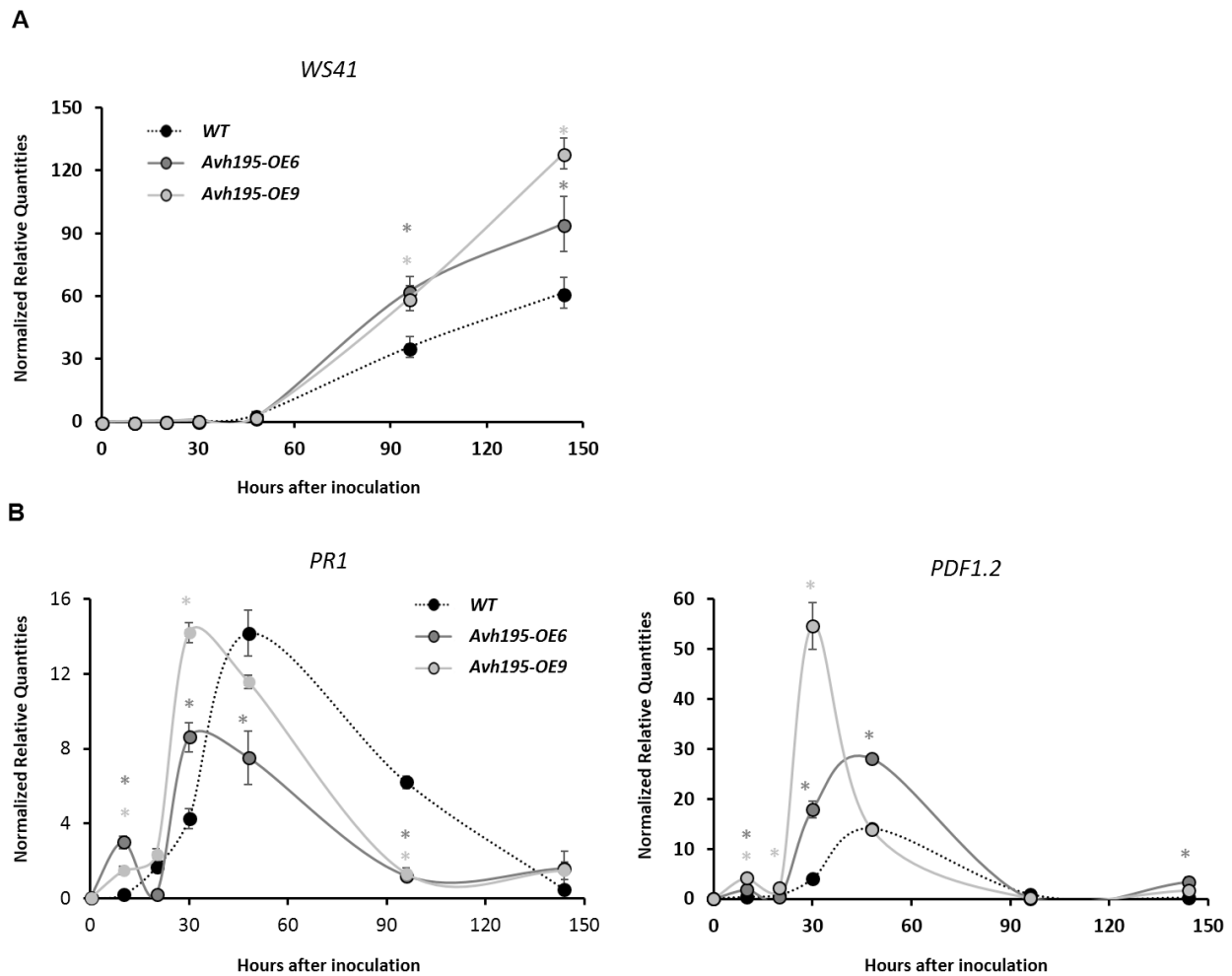


Figure 3.21: Avh195 promotes infection and changes the timely onset of plant defense responses.

Plants from the wild-type and from the transgenic *Arabidopsis* lines *Avh-OE6* and *Avh-OE9* were inoculated with *P. parasitica* zoospores and harvested at different time points after inoculation. RNA extracted from the samples were analyzed by RT-qPCR for the expression of marker genes allowing to analyze the development of oomycete biomass (A), the onset of plant defense responses (B).

- A. Oomycete biomass within plant tissues was determined by quantifying the accumulation of transcripts from the constitutively expressed *P. parasitica* gene *WS41*. RT-qPCR data were normalized with transcripts from both a constitutively expressed *P. parasitica* gene encoding a ubiquitin conjugating enzyme (*UBC*) and the constitutive *Arabidopsis* gene *At5g11770* encoding an NADH-Ubiquinone Oxidoreductase.
- B. The onset of plant defenses responses was assessed by determining the amounts of transcripts from the SA-dependent *PR1* gene, and from the JA- and ethylene-dependent *PDF1.2* gene, which are markers for defense responses against biotrophic and necrotrophic pathogens, respectively. RT-qPCR data were normalized with transcripts from the constitutive *Arabidopsis* gene *At5g11770*.

Shown in A-B are the means (+/-SD) from 3 replicates. Asterisks indicate significant differences with $p \leq 0.05$, according to Student's t-test.

3.4.3 *Avh195* promotes necrotrophy

To determine whether increased susceptibility of the transgenic plants results from changes in the *P. parasitica* life-cycle, we estimated the relative expression of *Phytophthora* genes that characterize the states of biotrophy, necrotrophy, and sporulation. Biotrophic and necrotrophic pathogen development were assessed by analyzing the expression of *HMP1* and *NPP1*, respectively (as described in Section 3.1.1). Sporulation of the oomycete was quantified *via* the expression of the *P. parasitica* ortholog of the sporulation-specific *CDC14* gene encoding a cyclin-dependent kinase that regulates the cell cycle, specifically expressed during sporulation [229].

Expression of *HMP1* in the WT followed the previously observed transient profile, with maximum transcript accumulations at 10hpi, and constant decline afterwards. At this time point, *HMP1* expression was lower in both transgenic lines, which instead accumulated significantly higher amounts of transcripts during a second wave of expression at 48hpi (**Figure 3.22**). By contrast, the expression of *NPP1* was accelerated in both transgenic lines, with transcripts starting to accumulate between 10 and 20hpi. In the WT, *NPP1* expression became detectable at 30hpi. Furthermore, the amounts of *NPP1* transcripts were significantly increased in plants from both transgenic lines, when compared to the WT, accumulating to maximum amounts between 30 and 48hpi and then declining continuously (**Figure 3.22**). Surprisingly, expression of the sporulation-associated *CDC14* gene was markedly decreased in plants expressing *Avh195*, when compared to the WT, at the later stages of infection between 96 and 144hpi (**Figure 3.22**). These experiments thus suggested that *P. parasitica* entered earlier the necrotrophic stage of infection in *Avh195*-expressing plants, and that this step of the life cycle was extended before the pathogen initiates reproduction. The correlation between an increased and accelerated expression in the transgenic lines of both *NPP1* by *P. parasitica*, and of *PDF1.2* by plants insinuates that *Avh195* promotes necrotrophy. If this is true, *Avh195* overexpressing lines should be more susceptible to infection with necrotrophic pathogens and more resistant to biotrophs.

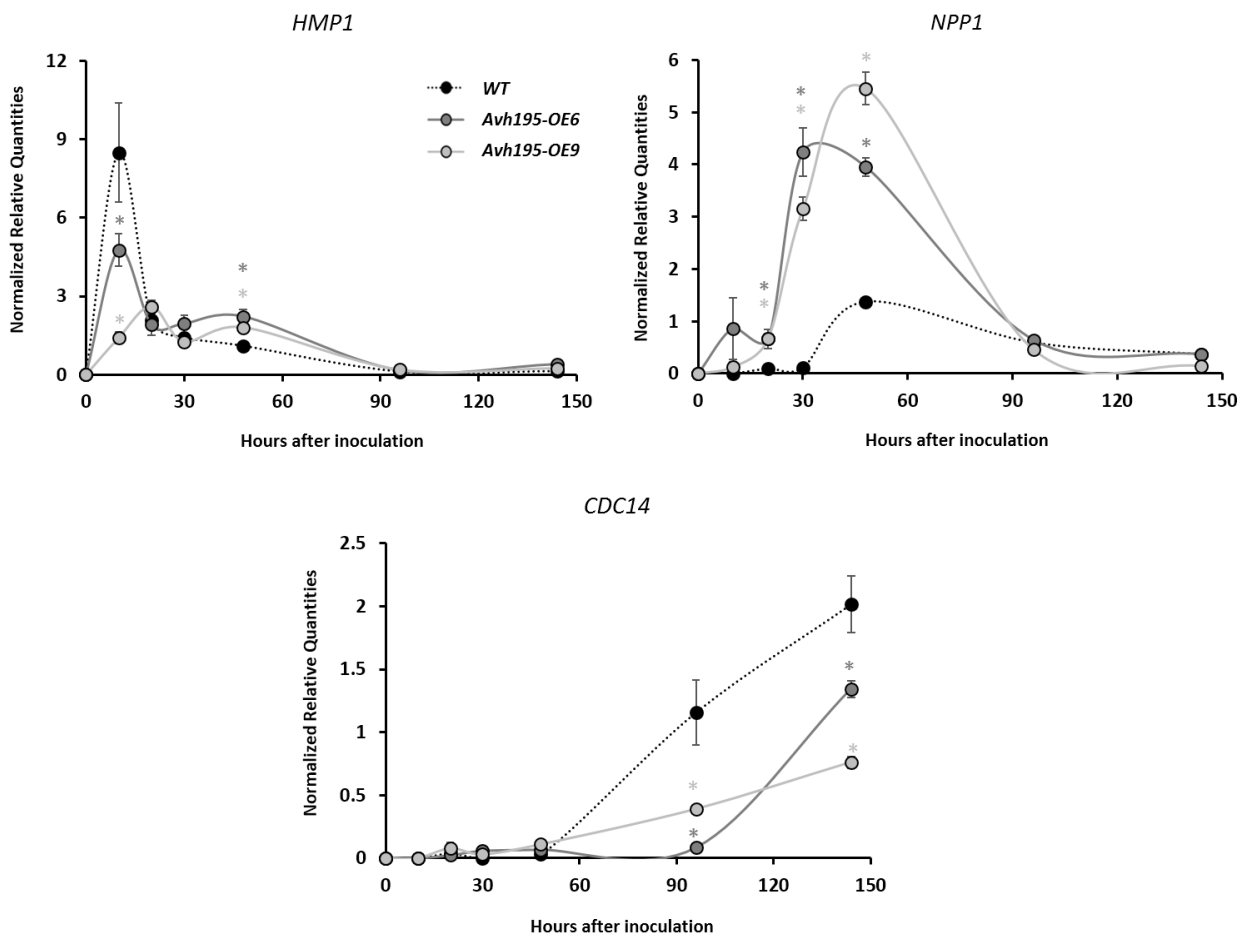


Figure 3.22: Expression of Avh195 in *A. thaliana* changes the timely onset of oomycete life style.

Plants from the wild-type and from the transgenic *Arabidopsis* lines *Avh-OE6* and *Avh-OE9* were inoculated with *P. parasitica* zoospores and harvested at different time points after inoculation. RNA extracted from the samples were analyzed by RT-qPCR for the expression of marker genes encoding Haustorium-specific Membrane Protein 1 (HMP1), Necrosis-inducing *Phytophthora* Protein 1, and the protein phosphatase CDC14, which represent marker genes for biotrophic growth, necrotrophy, and sporulation, respectively of *P. parasitica*. RT-qPCR data were normalized with transcripts from the constitutive *Phytophthora* genes WS41 and UBC. Shown are the means (+/-SD) from 3 replicates. Asterisks indicate significant differences with $p \leq 0.05$, according to Student's t-test.

We thus inoculated plants from the transgenic lines and from the WT with the obligate, biotrophic pathogen, *Hyaloperonospora arabidopsidis* (*Hpa*). To estimate the infection success, we determined the amount of asexual conidiospores that are produced at the end of the infection cycle. Sporulation rates were significantly higher in plants from the transgenic lines, when compared to the WT, thus indicating that Avh195 confers the plants with increased susceptibility to the biotrophic pathogen, rather than with increased resistance (**Figure 3.23**).

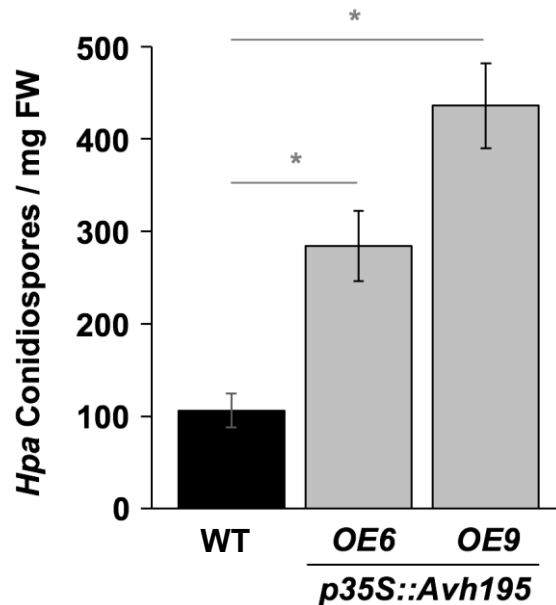


Figure 3.23: Overexpression of Avh195 in *A. thaliana* promotes susceptibility to biotrophic *H. arabidopsidis*.

Conidiospore production on wild-type (WT) Arabidopsis, and on 2 independent *Avh195*-overexpressing lines. The amount of conidiospores per mg fresh weight (FW) increased at least 3-fold in the transgenic lines, when compared to WT Arabidopsis. The bars represent mean values \pm SE for 20 samples. Statistically significant differences with $p \leq 0.001$ were determined by Student's t-test and are indicated with an *. The graph shows a representative experiment among 3 repetitions.

The data from the transgenic approach taken together show that the **Avh195 effector promotes infection by oomycete pathogens, which have either a biotrophic or a hemi-biotrophic lifestyle.**

To bring the Avh195-mediated early switch to necrotrophy in line with increased susceptibility to a pure biotroph, we suggest that the effector ameliorates the biotrophic stage of *P. parasitica* immediately after penetration. This might improve the early establishment of the pathogen in plant tissues and accelerate its development, which reflects as a faster switch to necrotrophic growth.

3.5 Trans-kingdom activity of Avh195

3.5.1 *Avh195 induces accumulation of acidic compartments in HeLa cells.*

During the setup of this work, besides the transient and stable transformations of plants and algae, we developed an additional approach that aimed at producing Avh195 protein for the exogenous application to cells from different model systems. We set up two different heterologous expression systems for the production of recombinant Avh195. The first one is *Escherichia coli*, for a rapid high-yield production and the second is *Pichia pastoris* to conserve post-translational modifications, such as glycosylation.

In both cases, yields were low. The recombinant proteins were poorly soluble in aqueous buffer, a finding that we could explain later by the membrane association of the effector (Section 3.2 of this Chapter). In addition, purification of the protein was not fully efficient or resulted in precipitation of the sample. Quantities and quality of the obtained protein were thus low, and we decided to abandon the approach for large scale analyses.

However, we obtained small quantities of soluble His-tagged Avh195 (**Avh195-His**) produced in *E. Coli*, which we used to perform qualitative assays on mammalian cultured cells in collaboration with the laboratory TOXALIM (INRA). We decided to perform our tests on HeLa cells, an immortalized human cell line, which was derived from cervical cancer cells that were taken from Henrietta Lacks in 1951. Those cells have an intact and well-defined autophagy pathway and are frequently used for studying autophagy and cell death. Since animal models are better explored than photosynthetic organisms for all mechanistic connections that exist between autophagy and PCD, and because numerous tools and assays are available to exploit the system [230], we considered this model as an alternative to validate the function of Avh195. Moreover, the analysis of autophagy perturbation of a non-photosynthetic organism, would further confirm the generality of the effector, which already demonstrated the ability to bind ATG8 proteins from both *Chlamydomonas* and *Arabidopsis* models.

To analyze the effect of recombinant purified Avh195-His on HeLa cells, we applied different doses of the protein on cultures of the human cell line. We first observed the uptake of Avh195 by HeLa cells over time. As shown in **Figure 3.24**, Avh195 accumulates mainly in the cytoplasm in a time-dependent manner, as shown by the immunofluorescence assay directed against the His tag. The observation of cells at 24h after the treatment with Avh195 also revealed that the protein induces

the formation of numerous refringent vesicles, readily visible under light microscopy (**Figure 3.25**). The aspect of those vesicles closely resembles the structures that accumulate in cells following treatment with chloroquine, a prototypical inhibitor of the fusion between autophagosomes and lysosomes leading to the accumulation of autophagic vesicles [231].

To characterize the nature of these structures, we used LysoSensor® DND189 to monitor the number of acidic compartments after Avh195 treatment. The number and the size of LysoTracker-positive structures were increased after Avh195 treatment in a dose-dependent manner. The effect of Avh195 on acidic vacuole accumulation was weaker than chloroquine but occurred in the same range of concentrations (**Figure 3.26**).

These results indicate that Avh195 induces accumulation of acidic compartment in HeLa cells, reflecting the activity of the autophagic flux inhibitor chloroquine.

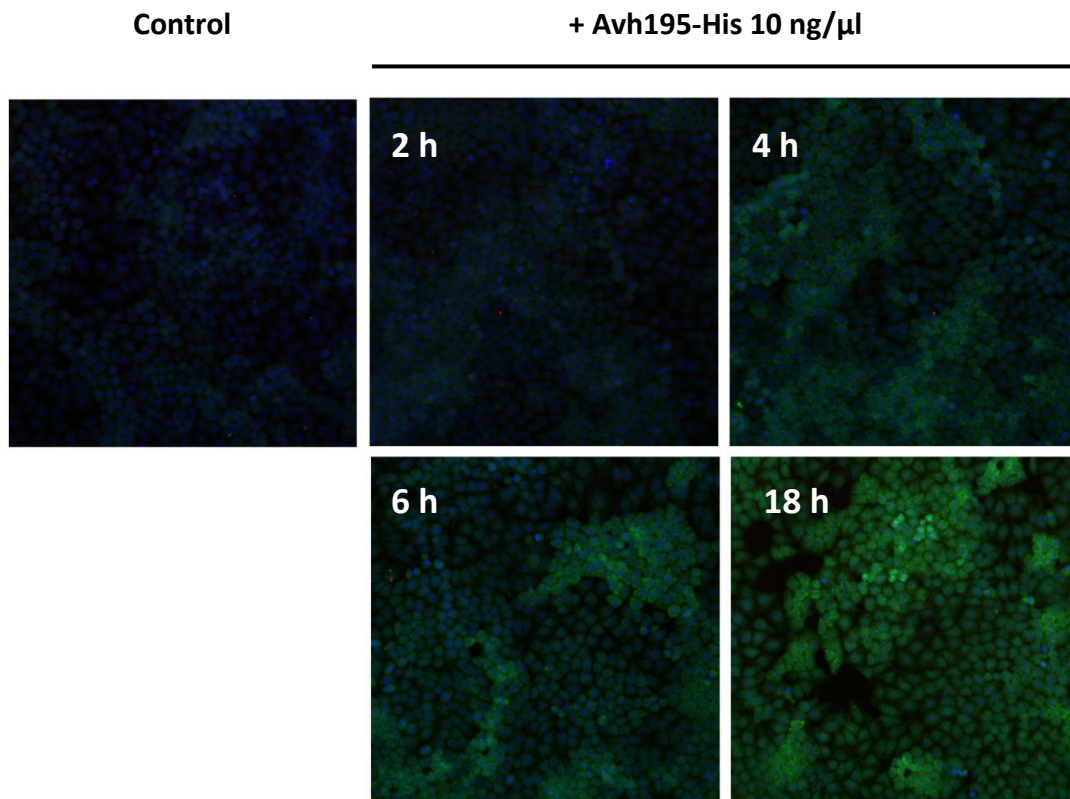


Figure 3.24: Exogenous Avh195 is taken up by mammalian cells.

HeLa cells were exposed to 10 ng/μL of Avh195-His protein. At the indicated time, cells were fixed and processed for indirect immunofluorescence analysis for the detection of Avh195 using anti-His antibody (green) and nuclei (Hoechst 33342, blue). Images were acquired with an inverted fluorescence microscope (Nikon®) equipped with a CCD camera (ORCA ER®, Hamamatsu Photonics), at 20× magnification.

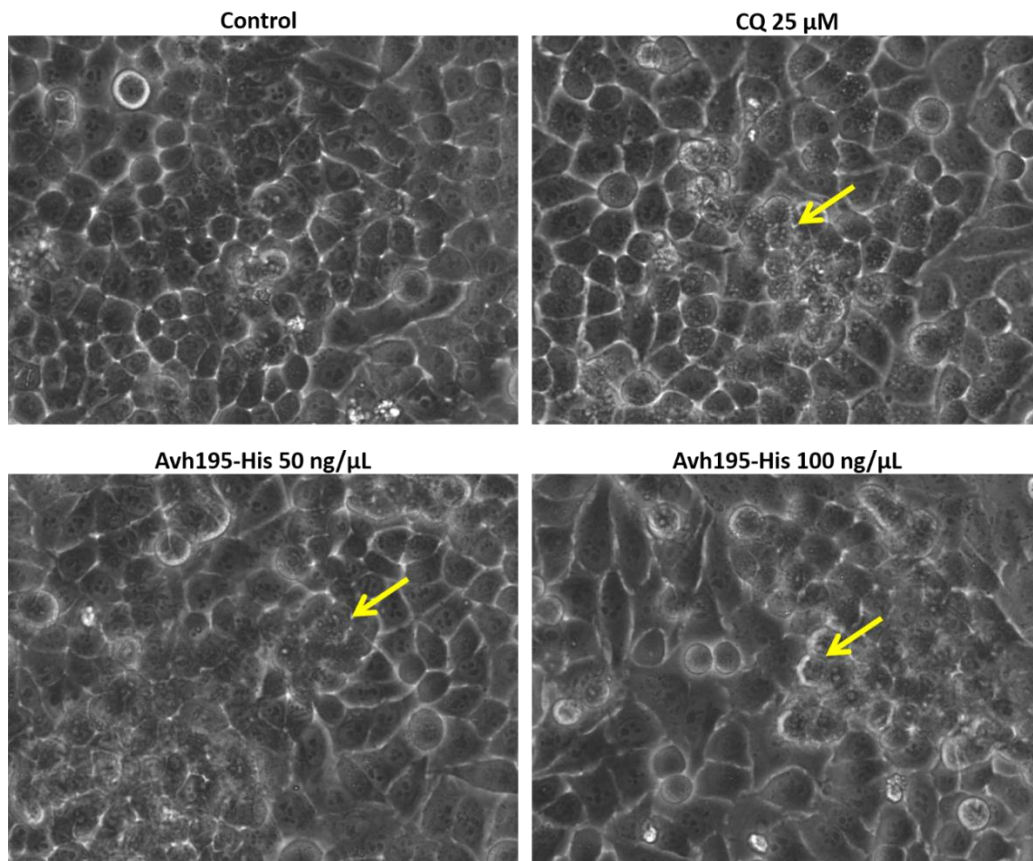


Figure 3.25: Morphological modifications induced by Avh195 treatments.

Phase contrast images of HeLa cells exposed for 24h to 25μM Chloroquine (CQ), an inhibitor of autophagy or 50 and 100ng/μL of Avh195-His purified protein. The arrow points cells presenting accumulation of refringent vesicles (granularity in the body of the cell) that are typically observed upon autophagy inhibition with Chloroquine. Cell morphology was examined under a light microscope (Nikon®) equipped with a CCD camera (ORCA ER®, Hamamatsu Photonics), at 20× magnification.

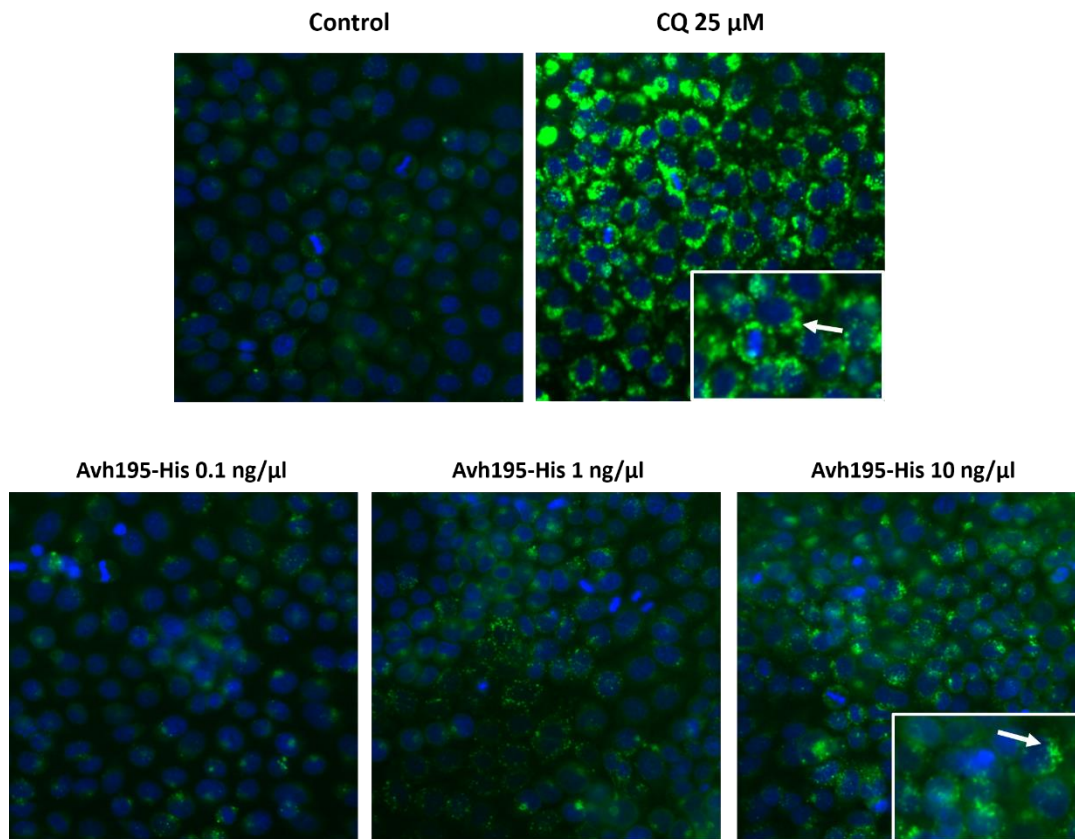


Figure 3.26: Exogenous Avh195 increases the accumulation of acidic vesicles.

HeLa cells were exposed to increased concentration of purified Avh195 (from 0.1 to 10 ng/μL) or 25 μM of Chloroquine (CQ) used for positive control for 24 h. Cells were then incubated with LysoSensor DND189 (green) and Hoechst 33342 (blue) for the detection of acidic vesicles and nuclei, respectively. Images were acquired with an inverted fluorescence microscope (Nikon®) equipped with a CCD camera (ORCA ER®, Hamamatsu Photonics), at 20× magnification.

3.5.2 Heterologous expression of Avh195 is cytotoxic for HeLa cells

To further elucidate the effect of Avh195 on the autophagic process, we decided to express a fusion protein of Avh195 coupled through its N- or C-terminus to green fluorescent protein (GFP) in HeLa cells. Under normal culture conditions, WT HeLa cells display an epithelial-like morphology, namely by forming a monolayer of polygonal adherent cells (**Figure 3.27 A**). Upon transfection with Avh195 overexpression vectors we observed a high cytotoxicity phenomenon, when compared to Mock treatments (Lipofectamine® 2000) or upon empty vectors transfections (**Figure 3.27 A**). This toxicity was reflected by phenotype alterations of the Avh195-expressing cells. Cells displaying the GFP signal of the Avh195 construct were spheroid and shrunken ((**Figure 3.27 A**, arrows and **B**). This phenotype eventually evolves to apoptosis-like cell death (**Figure 3.27 A**, arrowheads). Because of the cytotoxic effect of Avh195 on HeLa cells, it was impossible to perform molecular and biochemical assays to characterize the impacts of Avh195 on the autophagic process. We thus withdraw these analyses from the project.

However, the assays that we performed with HeLa cells further support the results that we obtained on *Chlamydomonas reinhardtii*. Here, Avh195 seems to interfere with autophagic flux like chloroquine, thus leading to the accumulation of autophagic vesicles. The toxic effects we observed with HeLa cells might reflect the lethal effects we observed upon heat-shock-induced overaccumulation of Avh195 in *Chlamydomonas* transgenic cells

To our knowledge, this work on the whole represents the first demonstration that an effector from a plant pathogen can provoke physiological alterations in cells from organisms, which are evolutionary as distant as plants, mammals, and algae, by targeting non-specifically conserved components of the autophagy machinery.

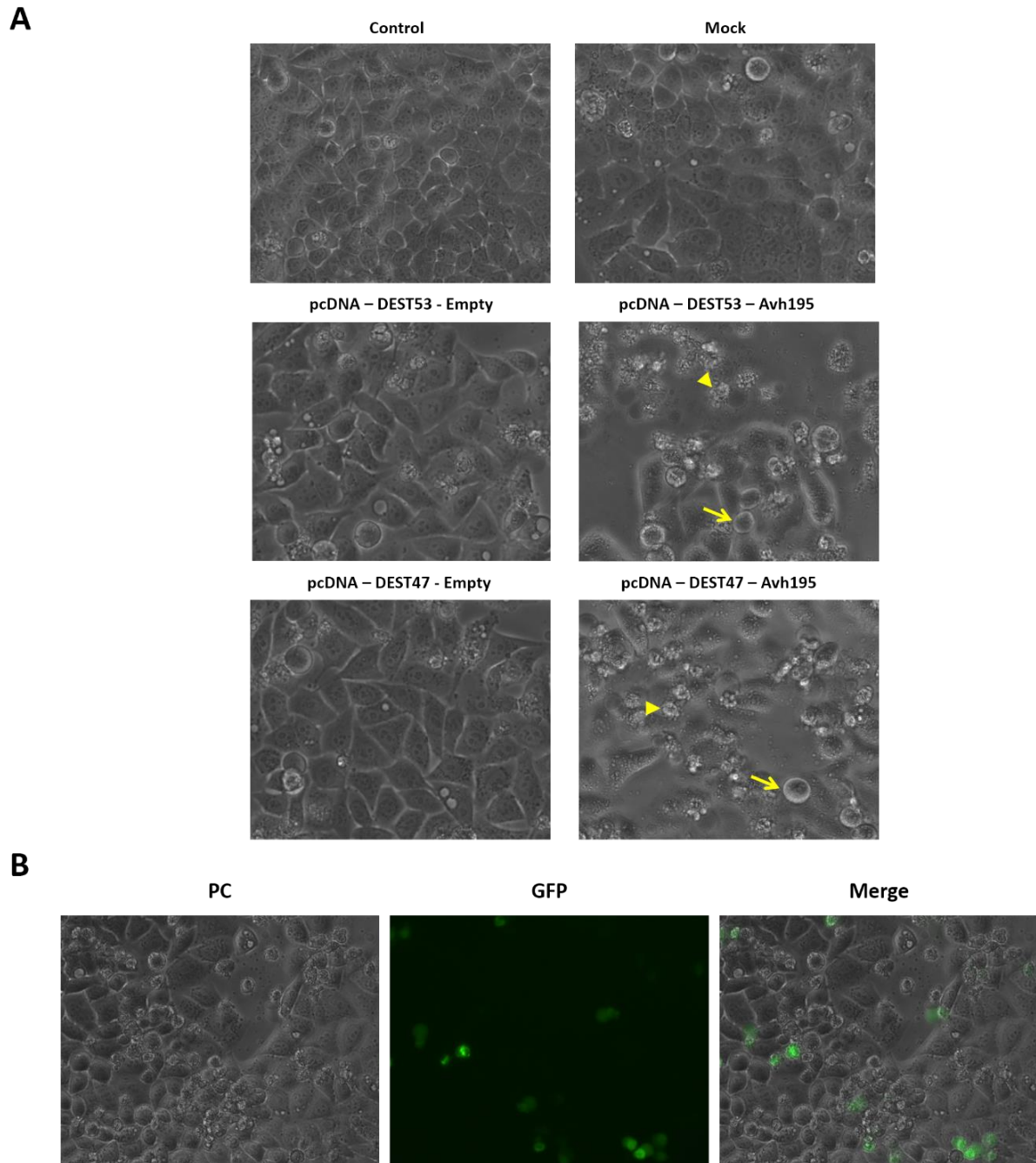


Figure 3.27: Morphological effect of Avh195 transfection.

- A.** Phase contrast images of HeLa cells transfected with vector encoding Avh195 tagged with green fluorescent protein (GFP) on the N-terminal (pcDNA-DEST53 constructs) or C-terminal (pcDNA-DEST47 constructs) as well as the corresponding empty vectors, using Lipofectamine® 2000. Control and Mock (upper lane) represent cells not exposed or exposed to Lipofectamine® 2000 alone respectively. Arrows indicate detached cells presenting spheroid and shrunk phenotype while arrowheads indicate apoptotic cells presenting membrane blebs.
- B.** Phase contrast (PC), Fluorescence (GFP) and merged images of HeLa cells transfected with Avh195-GFP encoding plasmid (pcDNA-DEST 47-Avh195-GFP) using Lipofectamine® 2000, 48 hours post-transfection. Cells expressing the foreign gene display green fluorescence and an altered phenotype.

Chapter 4: Discussion

This PhD work consisted in the molecular and functional characterization of a secreted effector protein from the plant pathogen *Phytophthora parasitica*, which takes part in the determination of the outcome of infection. We show in different photosynthetic systems that the *P. parasitica* Avh195 effector interferes with autophagy through interaction with ATG8. The effector thus slows down autophagic flux to favor pathogen development within host tissues.

As described in the introduction, the endomembrane system is composed of a set of membranous structures and organelles that form a functional unit dedicated to the trafficking of material through different compartments of the cells. In plants, this complex network emerged as essential for exchanges between plant and pathogens [232]. Numerous studies have shown that it is involved in endocytosis and signaling of immune receptors, the exocytosis of defense molecules, the relocalisation of proteins between different cellular compartments as well as their recycling. Given its importance for plant immunity, pathogens have evolved strategies to hijack the endomembrane system for the success of infection. One of the emerging targets is autophagy, a critical process in cell survival and homeostasis. During plant-pathogen interactions, autophagy enhances the survival of plant cells by degradation of damaged and toxic materials, and has an antimicrobial role, ensuring the degradation of pathogen-derived molecules [100].

During the last years, the effector protein PexRD54 from the oomycete *Phytophthora infestans* has been described as a perturbator of autophagy and endomembrane trafficking [89]. This protein is an RxLR effector, a typical class of secreted molecules that is translocated to the host cytoplasm during infection. The described interference of PexRD54 with autophagy in the host, represents the first report for such activity among this class of effectors. As described in the introduction PexRD54 is an interactant of ATG8CL, one of the nine members of the ATG8 family in potato (*S. tuberosum*). During infection, the autophagosomes labelled with ATG8CL are loaded with defense-related molecules, thanks to the cargo receptor Joka2, and are diverted towards the pathogen interface to restrict its growth. The binding of PexRD54 with ATG8CL not only disrupts the binding of Joka2, preventing the loading of antimicrobial autophagosomes, but also stimulates the formation of autophagosomes, thus providing membrane for the biogenesis of the EHM [89,188].

The RxLR effector presented in this work, Avh195, was initially identified as a potential perturbator of autophagy due to the presence of five ATG8-interacting motifs in the effector domain of the protein.

To test the actual existence of an interaction between Avh195 and ATG8, and to analyze effector activity, we developed the microalga *Chlamydomonas reinhardtii* as a model. The choice of this organism was initially driven by the genetic background of the microalga: the sequencing of nuclear and chloroplast genomes has been completed and annotated, revealing conservation of many genes of the photosynthetic lineage [200]. *Chlamydomonas* possesses most of the genes encoding the ATG core machinery, which are, unlike the situation in plants, single copy genes with conserved function in the microalga [143]. Phylogenetic analysis of the ATG8 gene family in *Arabidopsis thaliana* revealed the presence of 9 members, which diverge into three clades and differentiated in function and regulation. CrATG8 was identified as closely related to members of clades I and II, thus potentially representing 7 out of 9 members of Arabidopsis ATG8 gene family. This simplification has permitted to setup several techniques that collectively demonstrated the colocalization of Avh195 with the membrane-bound pool of ATG8, and the existence of an interaction between the two proteins. Interestingly, this interaction was not only confirmed for two members of Arabidopsis ATG8 gene family belonging to the clades I (ATG8D) and II (ATG8G), the most closely related to CrATG8, but also for ATG8H, a divergent paralog belonging to clade III. This result, besides validating the use of a simplified model organism, also indicates that the action of Avh195 is generalist since it targets multiple isoforms of ATG8. This result contrasts with the specificity of PexRD54: this effector binds the isoform ATG8CL, but not ATG8IL, another member of the protein family.

In addition to the single-gene status of ATG8, *Chlamydomonas* was retained as a heterologous system for functional analyses aiming to decipher the precise mechanism underlying the modulation of autophagy. Indeed, one of the advantages of this microalga is that foreign genes can be stably introduced in its genomes [233]: in our case we introduced Avh195 in *Chlamydomonas* nuclear genome to obtain constitutive overexpression of the effector. Since *Chlamydomonas* is amenable to flow cytometry without any preliminary treatment, maintaining the integrity of the organism, one can control whether effector expression in the cells has aberrant effects, before proceeding to further analyses. In *Chlamydomonas* expressing *Avh195*, we did not observe modifications other than the perturbation of autophagic flux and the accumulation of starch granules.

Chlamydomonas presents several other advantages to decipher effector biology, beyond autophagy-related studies. The synchronization of cultures is easily achieved by alternate light and dark periods, with two to three generations in a 24-hour period [209]. This synchronization generates homogeneous biological material, ensuring reliable monitoring for time-course studies.

For the analysis of perturbation of autophagy by Avh195 we choose to activate the machinery via inhibition of TOR signaling pathway. Several studies have demonstrated a conservation of the TOR complex in the alga, as well as the sensitivity of this complex to the macrolide rapamycin, a well-known inhibitor of TOR kinase [204,214]. The action of rapamycin relies on a conserved protein, FKBP12, which mediates the inhibitory effect of the drug on TOR kinase. Despite conservation, FKBP12 is unable to form a stable complex with rapamycin in higher plants, such as *A. thaliana* and *N. benthamiana*, that are indeed insensitive to treatment with this drug [234].

Molecular analyses of the transgenic *Chlamydomonas* lines revealed accumulation of *ATG* gene transcripts and of ATG8, as revealed in western blot experiments. The accumulation of ATG8 might be considered as a marker of autophagy induction. However, it may also reflect defect impaired completion of autophagy, through a defect in vacuolar degradation [235].

The different results obtained in the present study show that autophagy is impaired, although transiently, in *Chlamydomonas*. TEM analyses revealed the presence of smaller vesicles in transformants, when compared to WT cells. In addition, transformants display a delayed autophagy progression upon rapamycin treatment and accumulate cellular debris similarly to what is observed in *Chlamydomonas* cells treated with concanamycin A, an inhibitor of autophagic flux [219]. However, this effect appears to be transient since long-term observation of Avh195-overexpressing cells upon autophagy induction reveals that the signs of inhibition are partially relieved at the latter time point analyzed.

Besides, we noted an accumulation of starch in transformants, illustrated by an increase in starch granules per cell. A study conducted with *Arabidopsis thaliana* showed that *ATG* genes undergo a transcriptional regulation within 4h from onset of darkness. A mutation of *ATG* genes, or an inhibition of autophagy by the application of 3-methyladenine (3-MA) leads to starch accumulation [159]. The autophagic machinery thus appears complementary to the classic degradation of starch that occurs in the chloroplasts, therefore the accumulation of starch observed in *Chlamydomonas* would further indicate a negative modulation of autophagy.

Taken together, our observations on *Chlamydomonas* allowed to define a function for Avh195 on the autophagic machinery. Moreover, to our knowledge, this work provides the first report that an oomycete effector is active in a non-plant, but photosynthetic organism, making *Chlamydomonas* a promising model for further effector studies. The only other trans-kingdom activity has been shown for a CRN effector of the legume root pathogen *Aphanomyces euteiches*. This effector has been successfully expressed in *Xenopus laevis* embryos, where it triggers aberrant developmental modifications [236].

However, *Chlamydomonas* was not the sole heterologous system used in this work. To examine whether the activity of Avh195 is generalist and can target ATG8 proteins derived from phylogenetically distant organisms, we screened the properties of the effector on the mammalian HeLa cell line. This second model was chosen for the possibility to modulate and analyze each step of the autophagic flux thanks to a multitude of tools allowing detection and quantitation of autophagy and cell death [237]. Particularly with regard to cell death and apoptosis, HeLa cells represent a complement to *Chlamydomonas*: similar to higher green organisms, the description of hallmarks of programmed cell death are controversial and the existence of such mechanisms is still debated [238]. Although our work on HeLa cells was not much developed due to lethal effects of the effector, the obtained results supported our observations with *Chlamydomonas*. The application of recombinant Avh195 on HeLa cells promoted the accumulation of autophagosomes, similarly to late inhibition of autophagic flux by the drug Chloroquine, which prevents the fusion of autophagosomes with lysosomes and their acidification. Speculating that this result is once more provoked by the interaction between Avh195 and ATG8, this would strengthen the finding that the effector is able to bind ATG8 universally, regardless of the organism of origin. In mammals, ATG8 has evolved into a gene family composed by 6 members (LC3A, LC3B, LC3C, GABARAP, GABARAPL1, and GABARAPL2) that differentiated in function [239]. Interestingly, the abolition of all members of the LC3/GABARAP family does not impair autophagy in HeLa cells but rather results in a lower size and rate of autophagosome formation [240]. It is tempting to suppose that the effect of Avh195 observed in algae (namely the delay in vacuole coalescence) could be provoked by a (transient?) impairment of ATG8 action at the crescent autophagosome.

Despite the important contributions of the two heterologous model systems to the development of this work we have to take into account that they only represent a support for studies *in planta*. First, mammalian cells are phylogenetically distant from the plant lineage and even though organisms

belonging to those phyletic groups share some basic molecular machineries, transpositions of results from one model to the other must be made with caution. Second, *Chlamydomonas* cells were exploited for their convenience from a technical and methodological point of view but the reduced complexity of this model does not take into account the multifaceted aspects that autophagy covers in higher, multicellular organism, such as plants.

For this reason, a second important part of the work was carried out on plants, in order to observe the action of the effector in a natural context.

Cell death is the final stage of the HR, which is activated in plants upon the recognition of an invading pathogen, to limit its growth at the site of penetration [241]. Even though the mechanism by which autophagy promotes a confined HR remains unclear, many studies on ATG mutants have shown that autophagic functions are essential for the initiation of this response [178,242]. A particular role for autophagy was shown in the delimitation of cell death, as *ATG6* mutants are unable to restrict spreading of the HR induced by viral and bacterial pathogens [178,242]. However, other studies rather revealed a “pro-death” function of autophagy in the execution of HR triggered by avirulent pathogens in *Arabidopsis* [180].

Slight modulations of this fine-tuned machinery might thus have consequences for the success or the failure of infection. The analysis of Avh195 by transient overexpression in tobacco revealed that this effector does not induce cell death, conversely it is able to delay the development of symptoms related to cryptogein-induced HR-PCD. The transient nature of this effect is consistent with the transient effects of Avh195 on autophagy that we observed in *Chlamydomonas*. Modulations of host autophagy by Avh195 are thus subtle and do not interfere with vital parameters of the plant cells, but lead to a visible delay in the execution of HR. Moreover, we observed that Avh195 requires one or more AIMs for slowing down the progression of cryptogein-mediated cell death, as this activity is almost abolished in an effector, in which 3 of the 5 AIMs were mutated.

P. parasitica is a hemibiotrophic pathogen, which maintains host cells alive as a biotroph, before switching into a necrotrophic lifestyle. With regard to the function of Avh195 during infection we analyzed the mRNA level of the effector during *P. parasitica* infection. In two different pathosystems (*A. thaliana* and *S. lycopersicum*) we determined that the transcript is specifically accumulated during the biotrophic step of the *P. parasitica* infection cycle, indicating that the effector either promotes biotrophy, or prepares the switch to necrotrophy.

Several studies show that the plant autophagic machinery confers resistance to infection: as mentioned above, it can lead to the degradation of pathogen-derived molecules and also participate in the delivery of defense-related molecules at the pathogen interface [176,185,188]. Conversely, the manipulation of host autophagy by plant pathogens frequently aims at repressing plant defense responses [89,243].

In this work we showed that Avh195 thus does not act as a suppressor of defenses, but rather as an accelerator of infection. In Avh195-expressing transgenic Arabidopsis, the defense responses towards biotrophic and necrotrophic pathogens are activated, and occur earlier during the infection cycle than in the WT. During the interaction with Arabidopsis, the biotrophic phase of *P. parasitica* allows the oomycete to successfully establish in the root cortex and to reach the central cylinder, before setting up necrotrophic, invasive growth, and infecting the aerial parts of the plant [31]. The equilibrium between initial establishment within plant tissues and the development of biomass during invasive growth eventually determines the success of the oomycete life cycle. Avh195 is expressed during biotrophic growth only, where the effector slows down the development of hypersensitive cell death (a plant response to biotrophs).

Taken together, we can hypothesize that Avh195 acts during the biotrophic stage with two mechanisms. First, the transient inhibition of autophagy might slow down the autophagic degradation of pathogen-derived molecules and promote the establishment of the oomycete in plant tissues during the early stages of infection. Moreover, we suggest that Avh195 decelerates the pro-death function of the mechanism, and thus promotes biotrophy. This interpretation would be in line with the observation that the obligate biotrophic oomycete pathogen *Hpa* develops better in Avh195-expressing Arabidopsis, than in the WT. The observed earlier and intensified switch of *P. parasitica* to necrotrophy in the presence of Avh195 would then reflect a better biotrophic establishment and an acceleration of the life cycle.

Eventually, the transient action of Avh195 is relieved upon the switch to necrotrophy, when there is no more need for the pathogen to interfere with the HR.

The reduced sporulation rate at the end of the infection cycle observed for transgenic Arabidopsis expressing Avh195 may in turn reflect an improved nutrition of the pathogen: *Phytophthora* species may initiate their asexual reproduction following various environmental changes, among which nutrient limitation [33]. The prolonged increase in oomycete biomass and the simultaneously reduced sporulation rate in the presence of Avh195 may indicate that transgenic Arabidopsis plants

sustain nutrient supply to the pathogen longer than the WT. Sustained nutrient supply might also be a consequence of the Avh195-mediated interference with autophagic flux in the transgenic lines.

Conclusions and Perspectives

One of the keys of the success of plant parasitic oomycetes resides in the huge arsenal of molecules released during infection that participate in the complex crosstalk between the host and the pathogen. The numerous studies performed on effectors from the RxLR class revealed that part of such success is due to the rapid evolution of novel molecules developed by the pathogen to manipulate host plant defenses and metabolism. Autophagy is a process that potentially conjugates both aspects, and it appears to be targeted by different classes of plant pathogens, including oomycetes.

This work has contributed to the discovery of an RxLR effector from *P. parasitica* acting as an autophagy inhibitor, and uncovered a transient mode of action, which has never been described before. This finding reveals that the effector-mediated modulation of host cells is far more complex and fine-tuned than previously thought and surely opens new lines of research.

The development of new methodologies and model systems, such as the microalga *Chlamydomonas reinhardtii* presented in this work, will hopefully facilitate the study of RxLR effectors and the complex mechanisms of modulation of the host machinery. Here, this photosynthetic organism allowed the characterization of Avh195-dependent autophagy perturbation, through the generation of transgenic lines overexpressing the effector. The possibility to perform flow cytometry on *Chlamydomonas* revealed that Avh195 does not alter the physiology and fitness of the cell whereas TEM analysis of cells revealed a transitory inhibition of the autophagic flux. Together, our results helped comprehension and interpretation of the analysis of function of Avh195 performed in planta, such as the transient inhibition of hypersensitive cell death in tobacco and the facilitation of necrotrophic growth observed in *A. thaliana* transgenic lines. However, there are still many aspects of this work that will warrant ongoing and future experiments that will complete our understanding of the role of Avh195.

For example, we need to confirm that Avh195-dependent autophagy inhibition also occurs in plants and that it is related to the observed phenotypes. During my PhD thesis, we tried to demonstrate the impairment of the autophagic flux with a test based on the accumulation of NBR1, an autophagy receptor [244]. This receptor accumulates and aggregates when autophagy is inhibited and is considered a marker for impaired flux [226] NBR1 has not been identified yet in *Chlamydomonas* [245] and we could not detect a structural homolog of the receptor via immunoblot analysis of algae

protein extracts. NBR1 exists in plants, and we obtained an antibody targeting the Arabidopsis protein. The antibody will allow us to analyze the turnover of NBR1 in transgenic Arabidopsis overexpressing Avh195.

Going further, this work has collected many indications of autophagy inhibition but so far we did not decipher the exact mechanism by which this inhibition occurs. On the basis of the observation performed in *Chlamydomonas*, we can speculate that the inhibition derives from two distinct mechanisms. A first one is the perturbation of the biophysical properties of the membranes. The binding of Avh195 to ATG8 may interfere with the curvature and closure of phagophores, leading to a delayed completion of autophagic vesicles. This analysis could be performed by analyzing the accumulation of unclosed membranous structures in both *Chlamydomonas* and plant cells. An assay to observe defects in autophagosome completion has been developed for mammalian cells and consists in the visualization of GFP-tagged ATG5 on membranous structures: the closure of the phagophore releases ATG5 from the membranes and is indicative of a complete genesis of the autophagosome [246]. We might exploit the same methodology in *Chlamydomonas* and Arabidopsis and perform immunofluorescence experiments with antibodies directed against ATG5 to detect defects in the completion of autophagic vacuoles. The second mechanism that may contribute to autophagy inhibition is the perturbation of cargo catabolism inside the vacuole. Since Avh195 possesses numerous basic amino acids, it appears possible that the binding between Avh195 and ATG8 perturbs acidification of autophagosomes thus leading to defects in the catabolism of cargoes. To verify this hypothesis, we might perform enzymatic tests in both *Chlamydomonas* and Arabidopsis plants based on the activity of vacuolar hydrolases. One example could be represented by the γ -VPE enzyme, which is usually upregulated during senescence, and which appears to participate in vacuolar proteolytic activity during autophagy [144].

Throughout this work, we correlated the inhibition of autophagy to the direct binding of Avh195 with ATG8 via three out of five AIMs that are present in the effector domain of the protein, as confirmed by Y2H experiments. However, we are seeking to confirm that the alteration of those AIMs disrupts the interaction between the two proteins. Future experiments will be performed by producing the abolition of single AIMs as well as all of the five. This will permit the identification of important or dispensable sites to warrant the interaction. We will also need to implement additional tests to confirm the interaction in planta. One possibility is to get more detail on the subcellular localization of the two proteins by confocal imaging of agroinfiltrated tobacco in presence of

fluorescent reporters for different subcellular compartments (e.g. FM4-64 tracker for endocytic compartments). This approach could be complemented by co-immuno precipitation experiments that we sought to perform during my PhD thesis, but which requires optimization to be performed on microsomal fractions of protein extracts. In addition, we can consider a bioluminescence resonance energy transfer (BRET) based approach: this technique is similar to the fluorescence resonance energy transfer that is widely used to detect interaction between proteins, and has been successfully used in plants to detect interaction between ATG8 and ATG4 [247].

Despite we still lack some confirmations, this work showed that Avh195 has a generalist activity, being able to produce phenotypes related to autophagy inhibition in three photosynthetic heterologous systems (*C. reinhardtii*, Tobacco and *A. thaliana*) and a human cell line. Such peculiarity has never been observed for an oomycete effector so far.

Autophagy inhibition in *A. thaliana* Avh195 overexpressing lines was deduced by the results obtained during interaction with *P. parasitica* and *H. arabidopsidis*. On those plants we observed an acceleration of the whole infectious cycle and an intensified, prolonged necrosis. As discussed in the previous chapter, this could reflect an inhibition of autophagy since it could reduce its pro-death function during interaction with biotrophic pathogens which results in improved establishment of the pathogen. As a follow-up of this analysis we are going to analyze the influence of Avh195-overexpression in *A. thaliana* on the development of a strictly necrotrophic pathogen such as *Botrytis cinerea*. This analysis will help to rule out whether Avh195 promotes biotrophy or also conditions necrotrophy.

Since most of the experiments performed on *Arabidopsis* transgenic lines were solely based on transcriptional analysis, it would be interesting to test whether this corresponds to an actual alteration of a specific step, either during biotrophy or necrotrophy, of the infectious cycle of *P. parasitica*. Experiments might be performed by confocal imaging of transgenic plants infected with *P. parasitica* zoospores expressing GFP. A previous work conducted in our laboratory gave a detailed cellular description of the different steps of penetration and invasion of the oomycete in plant roots over a 30h time course [44]. Shifts in the timing or modifications in the behavior of the pathogen would help to determine the step of infection that is favored by Avh195.

In addition, we might perform the same panel of experiments with transgenic *Arabidopsis thaliana* expressing a hairpin RNAi construct, which would generate host-induced gene silencing (HIGS) of Avh195 in *Phytophthora parasitica* during interaction. Avh195-HIGS plants were generated during this PhD thesis, but were not included in the work since they need further steps of selections before

their utilization. Experiments conducted on these plants will further elucidate the role of Avh195 and will in particular allow to determine what consequences effector loss will have for the infectious cycle.

It emerged from experiments on *A. thaliana* that the activation of plant defenses is not impaired nor decreased in Avh195 overexpressing lines. Here again, we obtained this information from a transcriptional point of view, but it will be important to confirm the actual accumulation of PR1 and PDF1.2 proteins via immunoblotting, as witness of proactive and efficient defense response. To further investigate this aspect, we might also envisage the generation of Arabidopsis transgenics overexpressing both Avh195 and (GUS or GFP) reporter constructs for the transcriptional activation of PR1 and PDF1.2. These transgenic lines will provide a tool to observe *in vivo* the onset of plant defenses during Avh195 overexpression and to detect any perturbation in this response.

A question arising from our findings is why an effector that favors pathogen growth and targets a ubiquitous process has such a restricted distribution among *Phytophthora* species. As presented in the introduction, Avh195 was identified only in the genomes of *P. parasitica* and *P. infestans*. The non-specific binding of Avh195 to ATG8 might be considered as an ancestral character that was shaped by co-evolution with the host, leading to diversification [248]. Alternatively, it can represent the relatively recent acquisition from the common ancestor of *P. infestans* and *P. parasitica*. The analysis of the evolutionary history of this effector may help to point out also specific traits of *P. parasitica* lifestyle such as host specificity. In this regard it would be interesting to compare the Avh195 paralogs between *Phytophthora infestans* and *P. parasitica* for their expression profile, their target, and for other characteristics of PpAvh195 such as the transient action on autophagy. A comparison between the two species might open the intriguing perspective of understanding how a pathogen synchronizes the action of two effectors that target the same process with opposite effects. *P. infestans* PexRD54 [89] and Avh195 differ in sequence and only share the conserved characteristics of RxLR effectors and the presence of AIMs. The two effectors also differ in function: the first was proposed to promote autophagosome formation while the latter reduces the autophagic flux. Moreover, the different isoforms of ATG8 in plants have specific functions and regulations: PexRD54 targets autophagosomes specifically labelled by one of those isoforms, which were described as defense-related autophagosomes. Conversely Avh195 appears to target the machinery without such specificity. The possible competition (or coordination) between the two effectors targeting the same process might be analyzed by comparing the expression profiles of

Avh195 and PexRD54 during infection, and by characterizing the nature of different autophagosomes that may be generated during the plant-pathogen interaction.

However, the complexity of the interaction between effectors potentially targeting autophagy in the host is not limited to PexRD54 homologs. A master thesis project carried out in the laboratory (R. Hassanaly) revealed that Avh195 is not encoded by a single gene but is part of an expanded gene family composed of 8 (+2) members. Alignment of the ten sequences revealed an organization in 4 clades with an estimated sequence identity among members ranging from 45.7% to 97.6%. Only two of the analyzed sequences did not display all typical features of RxLR effectors (namely a signal peptide and the RxLR motif) but all isoforms contain 2 to 5 AIMs. Some of the AIMs appeared to be shared among the different isoforms whereas others were clade-specific (clades II and III). The expression profile of these genes was analyzed during *P. parasitica* infection in *N. tabacum*, revealing that Avh195 isoforms are differentially expressed throughout the infection cycle. Genes belonging to clade I (including the isoform of Avh195 presented in this work) are expressed during biotrophy whereas members of clades II and III are expressed in a second wave during necrotrophy. Interestingly, the analysis of HR upon agroinfiltration in tobacco revealed that another isoform of Avh195 belonging to the same clade is able to attenuate cell death.

The diversification of Avh195 in multiple isoform opens even more intriguing speculations. First, a correlation between the pattern of expression of clades and the distribution of AIMs was determined. We can hypothesize that members of clade I are expressed during biotrophy and inhibit autophagy in a general manner. Upon the switch to necrotrophy Clades II and III are expressed and their interaction with ATG8 might probably be different, leading to different effects on autophagy. Or even, they may target subclasses of autophagosomes that are formed during this stage of infection. It might thus be interesting to analyze the ability of members issued from each clade to bind different isoforms of ATG8 and to test their ability to either promote or to inhibit HR. A work similar to the one presented in this thesis, performed on other isoforms of Avh195, could help understanding how the two waves of effectors contribute to *P. parasitica* pathogenicity.

To conclude, even though this work alone will not lead to direct biotechnological implementations, it has surely improved our knowledge of the molecular mechanisms regulating the relationship between *Phytophthora* and the host plant and will contribute to the development of novel

strategies to fight oomycete diseases that are still deeply affecting agriculture and natural ecosystems.

Materials and Methods

I - Bioinformatic analysis

The Avh195 protein sequence was analyzed for its amino acid composition and theoretical pI using the ProtParam tool implemented at the ExPASy Bioinformatics Resources Portal (<https://www.expasy.org/>). The signal peptide was detected using SignalP V.4 at the same portal. Avh195 was also examined for the presence of AIMs, otherwise called LIR (LC3-interacting region) motifs [192,193]. This was achieved at the iLIR autophagy database hosted at <https://ilir.warwick.ac.uk>. Multiple alignments were conducted using Clustal Omega implemented in Seaview V. 4.0 [249]. Phylogenetic trees were constructed using the Maximum Likelihood (ML) method based on the LG model with a gamma rate of heterogeneity calculated in Mega 7.0 [250].

II - Vector construction

Plasmids used in this study were constructed based on the Gateway® Technology (Invitrogen®) following the instructions of the manufacturer except when otherwise indicated. All primers used in this study are listed in Section XV of this chapter.

- The **Avh195** coding sequence and its derived versions (**Avh195ΔED**, **Avh195ΔAIM**) were cloned without signal peptide from a full-length cDNA clone issued from *P. parasitica* 149 (from Spain collected on *Lycopersicon esculentum* 1975 A2).
- **Avh195ΔED** (Avh195 coding sequence deprived of its effector domain) was obtained by amplification with specific primers from a vector containing native version of Avh195.
- **Avh195ΔAIM** was generated by site-directed mutagenesis of Avh195 using a QuickChange II kit (Agilent®) according to the manufacturer's recommendations. Three primer pairs were specifically designed to alter one by one a selected AIM by replacement of hydrophobic residues of each site by an alanine.
- Chlamydomonas **CrATG8** coding sequence was amplified from cDNA sample issued from *Chlamydomonas reinhardtii* DW15-c2 strain.
- The coding sequences for *Arabidopsis thaliana* **AtATG8D**, **AtATG8G** and **AtATG8H** were amplified respectively from the Gateway-compatible plasmids G22544, U17226, and G82070

obtained from the Arabidopsis Biological Resource Center (ABRC) at the Ohio State University.

Vectors for in vivo overexpression

Amplification of target gene was carried out with HF Q5 Taq polymerase (New England Biolabs®) using overhanging primers flanked by attB1 and attB2 sites. PCR products were inserted by BP recombination into pDONR207 vector to generate Entry clones that were subsequently verified by DNA sequencing.

- For **transient overexpression in tobacco** *Avh195* and its derived versions *Avh195 Δ ED* and *Avh195 Δ AIM* were cloned into the pK7FWG2.0 (Plant systems biology®). Stop was included at the end to avoid GFP expression.
- For **in planta co-localization** assay *Avh195* was cloned into pK7GWF2.0 (Plant systems biology®) *in-frame* to the N-terminal GFP tag. *Chlamydomonas reinhardtii* *ATG8* coding sequence was cloned into pK7RWG2.0 (Plant Systems Biology®) *in-frame* to the N-terminal RFP tag.
- For **mbSUS Y2H assay** *Avh195* was cloned into vector pMetYC-DEST. The *Chlamydomonas reinhardtii* *CrATG8* coding sequence and *Arabidopsis thaliana* *AtATG8D*, *AtATG8G*, *AtATG8H* coding sequences were cloned in vector pNX32-DEST.
- For generation of ***Arabidopsis thaliana* overexpressing lines**, *Avh195* was cloned into pK7GWF2.0 vector (Plant Systems Biology®) with a codon stop to exclude the GFP tag from the construction (Plant systems biology®).
- For **overexpression in mammalian cells** *Avh195* coding sequence was cloned into pcDNA-DEST vectors (Thermo Fischer®) harboring a CMV promoter and providing fusion of the recombinant protein with GFP N-terminal tag (pcDNA-DEST53) or GFP C-terminal tag (pcDNA-DEST47).

All the constructions were firstly cloned in *Escherichia coli* electrocompetent strains ElectroMAX™DH10B™Cells (Invitrogen®). Transformed cells were cultivated in LB medium at 37°C on selective medium and the cells issued from the transformation process were tested via PCR for the presence of the construct. Plasmid was purified from validated clones with QIAprep Spin Miniprep (Qiagen®) and sequenced for validation (GENEWIZ™ - Beckman Genomics®). Verified clones were then stocked in LB 15% Glycerol at -80°C for long term conservation.

Transformation and expression of the expression vector in the final host will be described in the dedicated sections.

Vectors for recombinant protein production

Amplification of Avh195 coding sequence deprived of its signal peptide was carried out with HF Q5 Taq polymerase (New England Biolabs®) using primers flanked by EcoRI restriction enzymes sites. The amplicon was digested with the appropriate restriction enzyme according to manufacturer's instruction (New England Biolabs®) and cloned into vector pET28c (Merk Millipore®) allowing inducible expression of gene under control of IPTG. This construct was transformed into BL-21 electrocompetent cells (New England Biolabs®). Transformed cells were cultivated in LB medium at 37°C on selective medium and the cells issued from the transformation process were tested via PCR for the presence of the construct. Plasmid was purified from validated clones with QIAprep Spin Miniprep (Qiagen®) and sequenced for validation (GENEWIZ™ - Beckman Genomics®). Verified clones were then stocked in LB 15% Glycerol at -80°C for long term conservation.

III - RNA extractions and gene expression analysis

All RNA extractions were performed according to Laroche-Raynal [251] using PCI/CI method or with miRNAeasy kit (Qiagen®). Nucleic acids were pelleted overnight in 2,5 Volumes of EtOH and eventually resuspended in DPEC water. After DNase I treatment (Ambion®), RNA (1µg) was reverse-transcribed using IScript cDNA synthesis kits (BioRad®) or with Superscript IV RT (invitrogen®).

.

Reverse transcription-quantitative polymerase chain reaction (RT-qPCR) experiments were performed in AriaMX (Agilent®) thermocycler with 5µl of a 1:20 or 1:50 dilution of first-strand cDNA and SYBR Green, according to the manufacturer's instructions (Eurogentec®).

Primer pairs used for specific cDNA amplifications are listed in Section XV. Primers couples were designed using Primer3 software (<http://frodo.wi.mit.edu>) and their specificity was validated by the analysis of dissociation curves. Relative quantifications were made with the modified ΔC_t method employed by the qBase 1.3.5 software. qBase was also used to determine the stability of reference genes.

IV- SDS-page and Western blot analysis

All protein samples presented in the work were resuspended in Laemmli loading buffer and loaded on a 15% acrilamide/bisacrilamide SDS gel. Electrophoresis was performed until exit of dye front. Proteins were transferred on PVDF membrane using Biorad Trans-Blot® Turbo™ apparatus set for Mixed molecular weight transfer. Membranes were saturated in TBS (Tris HCl 25mM, NaCl 140mM, KCl 3mM) 5% milk, incubation of primary and secondary antibody was performed in TBS-Tween 0,1%, 2% milk, washing steps were performed before each step with TBS-Tween 0,1% solution. Eventually the membranes were irradiated with ECL reagent (Pierce®) and several exposition times were performed using photographic film and chemical reagents (Kodak®).

- To detect **GFP**-antigen membranes were incubated with primary antibody Anti-GFP (Chromotek® 3H9) and secondary antibody HRP-conjugated Goat anti-Rat (Chromotek®).
- To detect **Atg8**-antigen membranes were incubated with primary antibody Anti-Atg8 (Agrisera® AS14 2769) and HRP-conjugated secondary antibody Goat anti-Rabbit (Covalab®).
- To normalize the loaded sample from *Nicotiana tabacum*, membranes were probed with primary antibody recognizing the photosystem II **PsbO** (Agrisera® AS14 2769) and HRP-conjugated secondary antibody Goat anti-Rabbit (Covalab®).
- To normalize the loaded sample from *Chlamydomonas reinhardtii*, membranes were probed with a primary antibody recognizing the histone protein **H3** (Agrisera® AS10 710) diluted and HRP-conjugated secondary antibody Goat anti-Rabbit (Covalab®).

V - Recombinant protein production and purification

BL-21 electrocompetent cells transformed with plasmid vector pET28c-Avh195-*His*-tag were cultured in 4 ml LB medium at 37°C overnight. 24h later 2ml of the culture were used to seed 1L of terrific broth supplemented with kanamycin 30µg/ml and chloramphenicol 34µg/ml with constant aeration and agitation, kept at a constant temperature of 37°C. OD600 of the culture was monitored over time using a spectrophotometer. Synthesis of protein was induced by addition of 1mm/L IPTG. Three hours later the cell culture was collected by centrifugation 6000 rpm for 10 minutes and pellet was stored at -20°C.

One aliquot of the collected cell culture corresponding to about 150 ml was resuspended in 15 ml of Tris HCl pH 7.5 20mM and sonicated on ice with an amplitude of 25%, three pulses of 30 seconds each. The suspension was then filtered on glass fiber and diluted to a final volume of 30 ml with Tris HCl pH 7.5 20mM, NaCl 500mM and imidazole 20mM final concentrations.

The sample was purified by affinity chromatography on a 5 ml Ni-Sepharose His-Trap column, washed twice and eluted with Tris HCl pH 7.5 20mM, NaCl 500mM and imidazole 500mM final concentrations. Eluted sample was then loaded onto a PD10 column and eluted in Tris 20mM pH 7.5 then concentrated with a centrifugal filter Amicon® Ultra-4 10K (Merk-Millipore®). Protein content was determined with Bradford protein assay and sample purity was assessed on SDS page followed by silver staining.

Silver staining of polyacrylamide gels was performed as follows: gel was fixed in a solution of 50% methanol 12% acetic acid for 45 minutes, washed in 50% ethanol then dipped in 0.02% Na₂S₂O₃·5H₂O solution to remove background. Staining was performed in 0.02% AgNO₃ 0.07% Formaldehyde for 20 minutes and bands were revealed in 6% Na₂CO₃, 0.0004% Na₂S₂O₃·5H₂O, 0.05% Formaldehyde.

VI- Yeast two-hybrid assay

To determine interactions between membrane-associated Avh195 and ATG8, the mating-based split ubiquitin system (mbSUS) was used and employed as described [198]. Sequences encoding Avh195 and AtBi-1 were integrated as baits into pMetYC-DEST and transferred into the haploid Mat_a yeast strain THY.AP4. Sequences encoding *CrATG8*, *AtATG8D*, *AtATG8G*, and *AtATG8H* were cloned as preys into pNX32-DEST and transferred into the haploid Mat_{alpha} yeast strain THY.AP5. This strain was also transformed for positive and negative control with the prey plasmids, pNubWt-X-gate and empty pNX32-DEST, respectively. Mating between THY.AP4 and THY.AP5 transformants, and selection of diploids for growth on Synthetic Complete minimum (SC) medium complemented with adenine (A) and histidine (H) was performed as described [198]. Physical proximities between baits and preys were determined as autotrophic growth of yeast cells (from 10⁸ to 10⁴ cells per spot) at 30 °C on SC medium in the absence of adenine and histidine.

VII - *Arabidopsis thaliana* assays

***Arabidopsis thaliana* cultures**

In all this work *Arabidopsis* lines were from the Columbia genetic background (Col-0, N60000).

For cultures in **non-sterile** conditions *Arabidopsis thaliana* seeds were spread on a mixture of ground and sand and then placed 48h at 4°C for stratification. Then pots were placed in a climate chamber at with short photoperiod (8h light / 16h dark at 24 °C) for 3 weeks. Next, plants were transplanted in individual pot and left to in a climatic chamber at 24 °C with a 16h light /8h dark photoperiod until needed or until flowering.

For **in vitro** culture *Arabidopsis* seeds were surface-sterilized in 20% NaClO 80% EtOH, rinsed three times with 100% ethanol. Seeds were sown on MS 2/2 (1x Murashige and Skoog (MS) medium (Sigma®) supplemented with 2% sucrose (Prolabo®), and 2% agar), cold-stratified for two days and then incubated at 21°C under short-day conditions (8h light / 16h dark). After 6 days, plantlets were transferred to 96 well plates containing 30µl of the same medium which was overlaid with 25µl of liquid 0.5x MS supplemented with 1% sucrose for 8 days prior experimentations.

Generation of Arabidopsis thaliana stable genetic transformants

Arabidopsis plants were transformed with the destination vector pk7FWG2-Avh195 via the floral dip method [252]. Briefly, agrobacterium tumefaciens strain GV3101 containing the expression vector pK7WG2-Avh195 were cultivated in LB medium with antibiotics at 28°C. When OD = 1 bacteria were collected by centrifugation 4000 rpm x 10min and resuspended in transformation mix containing MS medium 0.5x, 5% sucrose, and 0,03% Silwett L-77, pH 5.7).

Arabidopsis inflorescences were inverted and dipped into agrobacterium suspension for 2 min. Once drained, plants were placed in a covered container and incubated under constant light for one day at 16°C then transferred in a long day room (16 hours light/8 hours dark, 21 °C) to allow senescence.

Seeds of transformed plants were harvested and selected in vitro on MS petri dishes via antibiotic selection (Kanamycin 50µg/ml). Transformation-derived plants were then allowed to self-pollinize until obtainment of homozygous plants.

***Arabidopsis thaliana – Phytophthora parasitica* interaction**

P. parasitica Dastur isolate 310 was initially isolated from tobacco in Australia, and was maintained in the *Phytophthora* collection at INRA, Sophia Antipolis, France. The conditions for *Phytophthora*

growth and zoospore production were as previously described [253]: mycelia were cultivated on V8-agar medium at 24°C in the dark. To produce zoospores, mycelia were cultivated for 1 week in V8 liquid medium at 24°C under continuous light. This material was then macerated and incubated for a further 4 days on water supplemented with 2% agar. The zoospores were released by a heat shock treatment: incubation at 4°C for 1h followed by incubation at 37°C for 30 min. Water (10 ml) was added in between incubations.

Zoospore suspension containing 10^3 cells was then used to inoculate 15 days old *Arabidopsis* plantlets grown in sterile conditions. Experiments were carried out in duplicate. At the defined time points after infection plantlets were collected and immediately frozen in liquid N₂.

RNA extraction and gene expression analysis

Frozen *Arabidopsis thaliana* plantlets (infected or not with *P. parasitica*) were ground with mortar and pestle in N₂ until pulverized then transferred to 2 ml test tube.

RNA extraction and gene expression analysis of *A. thaliana* - *P. parasitica* samples was performed as described in Section III. Relative expression of the target genes was calculated with the *NADH* and *OXA1* genes as references for *Arabidopsis* [45], *WS41* and *UBC* for *P. parasitica* [79].

Arabidopsis thaliana – Hyaloperonospora arabidopsidis interaction

Plants from the Col-0 wild-type and the Avh195-overexpressing lines were grown for 7 days in a soil-sand mixture at 20 °C under short-day conditions (8h light, 16h dark). Cotyledons from a population of about 500 plants per line were then spray-inoculated to saturation with Hpa isolate Noco2 conidiospores at 40,000 spores mL⁻¹. Inoculated plants were kept at 16 °C with a 16h photoperiod, first under 100 % relative humidity for 24h, then under 60 % relative humidity for 4 day, before relative humidity was increased again to 100 % for 48 hours to promote sporulation. Seven days after inoculation, 10 plantlets were repeatedly harvested (20 samples) from each line and placed into 20 tubes containing each 1.5mL water. After vortexing, the amount of released spores was determined with a hemocytometer and expressed as the amount of spores produced per mg of leaf fresh weight.

VIII - *Solanum lycopersicum* assays

Seeds of *Solanum lycopersicum* var. Marmande were surface-sterilized, sown on a mixture of ground and sand and placed in a climatic chamber at 24°C with a 16h light/8h dark photoperiod until development of 2-3 expanded leaves. Roots were water washed and plants were transferred to 2ml test tube containing 1.5ml of COIC medium for 2 days until experimentation.

***Solanum lycopersicum* – *Phytophthora parasitica* interaction**

P. parasitica isolate 709 from France (collected on *Lycopersicon esculentum*) was cultivated as described in 0. A zoospore suspension of $\times 10^5$ cells/tube was inoculated on roots of *S. lycopersicum*. At the defined time points after infection roots were collected and immediately frozen in N2.

RNA extraction and gene expression analysis

RNA extraction and gene expression analysis on *S. lycopersicum* - *P. parasitica* samples was performed as described in Section III. Relative expression of the target genes was calculated with *WS21*, *WS41* and *UBC* as reference genes for *P. parasitica* [79].

IX- *Nicotiana* species assays

Tobacco (*Nicotiana tabacum* var *xanthii* and *Nicotiana benthamiana*) plants were grown on a mixture of ground and sand in non-sterile conditions. The pots were placed in a climate chamber at with long photoperiod (16h light / 8h dark at 24 °C) for 3-4 weeks as previously described [79].

Transient overexpression in tobacco

Agrobacterium tumefaciens strain GV3101 transformed with the vector constructs of interest was grown in LB medium supplemented with 50 mg/ml rifampicin, 20 mg/ml gentamicin and 100 mg/ml spectinomycin until OD₆₀₀ reached 1.0. Then cells were pelleted, resuspended in infiltration buffer (10mM MgCl₂, 10mM 2-[N-morpholino] ethanesulfonic acid [MES], pH 5.6, 150μM acetosyringone) and adjusted to the appropriate optical density, then left 3h at room temperature in the dark before infiltration. Mix were prepared just before infiltration. Abaxial side of leaves of *N. tabacum* or *N. benthamiana* was infiltrated using a syringe without needle.

Cell death assay

Fully expanded leaves of 3-4 weeks old *N. tabacum* plants were infiltrated with suspensions of *A. tumefaciens* carrying pK7FWG2-Avh195 or its derived version (pK7WGF2-Avh195ΔED; pK7FWG2-Avh195ΔAIM) and/or Cryptogein (GenBank accession no. Z34459.1) previously cloned into the pK7FWG2 vector [79]. Infiltration was performed at a final OD₆₀₀ = 0.2 for the cell death inducer and OD₆₀₀ = 0.3 for the Avh195 constructs. Evaluation of the necrosis was carried out simultaneously on the three infiltration zones (Avh195 + Cryptogein / Avh195ΔED + Cryptogein or Avh195ΔAIM + Cryptogein). For each analyzed leaf a first score of 1 was attributed to the infiltrated patch presenting the least symptoms. We then compared the symptoms observed in the two neighboring patches and gave them a score ranging from 1 to 4 with 1 indicating absence of difference and 4 greatest difference.

Avh195 sub-cellular localization via live cell imaging

Fully expanded leaves of 3-4 weeks old *N. benthamiana* plants were infiltrated with suspensions of *A. tumefaciens* carrying pK7WGF2-GFP_Avh195 or pK7WGR2-RFP_CrATG8. Leaf patches were collected 72h after infiltration and mounted in water/sorbitol 0.8M for live cell imaging. Green and red fluorescence conferred by GFP- and RFP-tagged fusion proteins were detected in optical sections by confocal laser scanning microscopy on an inverted Zeiss LSM 880 microscope, equipped with Argon ion and HeNe lasers as excitation sources. For simultaneous imaging of GFP and RFP,

samples were excited at 488 nm for GFP and 561 nm for RFP. Confocal images were processed using the Zeiss ZEN 2 software.

Cell fractioning

Fully expanded leaves of 3-4 weeks old *N. benthamiana* plants were infiltrated with suspensions of *A. tumefaciens* carrying pK7FWG2-GFP_Avh195 or pK7RWG2-RFP_CrATG8. Leaf patches were collected 72h after infiltration and frozen in liquid nitrogen.

Frozen samples were crushed by mortar and pestle until pulverized then transferred to 15 ml tube.

For **cell fractioning** samples were resuspended in sucrose free microsome extraction buffer (100mM Tris HCl pH 7.4; 10mM KCl; 10mM EDTA; 1% Protease inhibitor cocktail; 12% Sucrose). Samples were centrifuged at low speed (1500 g x 10min at 4°C). The supernatant was collected, filtered on thin sieve to remove any floating leaf fragment then sucrose was added to a final concentration of 12%. Samples were centrifuged at 100000 g x 90 minutes at 4°C. At the end of centrifugation, the soluble fraction was collected in a new tube whereas the microsomal fraction was washed once in sucrose free extraction buffer and resuspended in 1 ml of fresh buffer.

To help the solubilization of the microsomes, the microsomal fraction samples were sonicated on ice intensity 30% with a 10-second pulse 3 times. Samples from both the soluble fraction and microsomal fraction were loaded on SDS-page followed by Western blot against GFP, Atg8 and PstO were performed as described in Section IV.

X - *Chlamydomonas reinhardtii* assays

***Chlamydomonas reinhardtii* cell culture**

Chlamydomonas reinhardtii strain *dw15.1* (nit1-305 cw15; mt+) is a cell wall-less strain derivative of *cw15* and is maintained at the CEA lab. Seed cells were cultivated in 250-ml flasks with 100 ml Tris Acetate Phosphate (TAP) medium under 12h /12h, light-dark cycle at 23°C with shaking. Transformant cells were maintained on agar plates containing antibiotic selection (Hygromycin B 7µg/ml).

In **heat shock** experiments, liquid cultures of *C. reinhardtii* in exponential growth were immersed in a water shaking bath at 42°C for 40min and subsequently put back at 23°C.

Where needed, Rapamycin 0.5µM or drug carrier (0,004% EtOH % and 0,001 % Tween) was added to liquid cultures at the beginning of light period.

Generation of Chlamydomonas reinhardtii transformant lines

Synthetic gene encoding *Avh195* was designed using the average codon usage implemented in the Codon Usage Database (<http://www.kazusa.or.jp/codon>). Gene synthesis was performed by GeneArt technologies and cloned in pChlamy_3 vector using KpnI and NotI restriction sites (Thermo Fisher®).

Nuclear transformation was performed using the electroporation method as previously described [254]. Briefly, the cells of *Chlamydomonas reinhardtii* WT strain *dw15* were grown to $1.0\text{--}2.0 \times 10^6$ cells/mL in TAP medium. Subsequently, 2.5×10^6 cells were harvested by centrifugation and suspended in 250µl of TAP medium supplemented with 40mM sucrose. Electroporation was performed by applying an electric pulse of 0.7 kV at a capacitance of 50 µF (GENE PULSER®, Bio-Rad), using 400 ng of *Scal*-linearized plasmids purified by agarose gel electrophoresis according to the manufacturer's instructions. The transgenic strains were selected directly on TAP/agar plates containing hygromycin B (30mg/L), and the plates were incubated under continuous fluorescent light ($20\mu\text{Mol m}^{-2} \text{s}^{-1}$) at 25°C.

Characterization of transformant lines by genotyping

Genotyping of *Avh195*-expressing *Chlamydomonas reinhardtii* was performed on total DNA extracts or cDNA samples. PCR analysis were performed on samples with combinations of specific primers.

Genomic DNA was extracted from cell pellet (5-6mm) issued of a petri dish culture resuspended in 200µl of Milliq water. Cells were spun down and then resuspended in 500µl of Chlamydomonas DNA extraction buffer (10mM Tris HCl pH 8.8; 10mM NaCl; 10mM EDTA; 1% SDS). DNA extraction was performed adding an equal volume of PCI: after vigorous shaking and centrifugation at 12000g x 10min the aqueous phase is collected and treated with RNase A 20µg/ml 37°C for 30 min. Then sample was extracted *twice* with an equal volume of *PCI and once* with *CI*. Precipitation of DNA was performed overnight adding 1,5 Volumes of EtOH 95% and 0,2M NaCl. Eventually sample was centrifuged 15000g x 15min at 4°C, pellet is washed in EtOH75% and resuspended in 50µl of Milliq water.

cDNA samples were prepared as described in Section III.

RNA extraction and gene expression analysis

Chlamydomonas reinhardtii frozen samples were directly resuspended in *Chlamydomonas* RNA extraction buffer (10mM Tris HCl pH 8.8; 600mM NaCl; 10mM EDTA; 4% SDS). For RNA extraction 5 ml of culture were collected by centrifugation 4000g x 5min, pelleted cells were frozen in N₂ and stored at -80°C; RNA was extracted as showed in Section III.

RT-qPCR experiments were performed as showed in Section III. Relative expression of the target genes was calculated with Cre02.g106550, Cre04.g227350 and Cre05.g232750 as reference genes [210]. In heat shock experiments the relative expression of the target genes was calculated with BTUB and CBLP as reference genes [210]. At least three biological replicates per experiment were analyzed.

Fluorescence staining and Microscopy observation

In experiments performed using the acidotropic dye LysoTracker® DND-189 (Thermo Fisher®) the probe was added to cells at 1µM final concentration. Cells were incubated at 37°C for 30min in the dark, rinsed twice in TAP medium and resuspended in a minimal volume then mounted on a glass slides for live cell imaging.

In experiments performed using the live/dead cell staining SYTOX® Green (Thermo Fisher®) the dye was added to 0.5µM final concentration and incubated at room temperature for 15 minutes in the dark. Cells were directly spotted on a glass slides for observation.

For both stainings, cells were analyzed with the epifluorescence microscope AxioimagerZ1 (Zeiss®) using GFP44 filter; images were acquired with the camera AxioCam MRm and analyzed with Zeiss ZEN 2102 pro® software and Fiji image processing software (<https://imagej.net/Fiji>).

Transmission Electron Microscopy

The wild type strain and selected transgenic strains were cultured in liquid medium until the exponential growth phase (2×10^6 cells/ml) under a 12h light/12h dark cycle. Rapamycin (0.5 μ M) was added at the start of the light period. After 4, 8, 12 and 24 hours of incubation, cells were collected, fixed in a mixture of Cacodylate buffer 0.1M and glutaraldehyde 2.5% and stored at 4°C. Cells were then rinsed with buffer and then postfixed in 1% osmium tetroxide in cacodylate buffer (0.1M). The final cell pellet was washed in water, dehydrated in acetone, and embedded in epoxy resin. Uranium- and lead citrate-contrasted thin sections (80 nm) were analyzed in a JEOL JEM-1400 120kV transmission electron microscope. Images were acquired with an 11 MegaPixel SIS Morada CCD camera (Olympus®).

Flow cytometry

The wild type strain and selected transgenic strains were cultured in liquid medium until the exponential growth phase under a 12h light/12h dark cycle.

For the analysis of cell proliferation and cell death a sample of unstained cells for each analyzed strain was collected at the beginning of the light period. Then 2×10^6 cells were stained with 7.5 μ M CFSE (Invitrogen®) 20 minutes in the dark with shaking then washed once in TAP medium and resuspended in appropriate amount of fresh medium to obtain a final concentration of 2×10^6 cell/ml. Cells were then treated with drug vehicle or Rapamycin 0.5 μ M; assessing the beginning of the light period as time $t=0$, samples were taken from cultures at 4, 8, 12 and 24h. Samples were counterstained with 4'-6-diamino-2-phenylindole (DAPI) (0.05 μ g/ml final) prior to analysis by flow cytometry. Flow cytometry analysis is performed on a SP6800 spectral cytometer (SONY Biotechnologies®) [255]. Data from single cells were then analyzed with Kaluza software (Beckman Coulter®).

Protein extraction and Western blot

To perform protein extraction of *Chlamydomonas* 10 ml of culture were collected by centrifugation 4000g x 5min and quickly frozen in N₂. Cell pellet was then resuspended in 250 μ l of Chlamydomonas Protein extraction buffer (10mM Tris HCl pH 7.5; 100mM NaCl; 0.1% EDTA; 0.1% NP-40; 1% Protease inhibitor cocktail; 5% Glycerol). Cells were lysed with 2 cycles of freeze at -80°C followed by thawing at RT, then centrifuged 16000g x 15min at 4°C. Soluble fraction was collected and total protein content was estimated with Bradford protein assay following manufacturer's instructions. 10 μ g of

total protein were resuspended in Laemmli buffer; SDS page and Western blot against Atg8 and H3 were performed as described in Section IV.

XI- HeLa cells assays

HeLa cell culture and treatments

HeLa cells were obtained from the American Type Culture Collection (ATCC) and maintained according to ATCC instructions. Briefly, HeLa cells were cultured in DMEM with 1% penicillin/streptomycin, 1% sodium pyruvate and 10% FBS, in humidified atmosphere at 37°C containing 95% CO₂ and 5% O₂. HeLa were plated at a concentration of 5000 cells/well in 96-well plate. 24h later, cells were exposed to 10 ng/μL of Avh-195 purified protein (Section V) for the indicated time.

Lysosome detection and immunostaining

After treatments or transfections, acidic vesicles were labelled with LysoSensor® Green DND-189 (50 nM) and the nuclear marker Hoechst 33342 (2.5 μg/ml final) at 37 °C. For the detection of Avh195, cells were fixed after treatments and Avh195 was detected using a specific primary antibody directed against His-Tag. After washing with PBS, secondary antibody coupled to AlexaFluor® 488 (Molecular Probes®) was added. Images were acquired with an inverted fluorescence microscope (Nikon®) equipped with a CCD camera (ORCA ER®, Hamamatsu Photonics), at 20× magnification.

Transient transfection of HeLa cells

HeLa cells were used to seed 96-well plates (500000 cells/well). Expression vectors pcDNA-DEST53-GFP_Avh195 and pcDNA-DEST47-Avh195_GFP and corresponding empty vectors were transfected using Lipofectamin® 2000 at reagent-to-DNA ratios of 3:1 according to the manufacturer conditions. After 48h of transfection, cells were observed under a light microscope (Nikon®) equipped with a CCD camera (ORCA ER®, Hamamatsu Photonics), at 20× magnification.

XII - Statistical analysis

All results showed are representative of two to three independent experiments. Statistical differences were assessed with Student's T-test.

XIII - Sequences

Domain	Start	End
Signal peptide	0	60
RxLR	163	175
EER	202	211
Effector domain	212	588
AIM Site 1 (KSYDDI)	370	387
AIM Site 2 (DRWIRL)	391	407
AIM Site 3 (PIWREV)	517	534

> *Avh195* - full coding sequence

ATGCGTCTGCCAATCATCGCTTCGTCGCAATGCTTACGTAAGTCTGCTAGCGGTGTGTATTCTATCGGCCTATGAACAAGAAGCTGTT
 GTCGCGCAAAACGCTCAGCGTTGGAGCTCAACTCATTCTGTTGCTGCTGCTGAAACCGGAGATACGTCTGGCAAACGCTCTTTAAGG
 TCTGACAGTATTCCGACTGTTGATGCTGAAGAGAGGGCCCTCCCAGGCATGACGAAGCTAACCGAGACGCTTAAGAAATGGATATCC
 GCATTGAGAAGCAAACCTGAGCAACAAGAAGTTGTGGTGGAACTACCAGAAGCTGGGTAACAAAAGCTTTCCGACTTAGATATCACC
 GGAATGTGGTTGAAAAACGGGAAAAGCTATGATGACATCTTCGACCGCTGGATTGACTCGATAAGTCACCGAGGCAAGCAGCCAA
 AAATTGCTGAATCATGGTACAACAACGAATGATCTCTACAAGGTCTTGCAGGAGCGTAATATGAACCTGAAACAATCAGACCGAT
 TTGGCGCGAAGTCGGACTGACAGAGTATCAACTTCGTGCCGCTCGTCACGCGGCTAGCGCCTTGTGA

> *Avh195* - protein sequence

MRLPYVLLLVAVCIIIASCNALSAEYQEA>VVAQNAQRWSSTHSVAAAETGDTSGKRLLRSDSIPTVDAEERALPGMTKLTETLKKWISALRS
 KLSNKKLWWNYQKLGKQLSDLDITGMWLKNGKSYDDIFDRWIRLDKSPRQAANKLLNHGTTTNDLYKVLKRNMNLETIRPIWREVG
 LTEYQLRAARHAASAL*

> *Avh195ΔAIM* - protein sequence without signal peptide

LSAEYQEA>VVAQNAQRWSSTHSVAAAETGDTSGKRLLRSDSIPTVDAEERALPGMTKLTETLKKWISALRSKLSNKKLWWNYQKLGKQ
 KLSLDLDITGMWLKNGKSAADAFDRAIRADKSPRQAANKLLNHGTTTNDLYKVLKRNMNLETIRPIAREAGLTEYQLRAARHAASAL*

> *Avh195ΔED* - protein sequence without signal peptide

LSAEYQEA>VVAQNAQRWSSTHSVAAAETGDTSGKRLLRSDSIPTVDAEER*

> *Avh195* without signal peptide for heterologous expression in *C. reinhardtii*

CTGTCCGCTACGAACAGGAGGCTGTGGTGGCGCAGAACGCTCAGCGGTGGAGCTCAACTCACTCCGTGGCGGCGCCGAGACCG
 GCGACACCTCTGGCAAGCGCCTCCTCAGGTCCGACTCGATCCCGACCGTCGACGCGGAGGAGCGGGCCCTGCCCGGCATGACGAAG
 CTGACCGAGACGCTTAAGAAGTGGATCTCCGACTGCGGAGCAAGCTGAGCAACAAGAAGCTGTGGTGGAACTACCAGAAGCTGGG
 CAAGCAGAAGCTGTCGGACCTGGACATCACCGCATGTGGCTGAAGAACGGGAAGAGCTACGACGACATCTTCGACCGCTGGATTG
 GACTCGACAAGTCGCCCCGCCAGGCGGCCAAAACTTGTGAATCACGGCACCACCAGAACGATCTCTACAAGGTGCTGCGCAAGC
 GCAACATGAACCTGGAGACCATCCGCCGATTTGGCGGAGGTCGGCCTGACAGAGTACCAACTGCGCGCCGCCGTCACGCGGCG
 AGCGCCCTG

XIV - Growth media

Bacteria

Luria Bertani Broth (LB)

Bacto-tryptone	10g
Yeast extract	5g
NaCl	10g
Water	up to 1000ml
Agar (solid medium)	15g

Terrific Broth (TB)

Bacto-tryptone	12g
Yeast extract	24g
Glycerol	4ml
Phosphate buffer (HK ₂ PO ₄ 0.72M; H ₂ KPO ₄ 0.17M)	100 ml
Water	up to 900ml

Yeast

Synthetic Complete (SC) medium (pH 6.0-6.3)

Yeast Nitrogen base	1.7g
(NH ₄)SO ₄	5g
Glucose	20g
Drop Out mixture	1.5g
Water	up to 1000ml
Agar (solid medium)	20g

Plant

Murashige and Skoog (MS) 2/2

MS	4.4g
Sucrose	20g
Water	up to 1000ml
Agar (solid medium)	20g

CO₂C nutritive solution 100x

HNO₃ (d=1.33)	31ml
(NH₄)HPO₄	14.5g
MgSO₄ 7·H₂O	12.5g
Ca(NO₃)₂ 4·H₂O	61g
KNO₃	22g
μCo₂C solution	10ml
EDTA Fe	250ml
Water	up to 1000ml

Stock solutions

- **μCo₂C solution**

(NH₄)₂MoO₄	50mg
H₃BO₃	1.5g
MnSO₄ 7·H₂O	2g
ZnSO₄ 7·H₂O	1g
CuSO₄ 5·H₂O	250mg
Water	up to 100ml

- **EDTA Fe**

FeSO₄ 7H₂O	5.57g
Na₂EDTA	7.45g
Water	up to 1000ml

Chlamydomonas

TAP medium

Beijerinck solution	50ml
Phosphate buffer	1ml
Hutner's trace elements	1ml
Acetic acid	1ml
Water	up to 1000ml
Agar (solid medium)	15g

Stock solutions

- **Beijerinck solution**

NH₄Cl	8g
MgSO₄ 7·H₂O	2g
CaCl₂ 2·H₂O	1g
Water	up to 1000ml

- **Phosphate buffer**

HK₂PO₄	10.6g
H₂KPO₄	5.3g
Water	up to 100 ml

- **Hutner's trace elements**

EDTA disodium salt	50g
ZnSO₄ 7·H₂O	11.4g
H₃BO₃	22g
MnCl₂ 4·H₂O	5.06g
CoCl₂ 6·H₂O	1.61g
CuSO₄ 5·H₂O	1.57g
(NH₄)₆Mo₇O₂₄ 4·H₂O	1.1g
FeSO₄ 7·H₂O	4.99g
KOH	12g
Water	up to 1000ml

XV - Primers

Vector constructions and verification

Name	Organism	Sequence 5'3'	Polarity	Comment
attB1_Avh195_F	<i>P. parasitica</i>	GGGGACAAGTTTGTACAAAAAAGCAGGCTTCACCATGCTATCGGCCTATGAACAA	+	Gateway cloning
attB2_Avh195_R	<i>P. parasitica</i>	GGGGACCACCTTTGTACAAGAAAGCTGGGTCTCACAAAGCGCTAGCCGCGTG	-	Gateway cloning
attB2_Avh195_ΔEER_R	<i>P. parasitica</i>	GGGGACCACCTTTGTACAAGAAAGCTGGGTcctcaCCTCTCTCAGCATC	-	Gateway cloning

195_AIM_S1_mut_F	<i>P. parasitica</i>	GAAAAACGGGAAAAGCGCTGATGACGCCCTTCGACCGCTGG	+	Site-directed mutagenesis
195_AIM_S1_mut_R	<i>P. parasitica</i>	CCAGCGGTGGAAGCGTCATCAGCGCTTTTCCCGTTTTTC	-	Site-directed mutagenesis
195_AIM_S2_mut_F	<i>P. parasitica</i>	CATCTTCGACCGCGCGATTTCGAGCCGATAAGTCACCG	+	Site-directed mutagenesis
195_AIM_S2_mut_R	<i>P. parasitica</i>	CGGTGACTTATCGGCTCGAATCGCGCGGTGGAAGATG	-	Site-directed mutagenesis
195_AIM_S3_mut_F	<i>P. parasitica</i>	CAATCAGACCGATTGCGCGCGAAGCGCGGACTGACAGAG	+	Site-directed mutagenesis
195_AIM_S3_mut_R	<i>P. parasitica</i>	CTCTGTACGTCGCGCTTCGCGCGCAATCGGTCTGATTG	-	Site-directed mutagenesis

EcoRI_Avh195 noSP_F	<i>P. parasitica</i>	GGGGACGAATTCCTATCGGCCTATGAACAAGAAGCT	+	Recombinant protein production
EcoRI_Avh195_R	<i>P. parasitica</i>	GGGGACGAATTCACAAGCGCTAGCCGCGTG	-	Recombinant protein production

attB1_CrATG8_F	<i>C. reinhardtii</i>	GGGGACAAGTTTGTACAAAAAAGCAGGCTTCACCATGGTTGGTCCCGACCCCGAC	+	Gateway cloning
attB2_CrATG8_R	<i>C. reinhardtii</i>	GGGGACCACCTTTGTACAAGAAAGCTGGGTCTCACAAAGCCAGCTCCTCCACA	-	Gateway cloning

pChlamy3_intron_F	<i>C. reinhardtii</i>	TGCTTGACGATTTGACTTGC	+	Chlamydomonas genotyping
pChlamy3_spliced_F	<i>C. reinhardtii</i>	TAAATGGCCAGGAGATTGCG	+	Chlamydomonas genotyping
pChlamy3_RBCS2 3'UTR_R	<i>C. reinhardtii</i>	TACCGCTTCAGCACTTGAGA	-	Chlamydomonas genotyping
pChlamy3_5'UTR_F	<i>C. reinhardtii</i>	GATAAACCGCCAGGGGGCC	+	Chlamydomonas genotyping
pChlamy3_3'UTR_R	<i>C. reinhardtii</i>	CAGCAAAGGTAGGGCGGGC	-	Chlamydomonas genotyping

qPCR

Name	Organism	Sequence 5'3'	Polarity	Comment
PR1a: At2g14610_F	<i>A. thaliana</i>	CGGAGCTACGCAGAACAAC	+	qPCR
PR1a: At2g14610_R	<i>A. thaliana</i>	CTCGCTAACCATGTTC	-	qPCR
PD_F1.2b: At2g26020_F	<i>A. thaliana</i>	ACCAACAATGGTGGAAAGCAC	+	qPCR
PD_F1.2b: At2g26020_R	<i>A. thaliana</i>	CACCTGTGAGCTGGGAAGAC	-	qPCR
NADH : AT5G11770_F	<i>A. thaliana</i>	GAAGTTGTGCCAATGGAGGT	+	qPCR
NADH : AT5G11770_R	<i>A. thaliana</i>	CCACCAATGCAAGAAATCCT	-	qPCR
Oxa1: AT5G62050_F	<i>A. thaliana</i>	AACAGGACTCAGCGATGTTG	+	qPCR
Oxa1: AT5G62050_R	<i>A. thaliana</i>	TACCTGATCTGCCTCCACCT	-	qPCR

Name	Organism	Sequence 5'3'	Polarity	Comment
qUBC_F1	<i>P. parasitica</i>	CCACTTAGAGCACGCTAGGA	+	qPCR
qUBC_R1	<i>P. parasitica</i>	TACCGACTGTCCTTCGTTC	-	qPCR
qWS21_F1	<i>P. parasitica</i>	CTCCAGAACGTGTACATCCG	+	qPCR
qWS21_R1	<i>P. parasitica</i>	TAGCGCCCTTCTCTCAG	-	qPCR
qWS41_F1	<i>P. parasitica</i>	TTCAAGTCCAGTGAGATCGG	+	qPCR
qWS41_R1	<i>P. parasitica</i>	TTGTGTCTTTGTGTGATGCG	-	qPCR
q195_F10	<i>P. parasitica</i>	AGGCAAGCAGCAAAAAC	+	qPCR
q195_R10	<i>P. parasitica</i>	CGGCACGAAGTGTACTCTG	-	qPCR
q195_F2	<i>P. parasitica</i>	CTTCGTGAATGCTCTATCG	+	qPCR
q195_R2	<i>P. parasitica</i>	CAGAGTATCTCCGGTTTCAG	-	qPCR
qNPP1_F	<i>P. parasitica</i>	CCCCAATGAACGTCTTAC	+	qPCR
qNPP1_R	<i>P. parasitica</i>	TGAACTGACACAGCCTTC	-	qPCR
qHMP1_F	<i>P. parasitica</i>	GATCGGTGAGACCATTTTCG	+	qPCR
qHMP1_R	<i>P. parasitica</i>	TGTTGAGGAACGTGCAAGC	-	qPCR

qCre195_1_F	<i>C. reinhardtii</i>	ATCTTCGACCGCTGGATTC	+	qPCR
qCre195_1_R	<i>C. reinhardtii</i>	TGGTCTCCAGGTTATGTTG	-	qPCR
qCre_ATG8	<i>C. reinhardtii</i>	CGACATTCAAGCAGGAGCATTCC	+	qPCR
qCre_ATG8	<i>C. reinhardtii</i>	TCTGCCTTCTCGACAATGACTGG	-	qPCR
qCre_VTI_1_2_F	<i>C. reinhardtii</i>	GGCAAAGCAGCTTCAGAAC	+	qPCR
qCre_VTI_1_2_R	<i>C. reinhardtii</i>	AAAGTCCGAAGTGGATGACC	-	qPCR
qCre_ATG6_F	<i>C. reinhardtii</i>	TTTGACAACGCGAGCGTGGATG	+	qPCR
qCre_ATG6_R	<i>C. reinhardtii</i>	TGTGACCAACAGAAGCACCTTG	-	qPCR
Cre_AMYA1_F	<i>C. reinhardtii</i>	TGTCTTGATTTGCCCAAGG	+	qPCR
Cre_AMYA1_R	<i>C. reinhardtii</i>	GGCCCATGATTTGTGGTG	-	qPCR
Cre_GWD1_F	<i>C. reinhardtii</i>	TTGTGTGTGAGGGAGCGAATTG	+	qPCR
Cre_GWD1_R	<i>C. reinhardtii</i>	GCTCCATCAAATCGAGAAGG	-	qPCR
Cre_STA2_F	<i>C. reinhardtii</i>	CGATGGTTTTGTGAGGTGCAG	+	qPCR
Cre_STA2_R	<i>C. reinhardtii</i>	ATCGACGGGCACAAAATG	-	qPCR
Cre_GPM1_F	<i>C. reinhardtii</i>	CGAGCGCTTTGAGAAAGCAAC	+	qPCR
Cre_GPM1_R	<i>C. reinhardtii</i>	GCGTACAAATCCGCTCAATGC	-	qPCR
Cre_BTUB_F	<i>C. reinhardtii</i>	CCCCCGCTGCACTTCTTC	+	qPCR
Cre_BTUB_R	<i>C. reinhardtii</i>	GTCGGCGGCGCACATCAT	-	qPCR
CBLP_F	<i>C. reinhardtii</i>	GCCACACCGAGTGGGTGCTGCGG	+	qPCR
CBLP_R	<i>C. reinhardtii</i>	CCTTGCCGCCGAGGCGCACAGCG	-	qPCR
RBCS2_F	<i>C. reinhardtii</i>	ATACTGCTCTCAAGTCTGAAGCG	+	qPCR
RBCS2_R	<i>C. reinhardtii</i>	AAAGACTGATCAGCACGAAACGG	-	qPCR

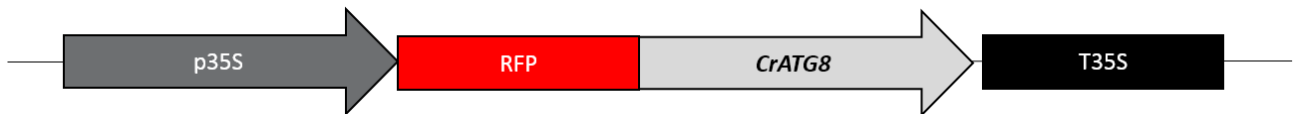
XVI - Vector constructions

Plant overexpression vectors

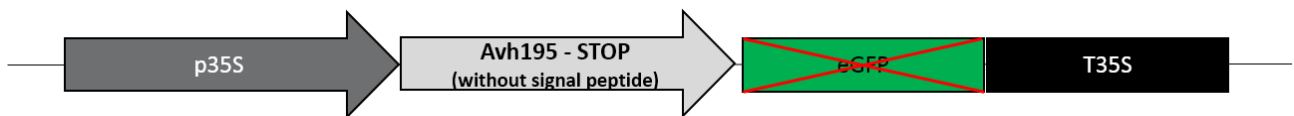
pK7WGF2-GFP_Avh195



pK7WGR2-RFP_CrATG8

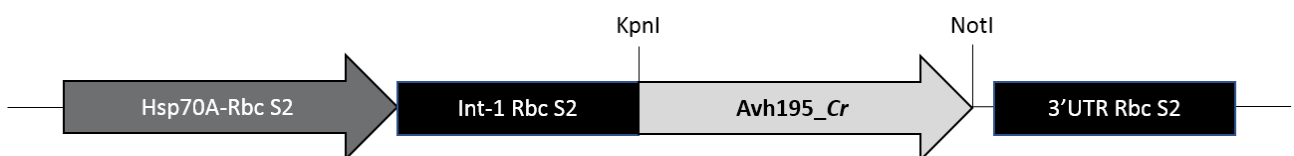


pK7FWG2-Avh195



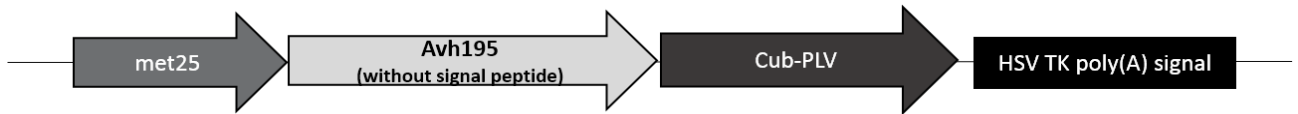
Chlamydomonas overexpression vector

pChlamy_3-Avh195

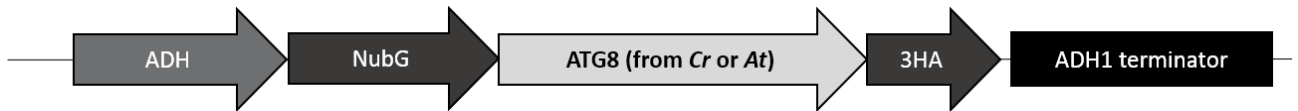


Yeast *mBSUS* vectors

pMetYC-DEST-Avh195

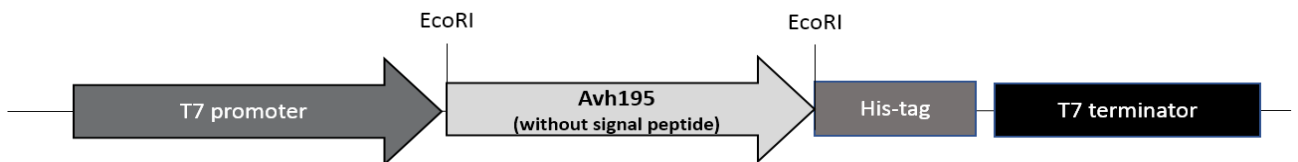


pNX32-DEST-ATG8



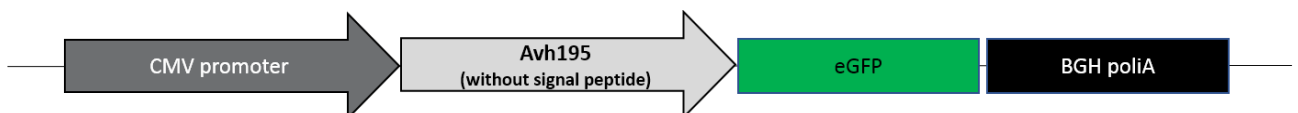
Recombinant protein production vector

pET28a-Avh195-His



HeLa overexpression vectors

pcDNA-DEST47-Avh195_GFP



pcDNA-DEST53-GFP_Avh195



Bibliography

1. André Lévesque C (2011) Fifty years of oomycetes-from consolidation to evolutionary and genomic exploration. *Fungal Divers* **50**: 35–46.
2. Beakes GW, Glockling SL, Sekimoto S (2012) The evolutionary phylogeny of the oomycete ‘fungi’. *Protoplasma* **249**: 3–19.
3. Cavalier-Smith T, Chao EY (2006) Phylogeny and megasystematics of phagotrophic heterokonts (kingdom Chromista). *J Mol Evol* **62**: 388–420.
4. Judelson HS (2017) Metabolic Diversity and Novelty in the Oomycetes. *Annu Rev Microbiol* **71**: 21–39.
5. Baldauf SL, Roger AJ, Wenk-Siefert I, Doolittle WF (2000) A kingdom-level phylogeny of eukaryotes based on combined protein data. *Science* **290**: 972–977.
6. Burki F (2014) The eukaryotic tree of life from a global phylogenomic perspective. *Cold Spring Harb Perspect Biol* **6**: a016147.
7. Derelle R, López-García P, Timpano H, Moreira D (2016) A Phylogenomic Framework to Study the Diversity and Evolution of Stramenopiles (=Heterokonts). *Mol Biol Evol* **33**: 2890–2898.
8. Tyler BM (2006) Phytophthora Genome Sequences Uncover Evolutionary Origins and Mechanisms of Pathogenesis. *Science (80-)* **313**: 1261–1266.
9. Matari NH, Blair JE (2014) A multilocus timescale for oomycete evolution estimated under three distinct molecular clock models. *BMC Evol Biol* **14**: 1–11.
10. Krings M, Taylor TN, Dotzler N (2011) The fossil record of the Peronosporomycetes (Oomycota). *Mycologia* **103**: 445–457.
11. Strullu-Derrien C, Kenrick P, Rioult JP, Strullu DG (2011) Evidence of parasitic Oomycetes (Peronosporomycetes) infecting the stem cortex of the Carboniferous seed fern *Lyginopteris oldhamia*. *Proc R Soc B Biol Sci* **278**: 675–680.
12. Thines M, Kamoun S (2010) Oomycete-plant coevolution: Recent advances and future prospects. *Curr Opin Plant Biol* **13**: 427–433.
13. Savory F, Leonard G, Richards TA (2015) The Role of Horizontal Gene Transfer in the Evolution of the Oomycetes. *PLoS Pathog* **11**: 1–6.
14. Jiang RHY, Tyler BM (2012) Mechanisms and Evolution of Virulence in Oomycetes. *Annu Rev Phytopathol* **50**: 295–318.
15. Phillips AJ, Anderson VL, Robertson EJ, Secombes CJ, van West P (2008) New insights into animal pathogenic oomycetes. *Trends Microbiol* **16**: 13–19.
16. Gaulin E, Jacquet C, Bottin A, Dumas B (2007) Root rot disease of legumes caused by *Aphanomyces euteiches*. *Mol Plant Pathol* **8**: 539–548.
17. Thines M (2014) Phylogeny and evolution of plant pathogenic oomycetes-a global overview. *Eur J Plant Pathol* **138**: 431–447.
18. Latijnhouwers M, De Wit PJGM, Govers F (2003) Oomycetes and fungi: Similar weaponry to attack plants. *Trends Microbiol* **11**: 462–469.

19. Kamoun S (2009) Plant Pathogens: Oomycetes (water mold). In, *Encyclopedia of Microbiology* pp 689–695. Elsevier Inc., Norwich, UK.
20. van West P (2006) *Saprolegnia parasitica*, an oomycete pathogen with a fishy appetite: new challenges for an old problem. *Mycologist* **20**: 99–104.
21. Kamoun S, Furzer O, Jones JDG, Judelson HS, Ali GS, Dalio RJD, Roy SG, Schena L, Zambounis A, Panabières F, et al. (2015) The Top 10 oomycete pathogens in molecular plant pathology. *Mol Plant Pathol* **16**: 413–434.
22. Derevnina L, Petre B, Kellner R, Dagdas YF, Sarowar MN, Giannakopoulou A, De la Concepcion JC, Chaparro-Garcia A, Pennington HG, van West P, et al. (2016) Emerging oomycete threats to plants and animals. *Philos Trans R Soc B Biol Sci* **371**: 20150459.
23. Randall E, Young V, Sierotzki H, Scalliet G, Birch PRJ, Cooke DEL, Csukai M, Whisson SC (2014) Sequence diversity in the large subunit of RNA polymerase I contributes to Mefenoxam insensitivity in *Phytophthora infestans*. *Mol Plant Pathol* **15**: 664–676.
24. Gisi U, Sierotzki H (2015) Oomycete Fungicides: Phenylamides, Quinone Outside Inhibitors, and Carboxylic Acid Amides. In, *Fungicide Resistance in Plant Pathogens* pp 145–174. Springer Japan, Tokyo, JP.
25. Fisher MC, Henk DA, Briggs CJ, Brownstein JS, Madoff LC, McCraw SL, Gurr SJ (2012) Emerging fungal threats to animal, plant and ecosystem health. *Nature* **484**: 186–194.
26. Agrios GN (2005) *Plant pathology*. Elsevier Academic Press, London, UK.
27. Pais M, Win J, Yoshida K, Etherington GJ, Cano LM, Raffaele S, Banfield MJ, Jones A, Kamoun S, Saunders DGO (2013) From pathogen genomes to host plant processes: the power of plant parasitic oomycetes. *Genome Biol* **14**: 211–221.
28. Martin FN, Blair JE, Coffey MD (2014) A combined mitochondrial and nuclear multilocus phylogeny of the genus *Phytophthora*. *Fungal Genet Biol* **66**: 19–32.
29. Meng Y, Zhang Q, Ding W, Shan W (2014) *Phytophthora parasitica*: a model oomycete plant pathogen. *Mycology* **5**: 43–51.
30. Panabières F, Ali GS, Allagui MB, Dalio RJD, Gudmestad NC, Kuhn ML, Guha Roy S, Schena L, Zampounis A (2016) *Phytophthora nicotianae* diseases worldwide: New knowledge of a long-recognised pathogen. *Phytopathol Mediterr* **55**: 20–40.
31. Attard A, Gourgues M, Callemeyn-Torre N, Keller H (2010) The immediate activation of defense responses in *Arabidopsis* roots is not sufficient to prevent *Phytophthora parasitica* infection. *New Phytol* **187**: 449–460.
32. Attard A, Gourgues M, Galiana E, Panabières F, Ponchet M, Keller H (2008) Strategies of attack and defense in plant-oomycete interactions, accentuated for *Phytophthora parasitica* Dastur (syn. *P. Nicotianae* Breda de Haan). *J Plant Physiol* **165**: 83–94.
33. Judelson HS, Blanco FA (2005) The spores of *Phytophthora*: Weapons of the plant destroyer. *Nat Rev Microbiol* **3**: 47–58.
34. Walker CA, van West P (2007) Zoospore development in the oomycetes. *Fungal Biol Rev* **21**: 10–18.
35. Hardham AR (2001) The cell biology behind *Phytophthora* pathogenicity. *Australas Plant Pathol* **30**: 91–98.
36. Hardham AR (2007) Cell biology of plant-oomycete interactions. *Cell Microbiol* **9**: 31–39.
37. Erwin DC, Ribeiro OK (1996) *Phytophthora diseases worldwide*. APS Press, St Paul, MN, USA.

-
38. Le Berre JY, Engler G, Panabières F (2008) Exploration of the late stages of the tomato-*Phytophthora parasitica* interactions through histological analysis and generation of expressed sequence tags. *New Phytol* **177**: 480–492.
 39. Shan W, Hardham AR (2004) Construction of a bacterial artificial chromosome library, determination of genome size, and characterization of an Hsp70 gene family in *Phytophthora nicotianae*. *Fungal Genet Biol* **41**: 369–380.
 40. Parasitica, *Phytophthora* genome : https://olive.broadinstitute.org/projects/phytophthora_parasitica.
 41. Panabieres F, Amselem J, Galiana E, Le Berre JY (2005) Gene identification in the oomycete pathogen *Phytophthora parasitica* during in vitro vegetative growth through expressed sequence tags. *Fungal Genet Biol* **42**: 611–623.
 42. Škalamera D, Wasson AP, Hardham AR (2004) Genes expressed in zoospores of *Phytophthora nicotianae*. *Mol Genet Genomics* **270**: 549–557.
 43. Kebdani N, Pieuchot L, Deleury E, Panabières F, Le Berre JY, Gourgues M (2010) Cellular and molecular characterization of *Phytophthora parasitica* appressorium-mediated penetration. *New Phytol* **185**: 248–257.
 44. Attard A, Evangelisti E, Kebdani-minet N, Panabières F, Deleury E, Maggio C, Ponchet M, Gourgues M (2014) Transcriptome dynamics of *Arabidopsis thaliana* root penetration by the oomycete pathogen *Phytophthora parasitica*. *BMC Genomics* **15**: 538-557.
 45. Le Berre J-Y, Gourgues M, Samans B, Keller H, Panabières F, Attard A (2017) Transcriptome dynamic of *Arabidopsis* roots infected with *Phytophthora parasitica* identifies VQ29, a gene induced during the penetration and involved in the restriction of infection. *PLoS One* **12**: e0190341.
 46. Kamoun S (2007) Groovy times: filamentous pathogen effectors revealed. *Curr Opin Plant Biol* **10**: 358–365.
 47. Dong S, Raffaele S, Kamoun S (2015) The two-speed genomes of filamentous pathogens: Waltz with plants. *Curr Opin Genet Dev* **35**: 57–65.
 48. Jones JDG, Dangl JL (2006) The plant immune system. *Nature* **444**: 323–329.
 49. Zipfel C (2008) Pattern-recognition receptors in plant innate immunity. *Curr Opin Immunol* **20**: 10–16.
 50. Brunner F, Rosahl S, Lee J, Rudd JJ, Geiler C, Kauppinen S, Rasmussen G, Scheel D, Nürnberger T (2002) Pep-13, a plant defense-inducing pathogen-associated pattern from *Phytophthora* transglutaminases. *EMBO J* **21**: 6681–6688.
 51. Nennstiel D, Scheel D, Nürnberger T (1998) Characterization and partial purification of an oligopeptide elicitor receptor from parsley (*Petroselinum crispum*). *FEBS Lett* **431**: 405–410.
 52. Fellbrich G, Romanski A, Varet A, Blume B, Brunner F, Engelhardt S, Felix G, Kemmerling B, Krzymowska M, Nürnberger T (2002) NPP1, a *Phytophthora*-associated trigger of plant defense in parsley and *Arabidopsis*. *Plant J* **32**: 375–390.
 53. Wawra S, Belmonte R, Löbach L, Saraiva M, Willems A, van West P (2012) Secretion, delivery and function of oomycete effector proteins. *Curr Opin Microbiol* **15**: 685–691.
 54. Stassen JHM, Van den Ackerveken G (2011) How do oomycete effectors interfere with plant life? *Curr Opin Plant Biol* **14**: 407–414.
 55. Ponchet M, Panabières F, Milat ML, Mikes V, Montillet JL, Suty L, Triantaphylides C, Tirilly Y, Blein JP (1999) Are elicitors cryptograms in plant-Oomycete communications? *Cell Mol Life Sci* **56**: 1020–1047.
-

56. Osman H, Mikes V, Milat ML, Ponchet M, Marion D, Prangé T, Maume BF, Vauthrin S, Blein JP (2001) Fatty acids bind to the fungal elicitor cryptogein and compete with sterols. *FEBS Lett* **489**: 55–58.
57. Anderson RG, Deb D, Fedkenheuer K, McDowell JM (2015) Recent Progress in RXLR Effector Research. *Mol Plant-Microbe Interact* **28**: 1063–1072.
58. Amaro TMMM, Thilliez GJA, Motion GB, Huitema E (2017) A Perspective on CRN Proteins in the Genomics Age: Evolution, Classification, Delivery and Function Revisited. *Front Plant Sci* **8**: 99–111.
59. Rehmany AP (2005) Differential Recognition of Highly Divergent Downy Mildew Avirulence Gene Alleles by RPP1 Resistance Genes from Two Arabidopsis Lines. *Plant Cell Online* **17**: 1839–1850.
60. Birch PR, Boevink PC, Gilroy EM, Hein I, Pritchard L, Whisson SC (2008) Oomycete RXLR effectors: delivery, functional redundancy and durable disease resistance. *Curr Opin Plant Biol* **11**: 373–379.
61. Kamoun S (2006) A Catalogue of the Effector Secretome of Plant Pathogenic Oomycetes. *Annu Rev Phytopathol* **44**: 41–60.
62. Win J, Krasileva K V., Kamoun S, Shirasu K, Staskawicz BJ, Banfield MJ (2012) Sequence divergent RXLR effectors share a structural fold conserved across plant pathogenic oomycete species. *PLoS Pathog* **8**: 8–11.
63. Boutemy LS, King SRF, Win J, Hughes RK, Clarke TA, Blumenschein TMA, Kamoun S, Banfield MJ (2011) Structures of Phytophthora RXLR effector proteins: A conserved but adaptable fold underpins functional diversity. *J Biol Chem* **286**: 35834–35842.
64. Whisson SC, Boevink PC, Moleleki L, Avrova AO, Morales JG, Gilroy EM, Armstrong MR, Grouffaud S, van West P, Chapman S, et al. (2007) A translocation signal for delivery of oomycete effector proteins into host plant cells. *Nature* **450**: 115–118.
65. Dou D, Kale SD, Wang X, Jiang RHY, Bruce N a, Arredondo FD, Zhang X, Tyler BM (2008) RXLR-Mediated Entry of Phytophthora sojae Effector Avr1b into Soybean Cells Does Not Require Pathogen-Encoded Machinery. *Plant Cell* **20**: 1930–1947.
66. Grouffaud S, van West P, Avrova AO, Birch PRJ, Whisson SC (2008) Plasmodium falciparum and Hyaloperonospora parasitica effector translocation motifs are functional in Phytophthora infestans. *Microbiology* **154**: 3743–3751.
67. Kale SD, Tyler BM (2011) Entry of oomycete and fungal effectors into plant and animal host cells. *Cell Microbiol* **13**: 1839–1848.
68. Yaeno T, Li H, Chaparro-Garcia A, Schornack S, Koshiba S, Watanabe S, Kigawa T, Kamoun S, Shirasu K (2011) Phosphatidylinositol monophosphate-binding interface in the oomycete RXLR effector AVR3a is required for its stability in host cells to modulate plant immunity. *Proc Natl Acad Sci* **108**: 14682–14687.
69. Tyler BM, Kale SD, Wang Q, Tao K, Clark HR, Drews K, Antignani V, Rumore A, Hayes T, Plett JM, et al. (2013) Microbe-independent entry of oomycete RxLR effectors and fungal RxLR-like effectors into plant and animal cells is specific and reproducible. *Mol Plant-Microbe Interact* **26**: 611–616.
70. Morgan W, Kamoun S (2007) RXLR effectors of plant pathogenic oomycetes. *Curr Opin Microbiol* **10**: 332–338.
71. Wang Q, Han C, Ferreira AO, Yu X, Ye W, Tripathy S, Kale SD, Gu B, Sheng Y, Sui Y, et al. (2011) Transcriptional programming and functional interactions within the Phytophthora sojae RXLR effector repertoire. *Plant Cell* **23**: 2064–2086.

-
72. Kelley BS, Lee SJ, Damasceno CMB, Chakravarthy S, Kim BD, Martin GB, Rose JKC (2010) A secreted effector protein (SNE1) from *Phytophthora infestans* is a broadly acting suppressor of programmed cell death. *Plant J* **62**: 357–366.
 73. Caillaud MC, Piquerez SJM, Fabro G, Steinbrenner J, Ishaque N, Beynon J, Jones JDG (2012) Subcellular localization of the Hpa RxLR effector repertoire identifies a tonoplast-associated protein HaRxL17 that confers enhanced plant susceptibility. *Plant J* **69**: 252–265.
 74. Sperschneider J, Catanzariti A-M, DeBoer K, Petre B, Gardiner DM, Singh KB, Dodds PN, Taylor JM (2017) LOCALIZER: subcellular localization prediction of both plant and effector proteins in the plant cell. *Sci Rep* **7**: 44598.
 75. McLellan H, Boevink PC, Armstrong MR, Pritchard L, Gomez S, Morales J, Whisson SC, Beynon JL, Birch PRJ (2013) An RxLR Effector from *Phytophthora infestans* Prevents Re-localisation of Two Plant NAC Transcription Factors from the Endoplasmic Reticulum to the Nucleus. *PLoS Pathog* **9**: e1003670.
 76. Qiao Y, Shi J, Zhai Y, Hou Y, Ma W (2015) *Phytophthora* effector targets a novel component of small RNA pathway in plants to promote infection. *Proc Natl Acad Sci* **112**: 5850–5855.
 77. Boevink PC, McLellan H, Gilroy EM, Naqvi S, He Q, Yang L, Wang X, Turnbull D, Armstrong MR, Tian Z, et al. (2016) Oomycetes Seek Help from the Plant: *Phytophthora infestans* Effectors Target Host Susceptibility Factors. *Mol Plant* **9**: 636–638.
 78. Liu T, Song T, Zhang X, Yuan H, Su L, Li W, Xu J, Liu S, Chen L, Chen T, et al. (2014) Unconventionally secreted effectors of two filamentous pathogens target plant salicylate biosynthesis. *Nat Commun* **5**: 4686–4696.
 79. Evangelisti E, Govetto B, Minet-Kebdani N, Kuhn ML, Attard A, Ponchet M, Panabières F, Gourgues M (2013) The *Phytophthora parasitica* RXLR effector Penetration-Specific Effector 1 favours *Arabidopsis thaliana* infection by interfering with auxin physiology. *New Phytol* **199**: 476–489.
 80. Zheng X, McLellan H, Friture M, Liu X, Boevink PC, Gilroy EM, Chen Y, Kandel K, Sessa G, Birch PRJ, et al. (2014) Functionally Redundant RXLR Effectors from *Phytophthora infestans* Act at Different Steps to Suppress Early flg22-Triggered Immunity. *PLoS Pathog* **10**: e1004057–e1004074.
 81. Freytag S, Arabatzis N, Hahlbrock K, Schmelzer E (1994) Reversible cytoplasmic rearrangements precede wall apposition, hypersensitive cell death and defense-related gene activation in potato/*Phytophthora infestans* interactions. *Planta* **194**: 123–135.
 82. Takemoto D, Jones DA, Hardham AR (2003) GFP-tagging of cell components reveals the dynamics of subcellular re-organization in response to infection of *Arabidopsis* by oomycete pathogens. *Plant J* **33**: 775–792.
 83. Hein I, Gilroy EM, Armstrong MR, Birch PRJ (2009) The zig-zag-zig in oomycete-plant interactions. *Mol Plant Pathol* **10**: 547–562.
 84. Koh S, Somerville S (2006) Show and tell: cell biology of pathogen invasion. *Curr Opin Plant Biol* **9**: 406–413.
 85. Lu YJ, Schornack S, Spallek T, Geldner N, Chory J, Schellmann S, Schumacher K, Kamoun S, Robatzek S (2012) Patterns of plant subcellular responses to successful oomycete infections reveal differences in host cell reprogramming and endocytic trafficking. *Cell Microbiol* **14**: 682–697.
 86. Bozkurt TO, Belhaj K, Dagdas YF, Chaparro-Garcia A, Wu CH, Cano LM, Kamoun S (2015) Rerouting of Plant Late Endocytic Trafficking Toward a Pathogen Interface. *Traffic* **16**: 204–226.
-

87. Chaparro-Garcia A, Schwizer S, Sklenar J, Yoshida K, Petre B, Bos JIB, Schornack S, Jones AME, Bozkurt TO, Kamoun S (2015) Phytophthora infestans RXLR-WY effector AVR3a associates with dynamin-related protein 2 required for endocytosis of the plant pattern recognition receptor FLS2. *PLoS One* **10**: e0137071.
 88. Du Y, Mpina MH, Birch PRJ, Bouwmeester K, Govers F (2015) Phytophthora infestans RXLR effector AVR1 interacts with exocyst component Sec5 to manipulate plant immunity. *Plant Physiol* **169**: 1975–1990.
 89. Dagdas YF, Beihaj K, Maqbool A, Chaparro-Garcia A, Pandey P, Petre B, Tabassum N, Cruz-Mireles N, Hughes RK, Sklenar J, et al. (2016) An effector of the Irish potato famine pathogen antagonizes a host autophagy cargo receptor. *Elife* **5**: 1–23.
 90. Boevink PC, Wang X, McLellan H, He Q, Naqvi S, Armstrong MR, Zhang W, Hein I, Gilroy EM, Tian Z, et al. (2016) A Phytophthora infestans RXLR effector targets plant PP1c isoforms that promote late blight disease. *Nat Commun* **7**: 10311–10325.
 91. Klionsky DJ (2008) Autophagy revisited: A conversation with Christian de Duve. *Autophagy* **4**: 740–743.
 92. Ohsumi Y (2014) Historical landmarks of autophagy research. *Cell Res* **24**: 9–23.
 93. Takeshige K, Baba M, Tsuboi S, Noda T, Ohsumi Y (1992) Autophagy in yeast demonstrated with proteinase-deficient mutants and conditions for its induction. *J Cell Biol* **119**: 301–311.
 94. Baba M, Takeshige K, Baba N, Ohsumi Y (1994) Ultrastructural analysis of the autophagic process in yeast: Detection of autophagosomes and their characterization. *J Cell Biol* **124**: 903–913.
 95. Tsukada M, Ohsumi Y (1993) Isolation and characterization of autophagy-defective mutants of *Saccharomyces cerevisiae*. *FEBS Lett* **333**: 169–174.
 96. Thumm M, Egner R, Koch B, Schlumpberger M, Straub M, Veenhuis M, Wolf DH (1994) Isolation of autophagocytosis mutants of *Saccharomyces cerevisiae*. *FEBS Lett* **349**: 275–280.
 97. Klionsky DJ (2007) Autophagy: from phenomenology to molecular understanding in less than a decade. *Nat Rev Mol Cell Biol* **8**: 931–937.
 98. Levine B, Klionsky DJ (2004) Development by self-digestion: Molecular mechanisms and biological functions of autophagy. *Dev Cell* **6**: 463–477.
 99. Eskelinen E-L, Saftig P (2009) Autophagy: a lysosomal degradation pathway with a central role in health and disease. *Biochim Biophys Acta* **1793**: 664–673.
 100. Üstün S, Hafrén A, Hofius D (2017) Autophagy as a mediator of life and death in plants. *Curr Opin Plant Biol* **40**: 122–130.
 101. Anding AL, Baehrecke EH (2017) Cleaning House: Selective Autophagy of Organelles. *Dev Cell* **41**: 10–22.
 102. Lynch-Day M, Klionsky DJ (2011) The Cvt pathway as a model for selective autophagy. *FEBS Lett* **584**: 1359–1366.
 103. Zaffagnini G, Martens S (2016) Mechanisms of Selective Autophagy. *J Mol Biol* **428**: 1714–1724.
 104. Kwon S II, Cho HJ, Jung JH, Yoshimoto K, Shirasu K, Park OK (2010) The Rab GTPase RabG3b functions in autophagy and contributes to tracheary element differentiation in *Arabidopsis*. *Plant J* **64**: 151–164.
 105. Melendez A, Neufeld TP (2008) The cell biology of autophagy in metazoans: a developing story. *Development* **135**: 2347–2360.
-

106. Maiuri MC, Zalckvar E, Kimchi A, Kroemer G (2007) Self-eating and self-killing: crosstalk between autophagy and apoptosis. *Nat Rev Mol Cell Biol* **8**: 741–752.
107. Suzuki K, Ohsumi Y (2007) Molecular machinery of autophagosome formation in yeast, *Saccharomyces cerevisiae*. *FEBS Lett* **581**: 2156–2161.
108. Marion J, Le Bars R, Besse L, Batoko H, Satiat-Jeunemaitre B (2018) Multiscale and Multimodal Approaches to Study Autophagy in Model Plants. *Cells* **7**: 1–17.
109. Zheng XF, Fiorentino D, Chen J, Crabtree GR, Schreiber SL (1995) TOR kinase domains are required for two distinct functions, only one of which is inhibited by rapamycin. *Cell* **82**: 121–130.
110. Loewith R, Hall MN (2011) Target of rapamycin (TOR) in nutrient signaling and growth control. *Genetics* **189**: 1177–1201.
111. Stephan JS, Yeh Y-Y, Ramachandran V, Deminoff SJ, Herman PK (2009) The Tor and PKA signaling pathways independently target the Atg1/Atg13 protein kinase complex to control autophagy. *Proc Natl Acad Sci* **106**: 17049–17054.
112. Torggler R, Papinski D, Kraft C (2017) Assays to Monitor Autophagy in *Saccharomyces cerevisiae*. *Cells* **6**: 1–24.
113. Farré J-C, Subramani S (2016) Mechanistic insights into selective autophagy pathways: lessons from yeast. *Nat Rev Mol Cell Biol* **17**: 537–552.
114. Yorimitsu T, Klionsky DJ (2005) Atg11 Links Cargo to the Vesicle-forming Machinery in the Cytoplasm to Vacuole Targeting Pathway. *Mol Biol Cell* **16**: 1593–1605.
115. Kijanska M, Peter M (2013) Atg1 kinase regulates early and late steps during autophagy. *Autophagy* **9**: 249–251.
116. Yeasmin AMST, Waliullah TM, Kondo A, Kaneko A, Koike N, Ushimaru T (2016) Orchestrated action of PP2A antagonizes atg13 phosphorylation and promotes autophagy after the inactivation of TORC1. *PLoS One* **11**: 1–20.
117. Kamada Y, Funakoshi T, Shintani T, Nagano K, Ohsumi M, Ohsumi Y (2000) Tor-mediated induction of autophagy via an Apg1 protein kinase complex. *J Cell Biol* **150**: 1507–1513.
118. Cheong H, Klionsky DJ (2008) Dual role of Atg1 in regulation of autophagy-specific PAS assembly in *Saccharomyces cerevisiae*. *Autophagy* **4**: 724–726.
119. Suzuki K, Kirisako T, Kamada Y, Mizushima N, Noda T, Ohsumi Y (2001) The pre-autophagosomal structure organized by concerted functions of APG genes is essential for autophagosome formation. *EMBO J* **20**: 5971–5981.
120. Stanley RE, Ragusa MJ, Hurley JH (2014) The beginning of the end: How scaffolds nucleate autophagosome biogenesis. *Trends Cell Biol* **24**: 73–81.
121. Rubinsztein DC, Shpilka T, Elazar Z (2012) Mechanisms of autophagosome biogenesis. *Curr Biol* **22**: R29–R34.
122. Obara K, Ohsumi Y (2008) Dynamics and function of PtdIns(3)P in autophagy. *Autophagy* **4**: 952–954.
123. Kihara A, Noda T, Ishihara N, Ohsumi Y (2001) Two distinct Vps34 phosphatidylinositol 3-kinase complexes function in autophagy and carboxypeptidase γ sorting in *Saccharomyces cerevisiae*. *J Cell Biol* **153**: 519–530.
124. Suzuki K, Kubota Y, Sekito T, Ohsumi Y (2007) Hierarchy of Atg proteins in pre-autophagosomal structure organization. *Genes to Cells* **12**: 209–218.

125. Reggiori F, Tucker KA, Stromhaug PE, Klionsky DJ (2004) The Atg1-Atg13 Complex Regulates Atg9 and Atg23 Retrieval Transport from the Pre-Autophagosomal Structure. *Dev Cell* **6**: 79–90.
126. Papinski D, Kraft C (2014) Atg1 kinase organizes autophagosome formation by phosphorylating Atg9. *Autophagy* **10**: 1338–1340.
127. Sugawara K, Suzuki NN, Fujioka Y, Mizushima N, Ohsumi Y, Inagaki F (2004) The crystal structure of microtubule-associated protein light chain 3, a mammalian homologue of *Saccharomyces cerevisiae* Atg8. *Genes to Cells* 611–618.
128. Suzuki NN, Yoshimoto K, Fujioka Y, Ohsumi Y, Inagaki F (2005) The Crystal Structure of Plant ATG12 and its Biological Implication in Autophagy. *Autophagy* **1**: 119–126.
129. Mizushima N, Noda T, Yoshimori T, Tanaka Y, Ishii T, George MD, Klionsky DJ, Ohsumi M, Ohsumi Y (1998) A protein conjugation system essential for autophagy. *Nature* **395**: 395–398.
130. Hanada T, Noda NN, Satomi Y, Ichimura Y, Fujioka Y, Takao T, Inagaki F, Ohsumi Y (2007) The Atg12-Atg5 Conjugate Has a Novel E3-like Activity for Protein Lipidation in Autophagy. *J Biol Chem* **282**: 37298–37302.
131. Kuma A, Mizushima N, Ishihara N, Ohsumi Y (2002) Formation of the approximately 350-kDa Apg12-Apg5-Apg16 multimeric complex, mediated by Apg16 oligomerization, is essential for autophagy in yeast. *J Biol Chem* **277**: 18619–18625.
132. Ichimura Y, Kirisako T, Takao T, Satomi Y, Shimonishi Y, Ishihara N, Mizushima N, Tanida I, Kominami E, Ohsumi M, et al. (2000) A ubiquitin-like system mediates protein lipidation. *Nature* **408**: 488–492.
133. Xie Z, Nair U, Klionsky DJ (2008) Atg8 Controls Phagophore Expansion during Autophagosome Formation. *Mol Biol Cell* **19**: 3290–3298.
134. Knorr RL, Nakatogawa H, Ohsumi Y, Lipowsky R, Baumgart T, Dimova R (2014) Membrane Morphology Is Actively Transformed by Covalent Binding of the Protein Atg8 to PE-Lipids. *PLoS One* **9**: e115357.
135. Noda NN, Ohsumi Y, Inagaki F (2010) Atg8-family interacting motif crucial for selective autophagy. *FEBS Lett* **584**: 1379–1385.
136. Yu Z-Q, Ni T, Hong B, Wang H-Y, Jiang F-J, Zou S, Chen Y, Zheng X-L, Klionsky DJ, Liang Y, et al. (2012) Dual roles of Atg8-PE deconjugation by Atg4 in autophagy. *Autophagy* **8**: 883–892.
137. Sánchez-Wandelmer J, Kriegenburg F, Rohringer S, Schuschnig M, Gómez-Sánchez R, Zens B, Abreu S, Hardenberg R, Hollenstein D, Gao J, et al. (2017) Atg4 proteolytic activity can be inhibited by Atg1 phosphorylation. *Nat Commun* **8**: 1–10.
138. Reggiori F, Ungermann C (2017) Autophagosome Maturation and Fusion. *J Mol Biol* **429**: 486–496.
139. Nakamura N, Matsuura a, Wada Y, Ohsumi Y (1997) Acidification of vacuoles is required for autophagic degradation in the yeast, *Saccharomyces cerevisiae*. *J Biochem* **121**: 338–344.
140. Yang Z, Huang J, Geng J, Nair U, Klionsky DJ (2006) Atg22 Recycles Amino Acids to Link the Degradative and Recycling Functions of Autophagy. *Mol Biol Cell* **17**: 5094–5104.
141. Yoshimoto K, Takano Y, Sakai Y (2010) Autophagy in plants and phytopathogens. *FEBS Lett* **584**: 1350–1358.
142. Shemi A, Ben-Dor S, Vardi A (2015) Elucidating the composition and conservation of the autophagy pathway in photosynthetic eukaryotes. *Autophagy* **11**: 701–715.
143. Avin-Wittenberg T, Honig A, Galili G (2012) Variations on a theme: Plant autophagy in comparison to yeast and mammals. *Protoplasma* **249**: 285–299.

144. Thompson AR, Vierstra RD (2005) Autophagic recycling: Lessons from yeast help define the process in plants. *Curr Opin Plant Biol* **8**: 165–173.
145. Bassham DC, Laporte M, Marty F, Moriyasu Y, Ohsumi Y, Olsen LJ, Yoshimoto K (2006) Autophagy in development and stress responses of plants. *Autophagy* **2**: 2–11.
146. Kellner R, De la Concepcion JC, Maqbool A, Kamoun S, Dagdas YF (2017) ATG8 Expansion: A Driver of Selective Autophagy Diversification?. *Trends Plant Sci* **22**: 204–214.
147. Suttangkakul A, Li F, Chung T, Vierstra RD (2011) The ATG1/ATG13 Protein Kinase Complex Is Both a Regulator and a Target of Autophagic Recycling in Arabidopsis. *Plant Cell* **23**: 3761–3779.
148. Hanaoka H, Noda T, Shirano Y, Kato T, Hayashi H, Shibata D, Tabata S, Ohsumi Y (2002) Leaf senescence and starvation-induced chlorosis are accelerated by the disruption of an Arabidopsis autophagy gene. *Plant Physiol* **129**: 1181–1193.
149. Patel S, Dinesh-Kumar SP (2008) Arabidopsis ATG6 is required to limit the pathogen-associated cell death response. *Autophagy* **4**: 20–27.
150. Xiong Y, Contento AL, Bassham DC (2005) AtATG18a is required for the formation of autophagosomes during nutrient stress and senescence in Arabidopsis thaliana. *Plant J* **42**: 535–546.
151. Doelling JH, Walker JM, Friedman EM, Thompson AR, Vierstra RD (2002) The APG8/12-activating enzyme APG7 is required for proper nutrient recycling and senescence in Arabidopsis thaliana. *J Biol Chem* **277**: 33105–33114.
152. Yoshimoto K, Hanaoka H, Sato S, Kato T, Tabata S, Noda T, Ohsumi Y (2004) Processing of ATG8s, ubiquitin-like proteins, and their deconjugation by ATG4s are essential for plant autophagy. *Plant Cell* **16**: 2967–2983.
153. Thompson AR, Doelling JH, Suttangkakul A, Vierstra RD (2005) Autophagic Nutrient Recycling in Arabidopsis Directed by the ATG8 and ATG12 Conjugation Pathways. *Plant Physiol* **138**: 2097–2110.
154. Phillips AR, Suttangkakul A, Vierstra RD (2008) The ATG12-Conjugating Enzyme ATG10 Is Essential for Autophagic Vesicle Formation in Arabidopsis thaliana. *Genetics* **135**: 1339–1353.
155. Surpin M, Zheng H, Morita MT, Saito C, Avila E, Blakeslee JJ, Bandyopadhyay A, Kovaleva V, Carter D, Murphy A, et al. (2003) The VTI family of SNARE proteins is necessary for plant viability and mediates different protein transport pathways. *Plant Cell* **15**: 2885–2899.
156. Qin G, Ma Z, Zhang L, Xing S, Hou X, Deng J, Liu J, Chen Z, Qu LJ, Gu H (2007) Arabidopsis AtBECLIN 1/AtAtg6/AtVps30 is essential for pollen germination and plant development. *Cell Res* **17**: 249–263.
157. Kim SH, Kwon C, Lee JH, Chung T (2012) Genes for plant autophagy: Functions and interactions. *Mol Cells* **34**: 413–423.
158. Michaeli S, Avin-Wittenberg T, Galili G (2014) Involvement of autophagy in the direct ER to vacuole protein trafficking route in plants. *Front Plant Sci* **5**: 1–5.
159. Wang Y, Yu B, Zhao J, Guo J, Li Y, Han S, Huang L, Du Y, Hong Y, Tang D, et al. (2013) Autophagy contributes to leaf starch degradation. *Plant Cell* **25**: 1383–1399.
160. Guiboileau A, Yoshimoto K, Soulay F, Bataillé MP, Avice JC, Masclaux-Daubresse C (2012) Autophagy machinery controls nitrogen remobilization at the whole-plant level under both limiting and ample nitrate conditions in Arabidopsis. *New Phytol* **194**: 732–740.
161. Han S, Wang Y, Zheng X, Jia Q, Zhao J, Bai F, Hong Y, Liu Y (2015) Cytoplasmic Glyceraldehyde-3-Phosphate Dehydrogenases Interact with ATG3 to Negatively Regulate Autophagy and Immunity in Nicotiana benthamiana. *Plant Cell* **27**: 1–16.

162. Michaeli S, Honig A, Levanony H, Peled-Zehavi H, Galili G (2014) Arabidopsis ATG8-INTERACTING PROTEIN1 Is Involved in Autophagy-Dependent Vesicular Trafficking of Plastid Proteins to the Vacuole. *Plant Cell* **26**: 4084–4101.
163. Zhou J, Wang J, Yu J-Q, Chen Z (2014) Role and regulation of autophagy in heat stress responses of tomato plants. *Front Plant Sci* **5**: 1–12.
164. Kim J, Lee H, Lee HN, Kim S-H, Shin KD, Chung T (2013) Autophagy-Related Proteins Are Required for Degradation of Peroxisomes in Arabidopsis Hypocotyls during Seedling Growth. *Plant Cell* **25**: 4956–4966.
165. Yoshimoto K, Shibata M, Kondo M, Oikawa K, Sato M, Toyooka K, Shirasu K, Nishimura M, Ohsumi Y (2014) Organ-specific quality control of plant peroxisomes is mediated by autophagy. *J Cell Sci* **127**: 1161–1168.
166. Ishida H, Yoshimoto K, Izumi M, Reisen D, Yano Y, Makino A, Ohsumi Y, Hanson MR, Mae T (2008) Mobilization of Rubisco and Stroma-Localized Fluorescent Proteins of Chloroplasts to the Vacuole by an ATG Gene-Dependent Autophagic Process. *Plant Physiol* **148**: 142–155.
167. Izumi M, Wada S, Makino A, Ishida H (2010) The Autophagic Degradation of Chloroplasts via Rubisco-Containing Bodies Is Specifically Linked to Leaf Carbon Status But Not Nitrogen Status in Arabidopsis. *Plant Physiol* **154**: 1196–1209.
168. Liu Y, Burgos JS, Deng Y, Srivastava R, Howell SH, Bassham DC (2012) Degradation of the endoplasmic reticulum by autophagy during endoplasmic reticulum stress in Arabidopsis. *Plant Cell* **24**: 4635–4651.
169. Pu Y, Bassham DC (2013) Links between ER stress and autophagy in plants. *Plant Signal Behav* **8**: e24297.
170. Kulich I, Žárský V (2014) Autophagy-related direct membrane import from ER/Cytoplasm into the vacuole or apoplast: A hidden gateway also for secondary metabolites and phytohormones? *Int J Mol Sci* **15**: 7462–7474.
171. Le Bars R, Marion J, Le Borgne R, Satiat-Jeunemaitre B, Bianchi MW (2014) ATG5 defines a phagophore domain connected to the endoplasmic reticulum during autophagosome formation in plants. *Nat Commun* **5**: 1–10.
172. Zhuang X, Cui Y, Gao C, Jiang L (2015) Endocytic and autophagic pathways crosstalk in plants. *Curr Opin Plant Biol* **28**: 39–47.
173. Pečenková T, Marković V, Sabol P, Kulich I, Žárský V, Goring D, Zárský V (2017) Exocyst and autophagy-related membrane trafficking in plants. *J Exp Bot* **69**: 1–11.
174. Yang X, Bassham DC (2015) New Insight into the Mechanism and Function of Autophagy in Plant Cells. *Int Rev Cell Mol Biol* **320**: 1–40.
175. Estrada-Navarrete G, Cruz-Mireles N, Lascano R, Alvarado-Affantranger X, Hernández A, Barraza A, Olivares JE, Arthikala MK, Cardenas L, Quinto C, et al. (2016) An autophagy-related kinase is essential for the symbiotic relationship between *Phaseolus vulgaris* and both rhizobia and arbuscular mycorrhizal fungi. *Plant Cell* **28**: 2326–2341.
176. Lenz HD, Haller E, Melzer E, Kober K, Wurster K, Stahl M, Bassham DC, Vierstra RD, Parker JE, Bautor J, et al. (2011) Autophagy differentially controls plant basal immunity to biotrophic and necrotrophic pathogens. *Plant J* **66**: 818–830.
177. Lai Z, Wang F, Zheng Z, Fan B, Chen Z (2011) A critical role of autophagy in plant resistance to necrotrophic fungal pathogens. *Plant J* **66**: 953–968.

-
178. Liu Y, Schiff M, Czymmek K, Tallóczy Z, Levine B, Dinesh-Kumar SP (2005) Autophagy regulates programmed cell death during the plant innate immune response. *Cell* **121**: 567–577.
 179. Kwon S II, Cho HJ, Kim SR, Park OK (2013) The Rab GTPase RabG3b Positively Regulates Autophagy and Immunity-Associated Hypersensitive Cell Death in Arabidopsis. *Plant Physiol* **161**: 1722–1736.
 180. Hofius D, Schultz-Larsen T, Joensen J, Tsitsigiannis DI, Petersen NHT, Mattsson O, Jørgensen LB, Jones JDG, Mundy J, Petersen M (2009) Autophagic Components Contribute to Hypersensitive Cell Death in Arabidopsis. *Cell* **137**: 773–783.
 181. Wang J, Ma C, Zhang M, Yang L, Chen W (2015) ATG5 is required to limit cell death induced by *Pseudomonas syringae* in Arabidopsis and may be mediated by the salicylic acid pathway. *Acta Physiol Plant* **37**: 1–11.
 182. Wang Y, Nishimura MT, Zhao T, Tang D (2011) ATG2, an autophagy-related protein, negatively affects powdery mildew resistance and mildew-induced cell death in Arabidopsis. *Plant J* **68**: 74–87.
 183. Häffner E, Konietzki S, Diederichsen E (2015) Keeping Control: The Role of Senescence and Development in Plant Pathogenesis and Defense. *Plants* **4**: 449–488.
 184. Yoshimoto K, Jikumaru Y, Kamiya Y, Kusano M, Consonni C, Panstruga R, Ohsumi Y, Shirasu K (2009) Autophagy Negatively Regulates Cell Death by Controlling NPR1-Dependent Salicylic Acid Signaling during Senescence and the Innate Immune Response in Arabidopsis. *Plant Cell* **21**: 2914–2927.
 185. Kabbage M, Williams B, Dickman MB (2013) Cell Death Control: The Interplay of Apoptosis and Autophagy in the Pathogenicity of *Sclerotinia sclerotiorum*. *PLoS Pathog* **9**: e1003287.
 186. Popa C, Li L, Gil S, Tatjer L, Hashii K, Tabuchi M, Coll NS, Ariño J, Valls M (2016) The effector AWR5 from the plant pathogen *Ralstonia solanacearum* is an inhibitor of the TOR signalling pathway. *Sci Rep* **6**: 1–14.
 187. Üstün S, Hafrén A, Liu Q, Marshall RS, Minina EA, Bozhkov P, Vierstra RD, Hofius D (2018) Bacteria exploit autophagy for proteasome degradation and enhanced virulence in plants. *Plant Cell* **30**: 668–685.
 188. Dagdas YF, Pandey P, Tumtas Y, Sanguankiatichai N, Belhaj K, Duggan C, Leary AY, Segretin ME, Contreras MP, Savage Z, et al. (2018) Host autophagy machinery is diverted to the pathogen interface to mediate focal defense responses against the Irish potato famine pathogen. *Elife* **2018**: e37476.
 189. Hafrén A, Macia J-L, Love AJ, Milner JJ, Drucker M, Hofius D (2017) Selective autophagy limits cauliflower mosaic virus infection by NBR1-mediated targeting of viral capsid protein and particles. *Proc Natl Acad Sci* **114**: E2026–E2035.
 190. Jupe J, Stam R, Howden AJM, Morris JA, Zhang R, Hedley PE, Huitema E (2013) *Phytophthora capsici*-tomato interaction features dramatic shifts in gene expression associated with a hemi-biotrophic lifestyle. *Genome Biol* **14**: 1–18.
 191. Alemu EA, Lamark T, Torgersen KM, Birgisdottir AB, Larsen KB, Jain A, Olsvik H, Øvervatn A, Kirkin V, Johansen T (2012) ATG8 family proteins act as scaffolds for assembly of the ULK complex: Sequence requirements for LC3-interacting region (LIR) motifs. *J Biol Chem* **287**: 39275–39290.
 192. Kalvari I, Tsompanis S, Mulakkal NC, Osgood R, Johansen T, Nezis IP, Promponas VJ (2014) iLIR: A web resource for prediction of Atg8-family interacting proteins. *Autophagy* **10**: 913–925.
 193. Jacomin A-C, Samavedam S, Promponas V, Nezis IP (2016) iLIR database: A web resource for LIR motif-containing proteins in eukaryotes. *Autophagy* **12**: 1945–1953.
-

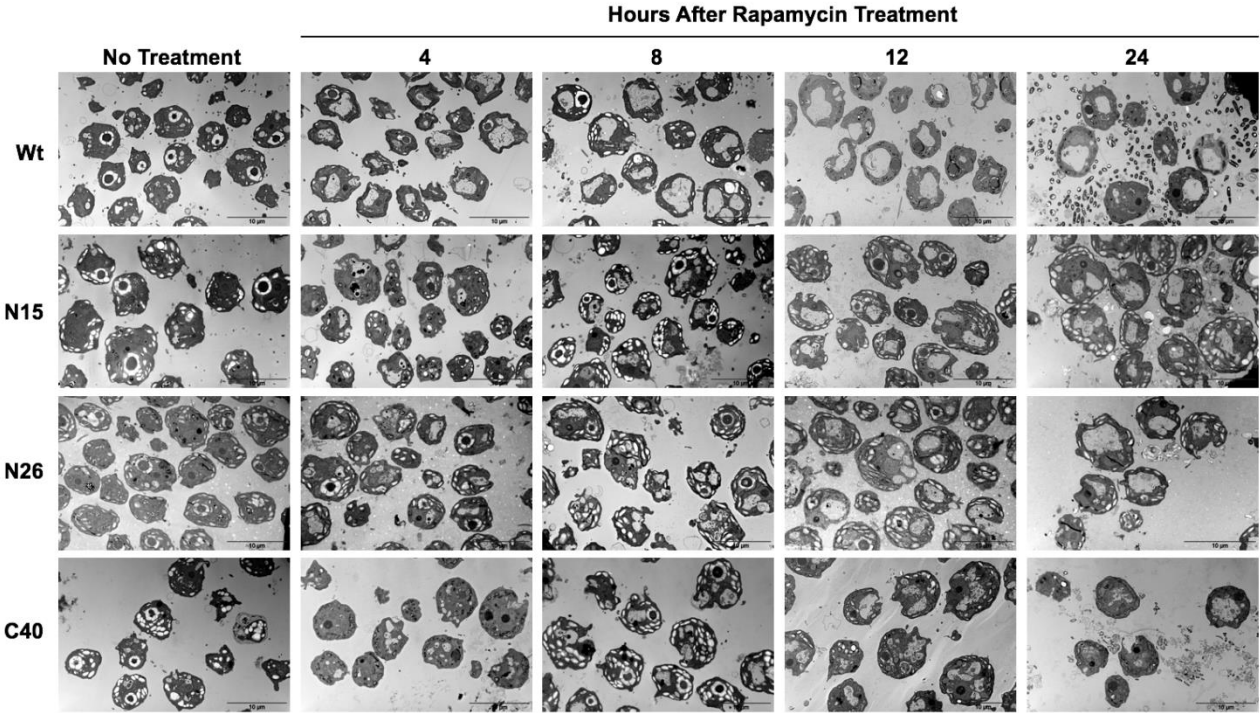
194. Krenek P, Samajova O, Luptovciak I, Duskocilova A, Komis G, Samaj J (2015) Transient plant transformation mediated by *Agrobacterium tumefaciens*: Principles, methods and applications. *Biotechnol Adv* **33**: 1024–1042.
195. Seo E, Woo J, Park E, Bertolani SJ, Siegel JB, Choi D, Dinesh-Kumar SP (2016) Comparative analyses of ubiquitin-like ATG8 and cysteine protease ATG4 autophagy genes in the plant lineage and cross-kingdom processing of ATG8 by ATG4. *Autophagy* **12**: 2054–2068.
196. Rose TL, Bonneau L, Der C, Marty-Mazars D, Marty F (2006) Starvation-induced expression of autophagy-related genes in *Arabidopsis*. *Biol Cell* **98**: 53–67.
197. Slavikova S, Ufaz S, Avin-Wittenberg T, Levanony H, Galili G (2008) An autophagy-associated Atg8 protein is involved in the responses of *Arabidopsis* seedlings to hormonal controls and abiotic stresses. *J Exp Bot* **59**: 4029–4043.
198. Grefen C, Obrdlik P, Harter K (2009) The determination of protein-protein interactions by the mating-based split-ubiquitin system (mbSUS). *Methods Mol Biol* **479**: 217–233.
199. Harris EH, Stern DB, Witman GB (2009) The Genus *Chlamydomonas*. In, *The Chlamydomonas Sourcebook*. Elsevier Inc., Oxford, UK.
200. Merchant SS, Prochnik SE, Vallon O, Harris EH, Karpowicz SJ, Witman GB, Terry A, Salamov A, Fritz-Laylin LK, Maréchal-Drouard L, et al. (2007) The *Chlamydomonas* genome reveals the evolution of key animal and plant functions. *Science* **318**: 245–250.
201. Jiang Q, Zhao L, Dai J, Wu Q (2012) Analysis of autophagy genes in microalgae: *Chlorella* as a potential model to study mechanism of autophagy. *PLoS One* **7**: e41826.
202. Pérez-Pérez ME, Crespo JL (2010) Autophagy in the model alga *Chlamydomonas reinhardtii*. *Autophagy* **6**: 562–563.
203. Pérez-Pérez ME, Florencio FJ, Crespo JL (2010) Inhibition of target of rapamycin signaling and stress activate autophagy in *Chlamydomonas reinhardtii*. *Plant Physiol* **152**: 1874–1888.
204. Crespo JLL, Díaz-Troya S, Florencio FJF (2005) Inhibition of target of rapamycin signaling by rapamycin in the unicellular green alga *Chlamydomonas reinhardtii*. *Plant Physiol* **139**: 1736–1749.
205. Pérez-Pérez ME, Couso I, Heredia-Martínez LG, Crespo JL (2017) Monitoring Autophagy in the Model Green Microalga *Chlamydomonas reinhardtii*. *Cells* **6**: 1–11.
206. Neupert J, Karcher D, Bock R (2009) Generation of *Chlamydomonas* strains that efficiently express nuclear transgenes. *Plant J* **57**: 1140–1150.
207. Barahimipour R, Strenkert D, Neupert J, Schroda M, Merchant SS, Bock R (2015) Dissecting the contributions of GC content and codon usage to gene expression in the model alga *Chlamydomonas reinhardtii*. *Plant J* **84**: 704–717.
208. Lumbreras V, Stevens DR, Purton S (1998) Efficient foreign gene expression in *Chlamydomonas reinhardtii* mediated by an endogenous intron. *Plant J* **14**: 441–447.
209. Cross FR, Umen JG (2015) The *Chlamydomonas* cell cycle. *Plant J* **82**: 370–392.
210. Zones JM, Blaby IK, Merchant SS, Umen JG (2015) High-Resolution Profiling of a Synchronized Diurnal Transcriptome from *Chlamydomonas reinhardtii* Reveals Continuous Cell and Metabolic Differentiation. *Plant Cell* **27**: 2743–2769.
211. Lyons AB (2000) Analysing cell division in vivo and in vitro using flow cytometric measurement of CFSE dye dilution. *J Immunol Methods* **243**: 147–154.

-
212. Rioboo C, O'Connor JE, Prado R, Herrero C, Cid A (2009) Cell proliferation alterations in *Chlorella* cells under stress conditions. *Aquat Toxicol* **94**: 229–237.
213. Schroda M, Blöcker D, Beck CF (2000) The HSP70A promoter as a tool for the improved expression of transgenes in *Chlamydomonas*. *Plant J* **21**: 121–131.
214. Couso I, Crespo JL (2017) The TOR Signaling Network in the Model Unicellular Green Alga *Chlamydomonas reinhardtii*. *Biomolecules* **7**: 1–13.
215. Jüppner J, Mubeen U, Leisse A, Caldana C, Wiszniewski A, Steinhäuser D, Giavalisco P (2018) The target of rapamycin kinase affects biomass accumulation and cell cycle progression by altering carbon/nitrogen balance in synchronized *Chlamydomonas reinhardtii* cells. *Plant J* **93**: 355–376.
216. Ylä-Anttila P, Vihinen H, Jokitalo E, Eskelinen E (2009) Monitoring Autophagy by Electron Microscopy in Mammalian Cells. In, *Methods in Enzymology* pp 143–164. Academic Press.
217. Park H, Eggink LL, Roberson RW, Hooper JK (1999) Transfer of proteins from the chloroplast to vacuoles in *Chlamydomonas reinhardtii* (Chlorophyta): a pathway for degradation. *Plant Biol* **538**: 528–538.
218. Shebanova A, Ismagulova T, Solovchenko A, Baulina O, Lobakova E, Ivanova A, Moiseenko A, Shaitan K, Polshakov V, Nedbal L, et al. (2017) Versatility of the green microalga cell vacuole function as revealed by analytical transmission electron microscopy. *Protoplasma* **254**: 1323–1340.
219. Couso I, Pérez-Pérez ME, Martínez-Force E, Kim H-S, He Y, Umen JG, Crespo JL, Bozhkov P (2017) Autophagic flux is required for the synthesis of triacylglycerols and ribosomal protein turnover in *Chlamydomonas*. *J Exp Bot* **69**: 1–13.
220. Wattedled F, Buléon A, Bouchet B, Ral J-P, Liénard L, Delvallé D, Binderup K, Dauvillée D, Ball S, D'Hulst C (2002) Granule-bound starch synthase I. A major enzyme involved in the biogenesis of B-crystallites in starch granules. *Eur J Biochem* **269**: 3810–3820.
221. Caspar T, Huber SC, Somerville C (1985) Alterations in Growth, Photosynthesis, and Respiration in a Starchless Mutant of *Arabidopsis thaliana* (L.) Deficient in Chloroplast Phosphoglucomutase Activity. *Plant Physiol* **79**: 11–17.
222. Koo KM, Jung S, Lee BS, Kim J-B, Jo YD, Choi H-I, Kang S-Y, Chung G-H, Jeong W-J, Ahn J-W (2017) The Mechanism of Starch Over-Accumulation in *Chlamydomonas reinhardtii* High-Starch Mutants Identified by Comparative Transcriptome Analysis. *Front Microbiol* **8**: 1–12.
223. Edner C, Li J, Albrecht T, Mahlow S, Hejazi M, Hussain H, Kaplan F, Guy C, Smith SM, Steup M, et al. (2007) Glucan, water dikinase activity stimulates breakdown of starch granules by plastidial beta-amylases. *Plant Physiol* **145**: 17–28.
224. Cao Y, Klionsky DJ (2007) Physiological functions of Atg6/Beclin 1: a unique autophagy-related protein. *Cell Res* **17**: 839–849.
225. Ishihara N, Hamasaki M, Yokota S, Suzuki K, Kamada Y, Kihara A, Yoshimori T, Noda T, Ohsumi Y (2001) Autophagosome requires specific early Sec proteins for its formation and NSF/SNARE for vacuolar fusion. *Mol Biol Cell* **12**: 3690–3702.
226. Klionsky DJ, Abdelmohsen K, Abe A, Abedin MJ, Abeliovich H, Arozena AA, Adachi H, Adams CM, Adams PD, Adeli K, et al. (2016) Guidelines for the use and interpretation of assays for monitoring autophagy (3rd edition). *Autophagy* **12**: 1–122.
227. Yan HZ, Liou RF (2006) Selection of internal control genes for real-time quantitative RT-PCR assays in the oomycete plant pathogen *Phytophthora parasitica*. *Fungal Genet Biol* **43**: 430–438.
-

228. Thomma BPHJ, Eggermont K, Penninckx IAMA, Mauch-Mani B, Vogelsang R, Cammue BPA, Broekaert WF (1998) Separate jasmonate-dependent and salicylate-dependent defense-response pathways in *Arabidopsis* are essential for resistance to distinct microbial pathogens. *Proc Natl Acad Sci* **95**: 15107–15111.
229. Ah Fong AM V., Judelson HS (2003) Cell cycle regulator Cdc14 is expressed during sporulation but not hyphal growth in the fungus-like oomycete *Phytophthora infestans*. *Mol Microbiol* **50**: 487–494.
230. Mizushima N, Yoshimori T, Levine B (2010) Methods in Mammalian Autophagy Research. *Cell* **140**: 313–326.
231. Mauthe M, Orhon I, Rocchi C, Zhou X, Luhr M, Hijlkema KJ, Coppes RP, Engedal N, Mari M, Reggiori F (2018) Chloroquine inhibits autophagic flux by decreasing autophagosome-lysosome fusion. *Autophagy* **14**: 1435–1455.
232. Park E, Nedo A, Caplan JL, Dinesh-Kumar SP (2017) Plant-microbe interactions: Organelles and the cytoskeleton in action. *New Phytol* **217**: 1012–1028.
233. Kumar SV, Misquitta RW, Reddy VS, Rao BJ, Rajam MV (2004) Genetic transformation of the green alga--*Chlamydomonas reinhardtii* by *Agrobacterium tumefaciens*. *Plant Sci* **166**: 731–738.
234. Menand B, Desnos T, Nussaume L, Berger F, Bouchez D, Meyer C, Robaglia C (2002) Expression and disruption of the *Arabidopsis* TOR (target of rapamycin) gene. *Proc Natl Acad Sci* **99**: 6422–6427.
235. Cheong H, Nair U, Geng J, Klionsky DJ (2008) The Atg1 kinase complex is involved in the regulation of protein recruitment to initiate sequestering vesicle formation for nonspecific autophagy in *Saccharomyces cerevisiae*. *Mol Biol Cell* **19**: 668–681.
236. Ramirez-Garcés D, Camborde L, Pel MJC, Jauneau A, Martinez Y, Néant I, Leclerc C, Moreau M, Dumas B, Gaulin E (2016) CRN13 candidate effectors from plant and animal eukaryotic pathogens are DNA-binding proteins which trigger host DNA damage response. *New Phytol* **210**: 602–617.
237. Yang KC, Sathiyaseelan P, Ho C, Gorski SM (2018) Evolution of tools and methods for monitoring autophagic flux in mammalian cells. *Biochem Soc Trans* **46**: 1–14.
238. Kasuba KC, Vavilala SL, D'Souza JS (2015) Apoptosis-like cell death in unicellular photosynthetic organisms - A review. *Algal Res* **12**: 126–133.
239. Schaaf MBE, Keulers TG, Vooijs MA, Rouschop KMA (2016) LC3/GABARAP family proteins: autophagy-(un)related functions. *FASEB J* **30**: 3961–3978.
240. Nguyen TN, Padman BS, Usher J, Oorschot V, Ramm G, Lazarou M (2016) Atg8 family LC3 / GAB ARAP proteins are crucial for autophagosome – lysosome fusion but not autophagosome formation during PINK1 / Parkin mitophagy and starvation. *J Cell Biol* **215**: 1–18.
241. Dodds PN, Rathjen JP (2010) Plant immunity: towards an integrated view of plant–pathogen interactions. *Nat Rev Genet* **11**: 539–548.
242. Patel S, Caplan J, Dinesh-Kumar S (2006) Autophagy in the control of programmed cell death. *Curr Opin Plant Biol* **9**: 391–396.
243. Zvereva AS, Golyaev V, Turco S, Gubaeva EG, Rajeswaran R, Schepetilnikov M V., Srour O, Ryabova LA, Boller T, Pooggin MM (2016) Viral protein suppresses oxidative burst and salicylic acid-dependent autophagy and facilitates bacterial growth on virus-infected plants. *New Phytol* **211**: 1020–1034.
244. Svenning S, Lamark T, Krause K, Johansen T (2011) Plant NBR1 is a selective autophagy substrate and a functional hybrid of the mammalian autophagic adapters NBR1 and p62/SQSTM1. *Autophagy* **7**: 993–1010.

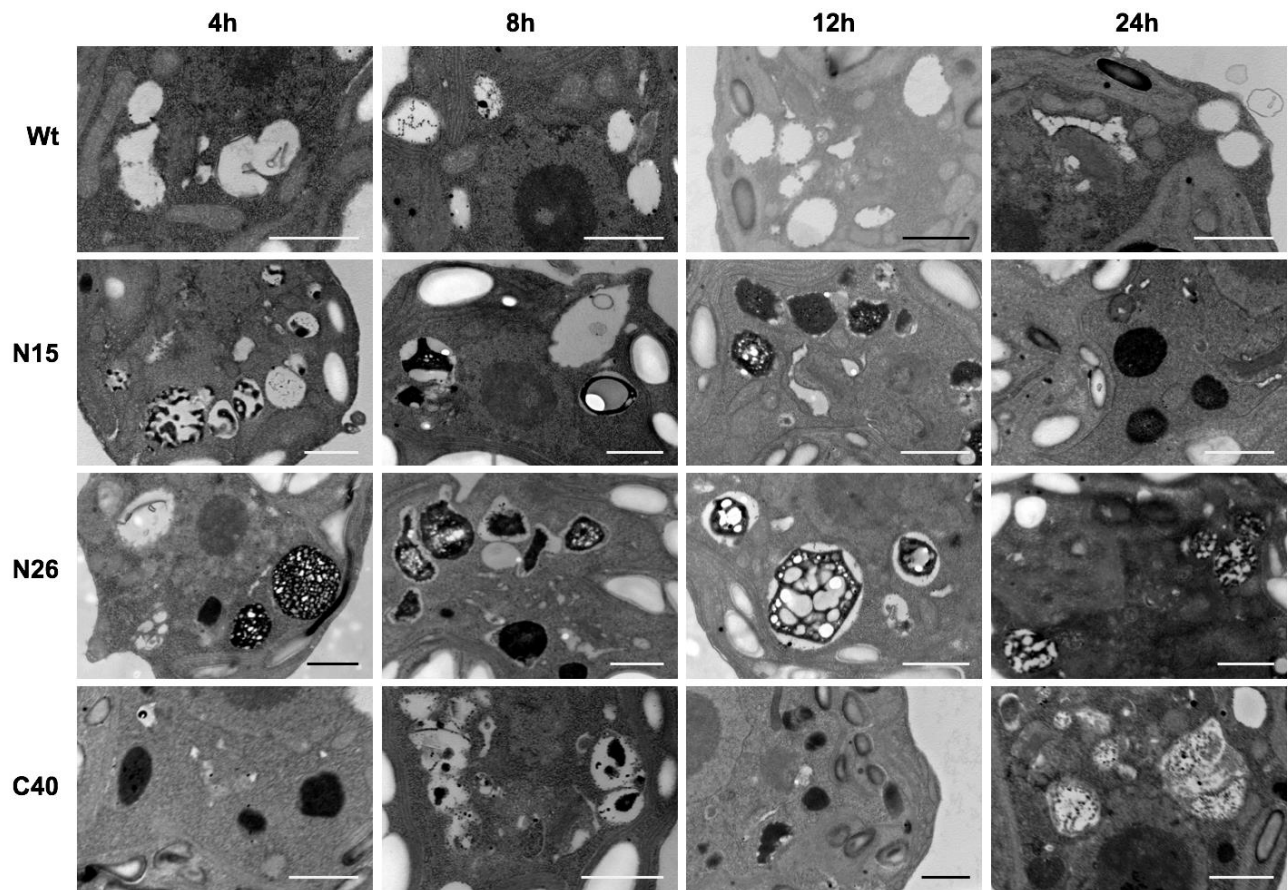
-
245. Duszenko M, Ginger ML, Brennand A, Gualdrón-López M, Colombo MI, Coombs GH, Coppens I, Jayabalasingham B, Langsley G, De Castro SL, et al. (2011) Autophagy in protists. *Autophagy* **7**: 127–158.
 246. Mizushima N, Yamamoto A, Hatano M, Kobayashi Y, Kabey Y, Suzuki K, Tokuhis T, Ohsumi Y, Yoshimori T (2001) Dissection of autophagosome formation using Apg5-deficient mouse embryonic stem cells. *J Cell Biol* **152**: 657–667.
 247. Park E, Woo J, Dinesh-Kumar SP (2014) Arabidopsis ATG4 cysteine proteases specificity toward ATG8 substrates. *Autophagy* **10**: 926–927.
 248. Upson JL, Zess EK, Białas A, Wu C hang, Kamoun S (2018) The coming of age of EvoMPMI: evolutionary molecular plant–microbe interactions across multiple timescales. *Curr Opin Plant Biol* **44**: 108–116.
 249. Gouy M, Guindon S, Gascuel O (2010) SeaView Version 4: A Multiplatform Graphical User Interface for Sequence Alignment and Phylogenetic Tree Building. *Mol Biol Evol* **27**: 221–224.
 250. Kumar S, Stecher G, Tamura K (2016) MEGA7: Molecular Evolutionary Genetics Analysis Version 7.0 for Bigger Datasets. *Mol Biol Evol* **33**: 1870–1874.
 251. Laroche-Raynal M, Aspart L, Delseny M, Penon P (1984) Characterization of radish mRNA at three developmental stages. *Plant Sci Lett* **35**: 139–146.
 252. Clough SJ, Bent AF (1998) Floral dip: A simplified method for *Agrobacterium*-mediated transformation of *Arabidopsis thaliana*. *Plant J* **16**: 735–743.
 253. Galiana E, Rivière MP, Pagnotta S, Baudouin E, Panabières F, Gounon P, Boudier L (2005) Plant-induced cell death in the oomycete pathogen *Phytophthora parasitica*. *Cell Microbiol* **7**: 1365–1378.
 254. Kong F, Liang Y, Légeret B, Beyly-Adriano A, Blangy S, Haslam RP, Napier JA, Beisson F, Peltier G, Li-Beisson Y (2017) *Chlamydomonas* carries out fatty acid β -oxidation in ancestral peroxisomes using a bona fide acyl-CoA oxidase. *Plant J* **90**: 358–371.
 255. Futamura K, Sekino M, Hata A, Ikebuchi R, Nakanishi Y, Egawa G, Kabashima K, Watanabe T, Furuki M, Tomura M (2015) Novel full-spectral flow cytometry with multiple spectrally-adjacent fluorescent proteins and fluorochromes and visualization of in vivo cellular movement. *Cytom Part A* **87**: 830–842.

Supplementary Figures



Supplementary Figure 1: Representative view of *Chlamydomonas* cells from the wild-type and transgenic lines expressing *Avh195*, as analyzed by TEM.

Micrographs show untreated cells, or cells that were incubated with 0.5 μ M rapamycin for 4h, 8h, 12h, and 24h. Bars represent 10 μ m.



Supplementary Figure 2: Accumulation of electron-dense, lysosome-like structures in cells from Avh195-expressing *Chlamydomonas* lines that were not treated with rapamycin.

High resolution TEM micrographs were recorded at different time points after onset of light over a 24h-day/night cycle. Appearance of the vesicle likely reflects basal autophagic flux within the cells. Bars represent 1 μ m.

